MODELING IMPACTS OF LAND-USE/LAND-COVER CHANGE AND VARIABLE PRECIPITATION ON HYDROLOGY AND WATER QUALITY OF A COASTAL WATERSHED IN TEXAS

A Thesis

by

CESAR R. CASTILLO

Submitted to the Office of Graduate Studies of
Texas A&M University
in partial fulfillment of the requirements for the degree of

MASTER OF SCIENCE

Chair of Committee,	Inci Guneralp
Committee Members,	Burak Guneralp
	Anthony Filippi
	Patricia Smith
Interdisciplinary Faculty Chair,	Ron Kaiser

August 2013

Major Subject: Water Management and Hydrological Science

Copyright 2013 Cesar R. Castillo

ABSTRACT

Land use/land cover (LULC) change and variations in precipitation can alter the quantity and quality of freshwater flows. The Mission-Aransas (M-A) estuary depends on inputs of freshwater and material from streams in order to maintain its ecological integrity. Freshwater inflow estimates for the M-A estuary have been established, but no analyses using scenarios of LULC change and precipitation variability have been conducted that inform how freshwater inflows could be impacted.

A land change analysis for the M-A region was conducted by classifying two Landsat images for the years 1990 and 2010. A large degree of LULC change occurred within the M-A region during this time; with 27.1% of the land area experiencing LULC change. Furthermore, developed land increased by 44.9%.

A SWAT hydrological model was developed to model the quantity and quality of freshwater inflows. SWAT was calibrated at a monthly scale using data from a stream gage. Model evaluations indicated that the model had a good performance rating with a Nash-Sutcliffe model efficiency coefficient (NS) of 0.66 and coefficient of determination (R^2) of 0.66 for the calibration period; and an NS of 0.76 and R^2 of 0.78 for the validation period.

Three LULC change scenarios and three precipitation scenarios were developed to be used in a scenario analysis with the calibrated SWAT model. Each LULC change scenario represents a different amount of developed land (3.4, 3.7, and 4.7% of

watershed area). Precipitation data was analyzed to select weather data for each precipitation scenario that each had different amounts of annual precipitation (763, 907, and 996 mm).

A scenario analysis was conducted that analyzed how stream/channel flows and loads of sediment, total nitrogen, and total phosphorus were impacted under scenario conditions. A general increase in all output variables was exhibited as the amount of precipitation and developed land increased; with impacts from precipitation variability outweighing impacts from varying amounts of developed land. Furthermore, sediment loads were the variable most impacted by differing amounts of developed land.

This study provides information on how LULC and precipitation can influence watershed hydrology that can be used in watershed management for the M-A region.

DEDICATION

I dedicate this work to my loving parents, my entire family, friends I've made throughout my educational and professional endeavors, and this wonderful and vastly interesting planet that we all share.

ACKNOWLEDGEMENTS

I would like to thank my committee chair, Dr. Inci Guneralp, and my committee members, Dr. Burak Guneralp, Dr. Anthony Filippi, and Dr. Patricia Smith, for their guidance, support, and patience throughout the course of this research and pursuit of my master's degree.

Thanks also go to good friends Katharine Bradley, Josh Litt, Keya Howard, Stephen Davis, Alan Lewis, Jannet Torres, Victor Garcia, and Askar Karimov for the constant laughs and lively conversations throughout my time in College Station. I would also like to thank Dr. Ron Kaiser, Dr. Rosario Sanchez, the late Dr. Val Silvey, and the remainder of the WMHS department faculty and staff for promoting a wonderful learning environment at Texas A&M University. I also want to extend my gratitude to the Office of Graduate Studies, which provided me with the Diversity Fellowship that funded my time spent pursuing my master's degree.

Finally, thanks to my loving parents, siblings, and friends in Texas and back in New Mexico for their never ending encouragement and support throughout the pursuit of my education.

TABLE OF CONTENTS

Page

LIST OF FIGURES

Page

LIST OF TABLES

CHAPTER I

INTRODUCTION

1.1 Introduction

The transformation of land surfaces for human use and changes in climate can disrupt the quantity and quality of freshwater flows. Like many other ecosystems, estuaries depend on inputs of freshwater and material that are transported by freshwater flows in order to maintain salinity gradients, sedimentation rates, and nutrient cycles inherent within the system. The Mission-Aransas (M-A) National Estuarine Research Reserve (NERR) on the Coastal Bend of Texas was established in 2006 with the primary mission of increasing the level of scientific knowledge and environmental stewardship associated with estuarine and coastal environments in Texas. Furthermore, the M-A NERR provides habitat for several species of fish and shellfish with commercial and recreational value, as well as crucial habitat for endangered species such as the whooping crane. Although freshwater inflow estimates and recommendations for the M-A system have been established, a lack of knowledge still exists over how land-use/land-cover (LULC) changes and variable precipitation could impact the quantity and quality of freshwater inflows.

1.2 Background

The analysis of hydrologic impacts as a result of a changing climate and the modification/transformation of land surfaces has become an area of thriving research

(Praskievicz and Chang 2011). Hydrologic impacts vary by location as a result of the differential levels of influence regional climate and land use can have on the hydrologic system. The transformation of land for various uses can degrade water quality and disrupt the partitioning of precipitation into runoff, evapotranspiration, and groundwater flow (Foley et al. 2005). Changes to freshwater flows can have a cascading effect on the dynamics of anthropogenic (Praskievicz and Chang 2009, Price 2011), riverine (Allan 2004), and coastal (Howarth et al. 2011) systems.

The hydrologic cycle controls the volume and timing of freshwater delivery and its chemical and sediment load to coastal ecosystems (Scavia et al. 2002). Estuaries and other systems are largely dependent on the quantity and quality of freshwater inflows. Freshwater inflows can be defined as inputs of freshwater from streams draining into estuaries. These inflows are important factors in the overall health of estuarine environments because they are major drivers of salinity gradients, sedimentation rates, and nutrient delivery. Furthermore, regional climate and LULC change can modify the hydrological characteristics of a watershed, potentially adversely affecting estuarine systems.

In Texas, the importance of freshwater inflows to estuaries has been recognized (Estevez 2002, Powell, Matsumoto, and Brock 2002). As estuaries provide habitat for several species of fish and shellfish of economic and recreational value, Texas has mandated the study of freshwater inflow requirements/recommendations for its estuaries (Powell, Matsumoto, and Brock 2002). This has involved the development and

application of the Texas Estuarine Mathematical Program (TexEMP) by the Texas Water Development Board (TWDB) and Texas Parks and Wildlife Department (TPWD). TexEMP incorporates hydrology, climate, fisheries harvests, upstream water uses, coastal bay hydrodynamics, and optimization procedures to develop estuary performance curves that are used to make freshwater inflow recommendations (Powell, Matsumoto, and Brock 2002, Chen 2010). The M-A NERR was established in 2006 and the TexEMP approach was applied to establish freshwater inflow recommendations for the estuary based on mean, minimum, and maximum flows (Chen 2010). However, as watersheds upstream of the M-A estuarine system become more developed and agricultural practices change, the hydrologic parameters used to establish the freshwater inflow recommendations may need to be revisited.

A large body of research has been conducted in an attempt to understand how hydrology is being impacted in different regions as a result of climate and LULC change (Praskievicz and Chang 2009, Price 2011). Urban and agricultural land uses have gained considerable amount of attention with regards to hydrologic impacts. A key study conducted by Tong and Chen (2002) found a strong statistical relationship between historical nutrient loads in surface water and agricultural and urban land uses for the state of Ohio. Furthermore, Tong and Chen (2002) simulated water quality parameters in watersheds of southwestern Ohio yielding similar results of higher nutrient loads in catchments with greater proportions of agricultural and urban land uses. Other hydrologic modeling studies that focused on historical urban expansion reported similar

results in the Conestoga River Basin, Pennsylvania (Chang 2004), the Muskegon River Basin, Michigan (Tang et al. 2005), and the Tualatin River Basin, Oregon (Franczyk and Chang 2009, Praskievicz and Chang 2011). Increased urbanization and agriculture in watersheds are characterized by the removal of permeable vegetative cover that reduces infiltration, allowing greater amounts of rainfall to be converted to surface runoff that washes out pollutants stored on the surface and in soil to receiving water bodies.

Regional climate and land use interact in complex ways to modify hydrology and water quality. Chang (2004) simulated hydrologic impacts in southeastern Pennsylvania from climate change and land-use change individually and interactively and found the climate (mostly precipitation) signal to be the dominant driver of surface water flows and nutrient loadings. Similar studies conducted by Franczyk and Chang (2009) and Praskievicz and Chang (2011) noted similar sensitivities to amounts of precipitation within a set of watersheds in northwest Oregon. Changes to seasonal precipitation are inferred to be the principal factor of hydrologic impacts within rainfed basins (Chang 2004, Franczyk and Chang 2009, Praskievicz and Chang 2011). Wetter time periods coupled with urban development increase surface water flows and the transport of pollutants and other materials within watersheds.

The pursuit of more informed and adaptive watershed management strategies has driven the use of modeling techniques that evaluate a variety of climate and LULC change scenarios. Climate and LULC change scenarios carry a large degree of uncertainty, due to the prediction/modeling methods (Praskievicz and Chang 2011) and

data availability (Breuer, Huisman, and Frede 2006). Nonetheless, scenario analysis can provide insight into how hydrologic variables can change in direction and magnitude (Chang 2004, Franczyk and Chang 2009, Praskievicz and Chang 2011). Generalized hydrologic models, such as the Soil and Water Assessment Tool (SWAT), used to simulate hydrologic impacts give results at the basin and subbasin scale, as these are the natural boundaries for any surface water analysis (Praskievicz and Chang 2009). These models allow a range of scenarios to be analyzed individually and in combination in order to infer whether precipitation or LULC can be considered the dominant signal of the hydrological and water quality characteristics of a watershed.

An increase in nutrient delivery to estuaries as a result of LULC change within upstream basins has been well documented in the literature (Correll, Jordan, and Weller 1992, Harris 2001, Arismendez et al. 2009, Howarth et al. 2011, Rebich et al. 2011). On the other hand, the influence of regional climate on water quality is largely dependent on the amount of rainfall a region receives (Howarth et al. 2011, Rebich et al. 2011). Changes to runoff and sediment flows will depend on the type, amount, and spatial configuration of LULC change, as well as the amount of rainfall. Sahoo and Smith (2009) noted how urbanization influenced differences between stream gages upstream and downstream (more than what would be expected) of San Antonio, Texas. The direction of change in precipitation projections for the Texas Gulf Coast varies amongst different general circulation models (Thomson et al. 2005). Watersheds upstream of the M-A estuarine system have been experiencing increases in the amount of urban land

cover, but whether or not this trend continues into the future is uncertain. No analysis on the quantity and quality of freshwater inflows entering the M-A estuarine system have previously been conducted using interactive scenarios of precipitation variability and LULC change. Scenario analysis can yield valuable information when there are uncertainties revolving around the types of changes in precipitation and LULC that may occur.

Watershed-based computer simulation systems are powerful tools when analyzing potential hydrologic impacts under LULC and precipitation scenarios. SWAT in particular, is very powerful in that it allows hydrology, sediment transport, and other water quality constituents to be simulated simultaneously within the same modeling system. Additionally, SWAT is computationally efficient and it has been widely applied in watersheds of various sizes with different hydrologic, geologic, and climatic conditions (Borah and Bera 2004, Arnold et al. 2012). Furthermore, SWAT was successfully applied by (Lee et al. 2011) for the coastal Matagorda Bay Watershed in Texas in order to estimate freshwater inflows for Matagorda Bay. This suggests that SWAT, and the graphical user interface ArcSWAT, can be applied to understand hydrologic impacts under various scenarios to freshwater inflows in the M-A region.

1.3 Research Objectives

The research presented in this thesis addressed the following question: How are streamflow, sediment flow, and nutrient transport into the Mission-Aransas estuarine system impacted by interactive variations in precipitation and land-use/land-cover

change? To address this question, this research was broken down into the following four objectives:

1) Gain an understanding of the quantity and spatial distribution of recent land use/land cover change within the Mission-Aransas Coastal Region.
2) Assess the capabilities of a SWAT hydrological model developed for the lower portions of the Aransas River Basin to predict freshwater inflows and the delivery of associated sediment and nutrient loads to the Mission-Aransas estuarine system.
3) Develop datasets of various scenarios of LULC change and precipitation that can be used as inputs to the SWAT hydrological model.
4) Analyze how SWAT simulations of the watershed hydrology and water quality for the Lower Aransas River Basin (LARB) are impacted under various scenarios of LULC change (increased development) and precipitation.

CHAPTER II

LAND CHANGE ANALYSIS OF THE MISSION-ARANSAS REGION

2.1 Introduction

The transformation of land surfaces for human use can disrupt the quantity and quality of freshwater flows, increase the potential for soil erosion, and lead to habitat loss/degradation. Coastal areas are not immune to potential issues associated with the transformation of land. In Texas, bays/estuaries and the drainage basins upstream from marine water bodies, are vital resources because these areas provide habitat for several fish and bird species of commercial and recreational value. Furthermore, development has continued to increase along the coast of Texas for industrial and municipal purposes. The Mission-Aransas region on the Coastal Bend of Texas is an area with a complex mix of natural and anthropogenic land surfaces. The bays and estuaries in the Mission-Aransas region are especially sensitive to changes in land use/land cover (LULC) within drainage basins upstream because it can disrupt inputs of freshwater and material that are vital in maintaining salinity gradients, sedimentation rates, and nutrient cycles within the system. To better understand how freshwater and material inputs are being impacted by LULC change, an understanding of the degree of LULC change within the region must first be established.

2.2 Objectives

The main objective presented in this chapter is to gain an understanding of the quantity and spatial distribution of recent land use/land cover change within the Mission-Aransas Coastal Region. To address this objective, this work was divided into four tasks:

1. Classify small portions of two Landsat Thematic Mapper images (for 1990 and 2010) that include much of the lower portions of the Aransas River Basin.
2. Conduct an accuracy assessment of the classified imagery and compute statistics that give estimates of the general accuracy of the classification procedure.
3. Describe the quantitative and spatial configuration of land use/land cover for 1990 and 2010.
4. Analyze how land use/land cover changed from 1990 to 2010 in terms of quantities and the spatial configuration of change.

2.3 Materials and Methodology

2.3.1 Study Area

The study area lies on the Coastal Bend of Texas just north of Corpus Christi. This area is part of the greater Mission-Aransas and Nueces basin region; and from this point the region will be referred to as the Mission-Aransas Coastal Region (MACR). It is situated in the northwestern corner of the Landsat scene on Path: 26 and Row: 41 of the Worldwide Reference System-2 (Figure II- 1a). This portion of the Landsat scene was chosen because the lower portions of the Aransas River basin (or Lower Aransas River Basin (LARB)) falls within the MACR (Figure II-1b), and the LARB is the focus in later

chapters of this thesis. The extent of the MACR lies between 27°47'23" - 28°19'49" north latitude and 96°58'12" - 97°54'36" west longitude.

The MACR has an area of 3745 km^2, which is about 12% of the total Landsat scene. Elevation in the region ranges from 0 to 74 meters above sea level with most relief occurring in the northwestern portions. The MACR has a semi-arid climate with mean annual precipitation of 864 mm and a mean temperature of 21.8 °C. However, the distribution of annual precipitation is skewed by seasonal tropical storms that occasionally bring large amounts of rainfall in late-summer and early-fall. Most of the MACR falls within the Aransas Watershed, but it also includes portions of the Mission and Nueces watersheds, all named after the principle river that flows within each watershed's respective boundaries. The eastern portions are coastal/near-shore environments that include all of Copano and Mission Bays, as well as portions of Aransas, Nueces, Corpus Christi, and Red Fish Bays (Figure II-2). Central portions are mostly dominated by cultivated land with rangeland and woodland occupying much of the northern portions of the region (Morehead, Beyer, and Dunton 2007).

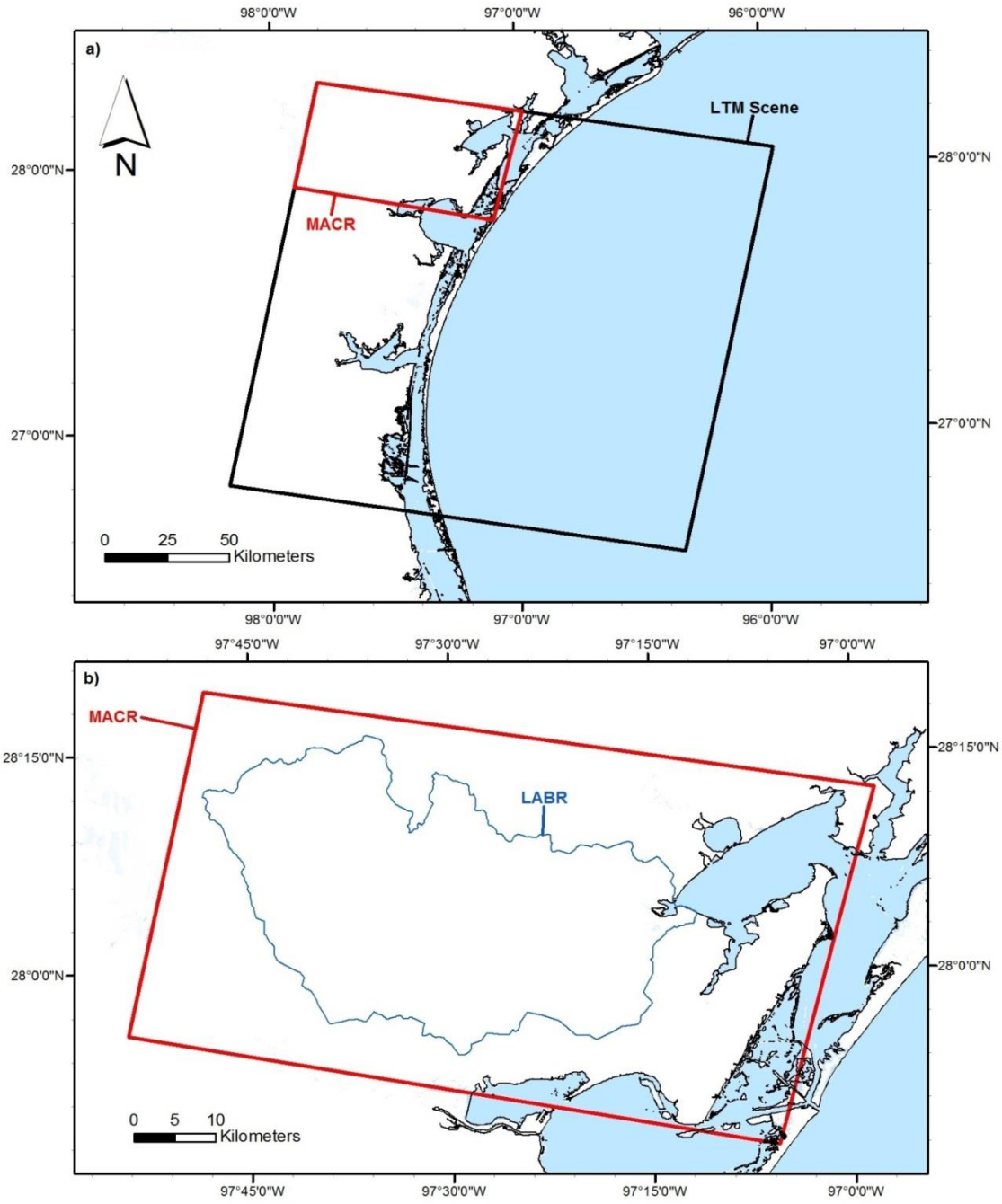

Figure II-1. a) Location map for Landsat Thematic Mapper (LTM) scene (Row: 26, Path: 41) used in the analysis. All image processing was conducted within the Mission-Aransas Coastal Region (MACR). b) Location map of the MACR along with identification the Lower Aransas River Basin (LABR).

The LARB lies in the central portions of the MACR (Figure II-2) and it has an area of 1406 km^2 that is about 38% of the MACR. It is composed of 12 subwatersheds (12-digit Hydrologic Unit Code) of the Aransas River and its tributaries. These streams/rivers flow in a general west to east direction towards the mouth of the Aransas River in the northeastern corner of the basin. In recent decades, cultivated lands have dominated much of the LARB, especially in southern portions with rangeland, woodland, and riverine environments in the northern portions. Most of the MACR and LARB fall within San Patricio County, but these areas also include portions of other counties (Table II-1). The MACR is predominantly rural with no large urban centers (Morehead, Beyer, and Dunton 2007). Cities and towns are generally situated near the coast or streams with the most populace urban areas in the MACR being Portland, Ingleside, Rockport, and Aransas Pass (Table II-2). The two most prominent urban areas entirely within the LARB are Sinton and Taft.

Table II-1. Texas counties that make up the Mission-Aransas Coastal Region (MACR) and the Lower Aransas River Basin (LARB).

County	MACR		LARB	
	Area (km^2)	**Percentage of Total Area**	**Area (km^2)**	**Percentage of Total Area**
San Patricio	1771.2	47.3%	1033.2	73.7%
Refugio	652.6	17.4%	110.9	7.9%
Bee	519.7	13.9%	247.5	17.7%
Aransas	441.9	11.8%	10.1	0.7%
Nueces	269.1	7.2%	0.0	0.0%
Jim Wells	80.8	2.2%	0.0	0.0%
Live Oak	11.2	0.3%	0.0	0.0%
Total	**3746.4**	**100.0%**	**1401.8**	**100.0%**

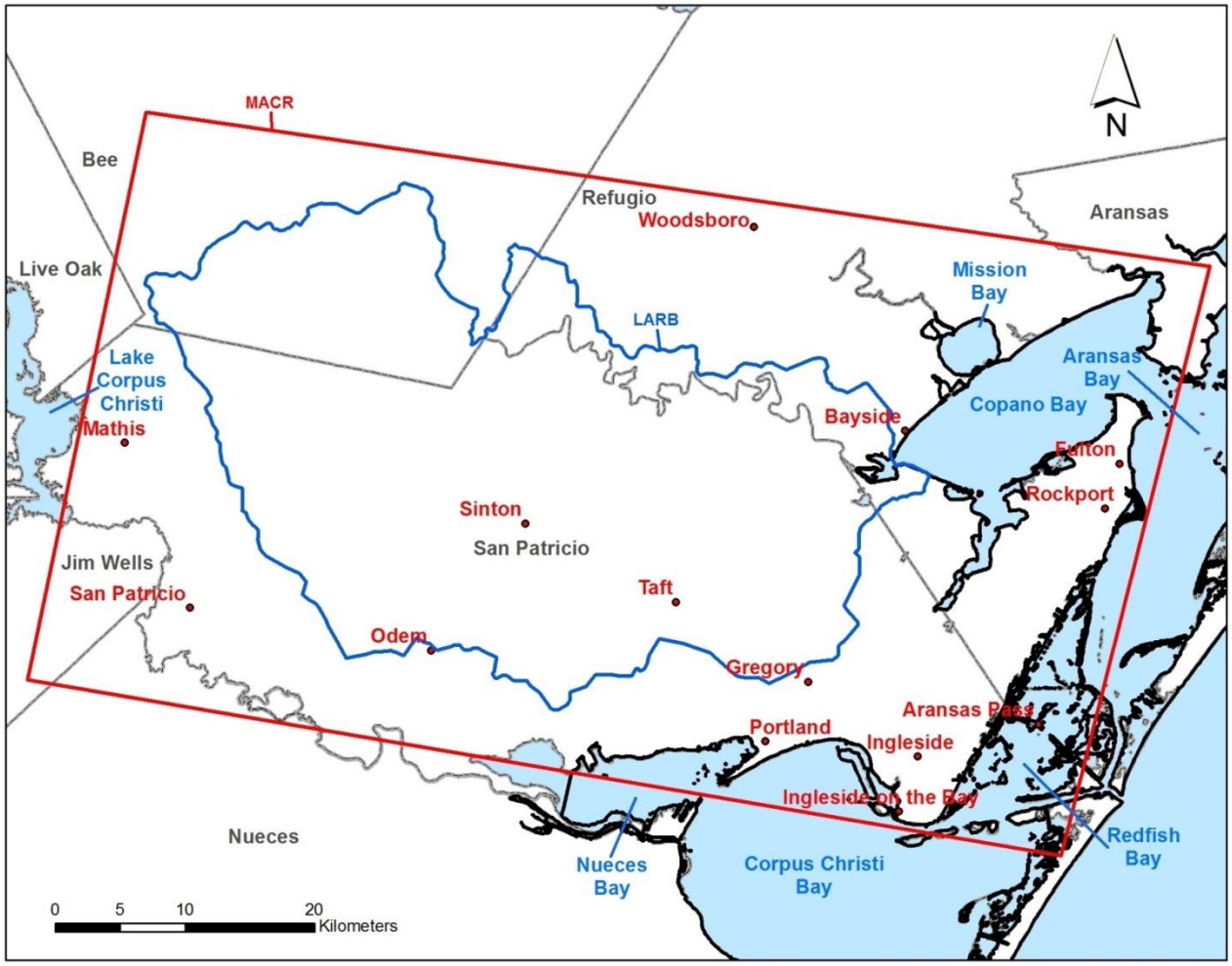

Figure II-2. County boundaries, cities/towns, and general geography within the Mission-Aransas Coastal Region (MACR) and Lower Aransas River Basin (LARB).

Table II-2. Cities/Towns that fall within the Mission-Aransas Coastal Region (MACR) along with their population in 2010.

Name	County	Designation	Population in 2010
Portland	San Patricio	City	15,099
Ingleside	San Patricio	City	9,387
Rockport	Aransas	City	8,766
Aransas Pass	Nueces/Aransas	City	8,204
Sinton	San Patricio	City	5,665
Mathis	San Patricio	City	4,942
Taft	San Patricio	City	3,048
Odem	San Patricio	City	2,389
Gregory	San Patricio	City	1,907
Woodsboro	Refugio	Town	1,512
Fulton	Aransas	Town	1,358
Ingleside on the Bay	San Patricio	City	615
San Patricio	San Patricio	City	395
Bayside	Refugio	Town	325
Total Urban Population			**63,612**

2.3.2 Data

Table II-3 lists the data used in the image classification procedures. The Landsat Thematic Mapper (LTM) images for 1990 and 2010 were used as the primary input for the LULC classification process. LTM imagery has six spectral bands at a spatial resolution of 30 m (Table II-4). Aerial photography for 1990, Google Earth (Google Inc 2011) imagery for the early 1990s, National Land Cover Dataset (NLCD) imagery for 1992, and Coastal Change Analysis Program imagery (CCAP) for 1996 were used as reference images in the designation of training areas/pixels for the classification algorithm and in the accuracy assessment of the 1990 LULC image/map. Aerial

photography that was downloaded from the United States Geological Survey (USGS) Earth Explorer (EE) website had to be spatially referenced.

Table II-3. Data used in the image classification and accuracy assessment

Name/Parameter	Description	Format	Spatial Resolution	Source
LTM Image for 17-Mar-1990	6 spectral bands	Raster	30 m	USGS EE
LTM Image for 25-Mar-2010	6 spectral bands	Raster	30 m	USGS EE
Aerial Photography for 1989	panchromatic and color infrared	Raster	1 and 3 m	USGS EE
Aerial Photography for 2010	color infrared	Raster	1 m	TNRIS
Google Earth Imagery	panchromatic and true color	Raster	various	Google Earth
Land Cover for 1992	aggregated to 7 classes	Raster	30 m	NLCD
Land Cover for 1996	aggregated to 7 classes	Raster	30 m	CCAP
Land Cover for 2006	aggregated to 7 classes	Raster	30 m	CCAP

Table II-4. Spectral bands for Landsat Thematic Mapper at 30 meter resolution.

Band Number	Spectral Range (μm)	Common Name
1	0.45-0.52	Blue
2	0.52-0.60	Green
3	0.63-0.69	Red
4	0.76-0.90	NIR
5	1.55-1.75	MIR1
7	2.08-2.35	MIR2

Aerial photography for 2010 from the Texas Natural Resources Information System (TNRIS) and CCAP LULC imagery for 2006 were used as reference images in

the designation of training areas for the classification algorithm and in the accuracy assessment for the 2010 LULC image generated in the classification procedure.

2.3.3 LULC Classification

The 1990 and 2010 LTM images were each classified independently to a modified Anderson Level I (Anderson et al. 1976) type of LULC classification. For a detailed description of the LULC characteristics for each class, the reader is referred to Anderson et al. (1976). Table II-5 lists the seven LULC classes used in this analysis and the differences in the naming of classes with the Anderson et al. (1976) scheme. Furthermore, the Anderson Level I scheme uses nine classes, but two of these classes are not found within the MACR because they are generally found at higher latitudes and highland environments. Excluding the classes that aren't found in the MACR, the most apparent difference between the LULC classes used here and the Anderson et al. (1976) scheme, are in how the pasture and forest/woodland classes are treated. Anderson et al. (1976) places pasture in the agriculture class, while this analysis groups pasture as part of the rangeland class. This is because the LULC data generated in this analysis will be used as an input to a hydrological model and hydrological properties of pasture are more similar to rangeland than cultivated crops. The Anderson Level I scheme also utilizes a forested land class, in this analysis a class of woodland was utilized because the MACR has a mix of trees and other woody vegetation. Separating large trees from other woody vegetation would require much more time and effort, given the 30 meter resolution of LTM imagery, and it was decided to aggregate these two similar classes into a woodland class.

Table II-5. Comparison between land use/land cover classes used in this analysis and Anderson Level I LULC classes.

LULC Classes	Anderson Level I Classes
1. Developed Land	1. Urban or Built-up Land
2. Cultivated Land	2. Agricultural Land
3. Rangeland	3. Rangeland
4. Woodland	4. Forest Land
5. Water	5. Water
6. Wetland	6. Wetland
7. Barren Land	7. Barren Land

All image classification procedures were conducted in ENVI 4.8 (ITT Visual Information Solutions 2009b). A portion of the full LTM images were classified. To minimize processing times, only the area of interest was included in the image processing.

Before the LTM images were classified, an atmospheric correction was conducted using the Fast Line-of-sight Atmospheric Analysis of Spectral Hypercubes (FLAASH) modeling tool in the Atmospheric Correction Module of ENVI. FLAASH is a first-principles atmospheric correction tool that corrects wavelengths in the visible through shortwave infrared regions by incorporating the MODTRAN4 (fourth version of MODTRAN) radiation transfer code (ITT Visual Information Solutions 2009a). The MODTRAN code allows for standard model atmospheres and aerosol types, along with parameter specifications unique to the scene and image, to be incorporated in the code and used in the correction procedure for each respective image. Before LTM images were used as inputs for FLAASH, they were radiometrically calibrated, scaled to the

appropriate units, and converted to band-interleaved-by-line (BIL) format using standard tools in ENVI. By specifying the sensor type, FLAASH automatically incorporates some of the necessary parameters, but other parameters needed to be specified that were dependent on the image and scene (Table II-6). The U.S. Standard atmospheric and maritime aerosol models were chosen because the images were acquired in early spring (other atmospheric models were specific to only the summer or winter) and the proximity of the MACR to the Gulf of Mexico.

Table II-6. Parameter specification for FLAASH processing.

Parameter	1990 Image	2010 Image
Atmospheric Model	U.S. Standard	U.S. Standard
Aerosol Model	Maritime	Maritime
Latitude for Scene Center	27.4340	27.4340
Longitude for Scene Center	-97.0670	-97.0670
Average Ground Elevation for Scene (km)	0.0170	0.0170
Initial Visibility (km)	40	40
Flight Date	18-Mar-90	25-Mar-10
Flight Time in GMT	16.3008	16.8089

Landsat images were classified using the Maximum Likelihood (ML) classification procedure in the ENVI Classification Module. Seven LULC classes (developed land, cultivated land, rangeland, woodland, open water, wetland, and barren land) were used in the image classification. The ML procedure requires that training areas for each class be specified within the respective image that is being classified. Reference maps/images (NLCD, CCAP, aerial photography, Google Earth), along with

computed normalized difference vegetation indices (NDVIs) and normalized difference water indices (NDWIs) were used to guide the selection of training areas. The generation of the LULC images for 1990 and 2010 was conducted in a trial-and-error fashion with a continual updating and editing of the training areas until the LULC images were considered suitable. Each class had a unique number of training pixels used for each image and class (Table II-7).

.

Table II-7. Count of pixels used as training areas for each land use/land cover (LULC) class for the image classification using the Maximum Likelihood classification procedure.

LULC Class	Number of Training Pixels	
	1990 Image	2010 Image
Developed Land	4,495	2,099
Cultivated Land	30,136	115,240
Rangeland	3,908	3,968
Woodland	1,491	663
Open Water	242,071	149,832
Wetland	4,343	2,477
Barren Land	1,171	2,182

A 3-by-3 majority filter was applied to the final output from the ML classification in order to eliminate extraneous pixels within the images. As a final step, pixels were manually edited using the Spatial Pixel Editor in ENVI to change areas that were obviously misclassified. Built-up areas, irregular cultivated lands (e.g. continuously flooded agriculture, areas where overland flows accumulate, fallow land), and areas influenced by changes in surface water elevations (tidal and riverine) were generally the locations that needed the most manual editing.

2.3.4 Accuracy Assessment of LULC Images

The accuracy of the LULC images for 1990 and 2010 was assessed using reference images from the same year or from a year as close as possible to 1990 or 2010 (Table II-3). Reference images were overlayed with the LULC images and compared/interpreted visually. The accuracy assessment and any associated image processing was conducted in ArcGIS 9.3.1 (ESRI 2009) and Google Earth (Google Inc 2011).

Aerial photographs for 1989 (collected as part of the National Aeronautics and Space Administration (NASA)'s National Aerial Photography Program (NAPP)), 1992 NLCD imagery, Google Earth imagery, 1996 CCAP imagery, 2006 CCAP imagery, and color-infrared aerial photographs for 2010 were used in the overlay comparison with the generated 1990 and 2010 LULC images. Pre-processing was required for some the reference imagery before they could be used in the accuracy assessment: the aerial photography for 1989 had to be spatially referenced; 1992 NLCD imagery was aggregated to seven LULC classes similar to those used in this analysis (Table II-8); and CCAP imagery was also aggregated to seven LULC classes (Table II-9).

Congalton and Green (2009) recommend a minimum sample size of 50 sites/points per class when conducting an accuracy assessment of classified imagery. A stratified random sample with 50 sample sites per LULC class (total of 350 sites per image) was generated in ENVI. The sample points were converted to ESRI shapefiles and Google Keyhole Markup Language (KML) files in order to conduct the accuracy assessment in ArcGIS and Google Earth. In determining how the predicted LULC class

compared to the actual LULC on the ground, a hierarchical approach was used in the comparison with the reference images. For the 1990 LULC image, it was first compared to the NAPP aerial photography for 1989; if the actual LULC could not be determined then it was compared to the aggregated 1992 NLCD image. As the NLCD imagery was generated for a more regional/national exercise, it would often neglect small patches of one type of LULC within another (e.g. development within large cultivated areas). To assess the LULC further it was also compared to aerial photography compiled in Google Earth for 1995 (1990 in some areas) and 1996 CCAP imagery. A similar approach was used for the 2010 LULC image; the 2010 LULC image was first compared to county composite color-infrared aerial photography for 2010; and compared to Google Earth and 2006 CCAP imagery when the exact LULC on the ground was difficult to determine using the aerial photography.

In order to quantitatively determine the accuracy of the 1990 and 2010 LULC imagery, error/confusion matrices were computed. Using the error matrices, three types of accuracy were computed (producer's, user's, and overall) along with a standard Kappa index, as recommended by Congalton and Green (2009). Producer's accuracy is the ratio between the value in the major diagonal for a specific class and the total for the column in the error matrix. Similarly, the user's accuracy is ratio between the value in the major diagonal and the total for the row in the error matrix. Overall accuracy is the ratio between the sum of the major diagonal and the sum of the error matrix. For producer's and user's accuracy, a value greater than or equal to 80% is considered suitable and values lower than 80% were analyzed on a case-by-case basis to conclude if

they were considered acceptable. Anderson et al. (1976) recommend a target overall accuracy of 85% for studies that classify Landsat imagery. The standard Kappa index is commonly used in accuracy assessment to quantitatively determine if an error matrix is different from another matrix (Congalton and Green 2009). An estimate of Kappa (KHAT), which is a measure of agreement between the classified image and the reference data as indicated by the major diagonal (Congalton and Green 2009), and its variance can be used to test if an image classification is significantly better than a randomly generated image using a standard normal Z-test.

Table II-8. Aggregated National Land Cover Data land use/land cover (LULC) classes.

Aggregated LULC Class	Original NLCD LULC Class
1. Developed Land	21. Low Intensity Residential
	22. High Intensity Residential
	23. Commercial/Industrial/Transportation
	85. Urban/Recreational Grasses
2. Cultivated Land	82. Row Crops
	83. Small Grains
3. Rangeland	51. Shrubland
	71. Grassland/Herbaceous
	81. Pasture/Hay
4. Forest Land/Woodland	41. Deciduous Forest
	42. Evergreen Forest
	43. Mixed Forest
5. Water	11. Open Water
6. Wetland	91. Woody Wetlands
	92. Emergent Herbaceous Wetlands
7. Barren Land	31. Bare Rock/Sand/Clay
	32. Quarries/Strip Mines/Gravel Pits

Table II-9. Aggregated Coastal Change Analysis Program land use/land cover (LULC) classes.

Aggregated LULC Class	Original CCAP LULC Class
1. Developed Land	2. Developed, High Intensity
	3. Developed, Medium Intensity
	4. Developed, Low Intensity
	5. Developed, Open Space
2. Cultivated Land	6. Cultivated Crops
3. Rangeland	7. Pasture/Hay
	8. Grassland/Herbaceous
	12. Scrub/Shrub
4. Forest Land/Woodland	9. Deciduous Forest
	10. Evergreen Forest
	11. Mixed Forest
5. Water	21. Open Water
	22. Palustrine Aquatic Bed
	23. Estuarine Aquatic Bed
6. Wetland	13. Palustrine Forest Wetland
	14. Palustrine Scrub/Shrub Wetland
	15. Palustrine Emergent Wetland (Persistent)
	16. Estuarine Forested Wetland
	17. Estuarine Scrub/Shrub Wetland
	18. Estuarine Emergent Wetland
7. Barren Land	19. Unconsolidated Shore
	20. Barren Land

The reporting of Kappa indices has become a standard within the literature, when accuracy assessments are conducted on classified imagery. Pontius and Millones (2011) have reported several issues regarding the use of Kappa indices and they recommend using a method that quantifies quantity and allocation disagreement. Quantity disagreement is the amount of difference between the reference imagery and the classified image in the proportions of the LULC classes, while allocation disagreement is

the amount of difference between the reference imagery and the classified image due to a less than optimal match in the spatial allocation of the LULC classes (Pontius and Millones 2011). These two types of disagreement between reference and classified imagery are computed using samples of pixels from the total number of pixels (population) to estimate the disagreement for the entire image (or population).

2.3.5 LULC Change

The LULC change from 1990 to 2010 was characterized collectively for the MACR and LARB, and on a pixel-by-pixel basis. Change/transition matrices were computed using the Tabulate Area function in the Spatial Analyst extension for ArcGIS. Using the change matrix, the percent difference (PD) from 1990 to 2010 for each LULC class was computed. PD is represented by Equation II-1:

$$PD = \left(\frac{A_{2010} - A_{1990}}{A_{1990}}\right) * 100\% \qquad \text{II-1}$$

where A_{2010} is the areal coverage for a respective LULC class in 2010 and A_{1990} is the areal coverage for the same LULC class in 1990.

The Raster Calculator, of the Spatial Analyst extension in ArcGIS, was employed in order to generate Boolean change maps that depicted areas that experienced some form of LULC change within the MACR and LARB. To gain insight on the spatial distribution of the types of LULC change that occurred, change maps of LULC were generated that identify the type of change that occurred. The LULC change maps were constructed by first reclassifying the LULC codes for each image (Table II-10). Using

the Minus tool in the Math Toolbox of Spatial Analyst, the reclassified 2010 LULC code was subtracted from the 1990 LULC code for every pixel in the MACR and LARB. Table II-11 depicts all possible outcomes of LULC change for the Minus tool operation and how they are classified in terms of LULC change from 1990 to 2010.

Table II-10. Reclassification of land use/land cover (LULC) codes for change map.

LULC Classes	Original LULC Code	Reclassified LULC Code
Developed Land	1	1
Cultivated Land	2	10
Rangeland	3	100
Woodland	4	1000
Water	5	10000
Wetland	6	100000
Barren Land	7	1000000

Table II-11. Possible land use/land cover (LULC) change outcomes using by subtracting 2010 LULC codes from 1990 LULC codes.

LULC Classes	LULC Change Code	LULC Classes	LULC Change Code
Developed to Cultivated	-9	Woodland to Water	-9000
Developed to Rangeland	-99	Woodland to Wetland	-99000
Developed to Woodland	-999	Woodland to Barren	-999000
Developed to Water	-9999	Water to Developed	9999
Developed to Wetland	-99999	Water to Cultivated	9990
Developed to Barren	-999999	Water to Rangeland	9900
Cultivated to Developed	9	Water to Woodland	9000
Cultivated to Rangeland	-90	Water to Wetland	-90000
Cultivated to Woodland	-990	Water to Barren	-990000
Cultivated to Water	-9990	Wetland to Developed	99999
Cultivated to Wetland	-99990	Wetland to Cultivated	99990
Cultivated to Barren	-999990	Wetland to Rangeland	99900
Rangeland to Developed	99	Wetland to Woodland	99000
Rangeland to Cultivated	90	Wetland to Water	90000
Rangeland to Woodland	-900	Wetland to Barren	-900000
Rangeland to Water	-9900	Barren to Developed	999999
Rangeland to Wetland	-99900	Barren to Cultivated	999990
Rangeland to Barren	-999900	Barren to Rangeland	999900
Woodland to Developed	999	Barren to Woodland	999000
Woodland to Cultivated	990	Barren to Water	990000
Woodland to Rangeland	900	Barren to Wetland	900000

2.4 Results and Discussion

2.4.1 Accuracy Assessment of LULC

A sample of 50 sites/pixels per LULC class (350 total sites per image) was used to construct an error matrix for each LULC image generated in the classification procedure. Tables II-12 and II-13 are the error matrices from the accuracy assessment of the LULC classification for 1990 and 2010, respectively. For 1990, it is no surprise that

open water and cultivated land were the LULC classes with the most agreement between the classified and reference imagery and this is largely because these classes were the easiest to identify in the LTM image and consequently had significantly higher training pixels assigned to them. Woodland and wetland were the LULC classes that had the least amount of agreement between the classified and reference imagery and this is because the coarse resolution of LTM imagery (30 m) made it difficult to separate these classes from each other and other similar classes (e.g. woodland can be similar to rangeland, wetland can be similar to shallow water or vegetated areas with high soil moisture). For 2010, results are similar to 1990 with open water and cultivated land being the classes with the most agreement between classified and reference imagery for much of the same reasons. Again, woodland is the class with the least amount of agreement as rangeland was commonly misclassified as woodland, but this is to be expected as the classes have fairly similar vegetation and some areas are complex mosaics of the two classes. Furthermore, barren land had the second lowest amount of agreement because open water and wetlands were commonly misclassified as barren land, but as barren land is commonly found at the interface of land and water (beaches and exposed soil near water bodies), the disagreement could be influenced by variations in water elevations (e.g. tidal and river flow fluctuations).

Table II-12. Error matrix for 1990 classified land use/land cover (LULC) image using 350 sample points.

		Reference Imagery							
		Developed	**Cultivated**	**Rangeland**	**Woodland**	**Water**	**Wetland**	**Barren**	**Row Total**
Classified Imagery	**Developed**	44	1	1	0	0	1	3	50
	Cultivated	0	50	0	0	0	0	0	50
	Rangeland	2	2	45	1	0	0	0	50
	Woodland	2	1	4	38	0	5	0	50
	Water	0	0	0	0	50	0	0	50
	Wetland	0	2	0	6	2	40	0	50
	Barren	1	1	3	0	2	2	41	50
	Column Total	49	57	53	45	54	48	44	350

Table II-13. Error matrix for 2010 classified land use/land cover (LULC) image using 350 sample points.

		Reference Imagery							
		Developed	**Cultivated**	**Rangeland**	**Woodland**	**Water**	**Wetland**	**Barren**	**Row Total**
Classified Imagery	**Developed**	43	1	4	0	1	0	1	50
	Cultivated	0	49	1	0	0	0	0	50
	Rangeland	1	4	43	2	0	0	0	50
	Woodland	0	0	18	32	0	0	0	50
	Water	0	0	0	0	50	0	0	50
	Wetland	1	0	0	5	3	41	0	50
	Barren	3	1	0	0	4	5	37	50
	Column Total	48	55	66	39	58	46	38	350

The error matrices were used to compute statistics that would give a measure of the degree of accuracy for each LULC image. Table II-14 provides the producer's and user's accuracy for each LULC class for 1990 and 2010. For 1990, open water and barren land are the only classes with a producer's accuracy greater than or equal to 90%, which is the result of having a low number of errors of omission. In this respect, the other five classes have a producer's accuracy between 80 and 90%. Nonetheless, the producer's accuracy for every class in 1990 can be considered suitable for the scope of this analysis. As for the user's accuracy, three classes (cultivated land, rangeland, and open water) have values of greater than or equal to 90%, which is the result of a low number of errors of commission and the accuracy is considered well-suited for this analysis. Three out of four of the other classes have a user's accuracy greater than or equal to 80% and less than 90%, which again is considered suitable for this analysis. Woodland has a user's accuracy of 76% that is lower than any other measure of accuracy for the 1990 LULC image, but the user's accuracy is considered acceptable as errors of commission were mostly associated with rangeland and wetland and these classes can be fairly similar to woodland.

For the 2010 LULC image, the producer's and user's accuracy was generally lower than values for 1990 (Table II-14). Barren land is the only class that had a producer's accuracy greater than or equal to 90%. Five of the other six classes (developed land, cultivated land, woodland, open water, wetland, and barren land) have a producer's accuracy greater than or equal to 80% and less than 90% and are considered suitable. Rangeland has a producer's accuracy of 65% due to 18 errors of omission

associated with woodland, but due to the similarities in these classes, the producer's accuracy for rangeland is considered acceptable. As for the user's accuracy, five out of the seven classes (developed land, cultivated land, rangeland, open water, and wetland) fall within the suitable range because they have a user's accuracy greater than 80%. Woodland has a user's accuracy of 64%, but this is due to errors of commission associated with rangeland and woodland and it was considered acceptable. Barren land has a user's accuracy of 74% mostly due to errors of commission associated with water and wetland classes, but as barren land is commonly found at the interface of land and water, the user's accuracy for barren land is considered acceptable.

Table II-14. Producer's and user's accuracy for the 1990 and 2010 land use/land cover (LULC) imagery.

Class	1990		2010	
	Producer's Accuracy	User's Accuracy	Producer's Accuracy	User's Accuracy
Developed	89.8%	88.0%	89.6%	86.0%
Cultivated	87.7%	100.0%	89.1%	98.0%
Rangeland	84.9%	90.0%	65.2%	86.0%
Woodland	84.4%	76.0%	82.1%	64.0%
Water	92.6%	100.0%	86.2%	100.0%
Wetland	83.3%	80.0%	89.1%	82.0%
Barren	93.2%	82.0%	97.4%	74.0%

The error matrices were also used to estimate the overall accuracy and parameters for the standard Kappa analysis. Table II-15 lists the overall accuracy, estimate of the Kappa statistic (KHAT), the variance of KHAT, and the standard normal

Z-statistic of the Kappa analysis for the 1990 and 2010 LULC images. The 1990 image has an overall accuracy of 88.0% that is greater than the target accuracy of 85.0% specified by Anderson et al. (1976), while the 2010 image has an overall accuracy of 84.3% and it is considered acceptable as the overall accuracy is nearly 85%. The standard Kappa analysis involved computing an estimate of Kappa (KHAT), the variance of KHAT, and the standard normal Z-statistic for KHAT. A KHAT value greater than 0.80 is considered strong agreement between classified and reference imagery (Congalton and Green 2009), and both the 1990 and 2010 LULC images have KHAT values greater than 0.80. With the Z-statistic, it can be determined if the classified image is significantly better than one generated at random (Congalton and Green 2009). As the Z-statistics for the 1990 and 2010 image are 42.5 and 36.1, respectively; it can be concluded that that the classified images are better than images generated at random even at a 99% confidence-level (Z-statistic = 2.58).

Table II-15. Overall accuracy and estimates of Kappa parameters (variance and standard normal Z-statistic) for 1990 and 2010 land use/land cover (LULC) images.

Image	Overall Accuracy	KHAT	Var(KHAT)	Z(KHAT)
1990 LULC	88.0%	0.86	0.00041	42.5
2010 LULC	84.3%	0.82	0.00051	36.1

To further verify the accuracy of the 1990 and 2010 LULC images, a technique reported by Pontius and Millones (2011) where quantity and allocation disagreement in the sample is used to estimate the overall agreement and quantity and allocation

disagreement for the entire image (or population). Table II-16 lists the overall agreement, quantity and allocation disagreement for the sample and population of pixels for each image. As before, the disagreement between the classified and reference imagery is greater for the 2010 LULC image. The overall agreement for the 1990 and 2010 classifications is 93% and 89%, respectively, which is considered suitable for this analysis. Both types of disagreement are less than 10% for the 1990 and 2010 images, which is also considered suitable.

Table II-16. Quantity and allocation disagreement statistics for 1990 and 2010 land use/land cover (LULC) images.

Image	Sample			Population		
	Overall Agreement (%)	Quantity Disagreement (%)	Allocation Disagreement (%)	Overall Agreement (%)	Quantity Disagreement (%)	Allocation Disagreement (%)
1990 LULC	88	4	8	93	3	4
2010 LULC	84	8	7	89	4	7

The classification of the 1990 image was generally more accurate than that of the 2010 image. Similarities between the LULC classes were noted when evaluating classes that had a lower level of accuracy than originally targeted. Another factor that could have influenced the accuracy of the classifications is precipitation events prior to the LTM image acquisition. Rainfall events occurred the day before and on the day of image acquisition for the 2010 LTM image (Figure II-3). It is a modest amount of rainfall just before the image was acquired in 2010, but any amount of rainfall can influence soil

moisture and puddling of water on the surface that can influence image classification. Furthermore, some of the errors (e.g. woodland classified as wetland) in the 1990 image could have been influenced by the two larger rain events that occurred weeks before the image was acquired.

Overall, the classification of the 1990 and 2010 images to seven LULC classes (Table II-5) is considered suitable for the scope of this analysis.

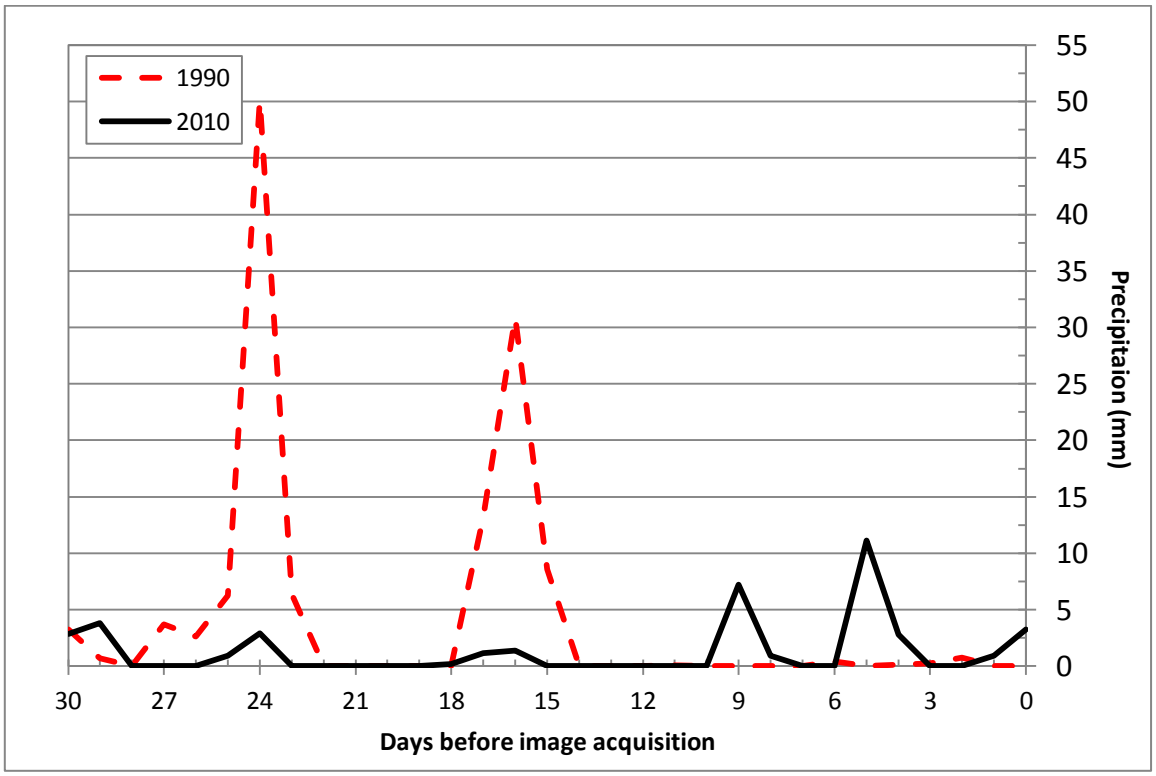

Figure II-3. Average precipitation per day from 4 weather stations (USC00417170, USC00417704, USC00418354, and USC00419559) in the Mission-Aransas Coastal Region (MACR) 30 days before each Landsat Thematic Mapper image was acquired. Note: precipitation data is from the GHCND database of the National Climatic Data Center.

2.4.2 LULC Classification

2.4.2.1 Mission-Aransas Coastal Region (MACR)

Maps of LULC were constructed by classifying the 1990 and 2010 LULC imagery using the ML classification procedure (Figures II-4 and II-5). For both LULC maps, developed land is mostly situated along the coast or near cultivated areas. Cultivated land dominates the south-central portions of the MACR, with another large patch west of Mission and Copano Bays. Rangeland occupies much of the northern and southwestern portions, along with small patches littered throughout the MACR. Woodland is mostly found near coastal and riverine environments, and within areas with large amounts of scattered development. Open water dominates the far-eastern and southeastern portions of the MACR, as these areas are where the bays and estuaries are found. Wetlands are generally found along the coast separating open water from the mainland and within riparian environments. Most of the barren land within the MACR is found at the boundary between open water and land that is composed of beach environments, in areas near meanders of streams/rivers, and in industrial/mining facilities.

In 1990, the dominant LULC classes are cultivated land and rangeland as they occupy 36.9% and 28.9% of the MACR, respectively (Table II-17). Barren and developed lands contribute the least to the total MACR area they represent 1.3% and 3.5% of the total area, respectively. For 2010, cultivated land and rangeland remain the dominant classes within the MACR, but the proportions that they represent declined to 34.3% and 27.7%, respectively. Similarly, barren and developed lands remained the

classes that encompass the smallest proportion of the MACR, but the proportions increased to 1.7% and 5.1%, respectively.

The most noticeable differences between the 1990 and 2010 LULC maps (Figures II-4 and II-5) are significant expansions of woodland and developed land in the 2010 image. These expansions have generally been at the expense of rangeland and cultivated land.

Table II-17. Aerial coverage and percentage of total area that each land use/land cover (LULC) encompasses for the Mission-Aransas Coastal Region (MACR) and Lower Aransas River Basin (LARB) in 1990 and 2010.

LULC Class	1990				2010			
	MACR		LARB		MACR		LARB	
	Area (km^2)	% of Total Area	Area (km^2)	% of Total Area	Area (km^2)	% of Total Area	Area (km^2)	% of Total Area
Developed Land	131.7	3.5%	28.1	2.0%	190.8	5.1%	35.0	2.5%
Cultivated Land	1382.1	36.9%	830.5	59.1%	1282.8	34.3%	798.7	56.8%
Rangeland	1081.9	28.9%	416.1	29.6%	1037.0	27.7%	366.4	26.1%
Woodland	361.5	9.7%	80.1	5.7%	396.0	10.6%	141.0	10.0%
Open Water	451.6	12.1%	4.9	0.4%	458.3	12.2%	4.6	0.3%
Wetland	288.3	7.7%	40.3	2.9%	316.1	8.4%	54.9	3.9%
Barren Land	47.8	1.3%	5.7	0.4%	63.9	1.7%	5.1	0.4%
Total	**3744.9**	**100.0%**	**1405.8**	**100.0%**	**3744.9**	**100.0%**	**1405.8**	**100.0%**

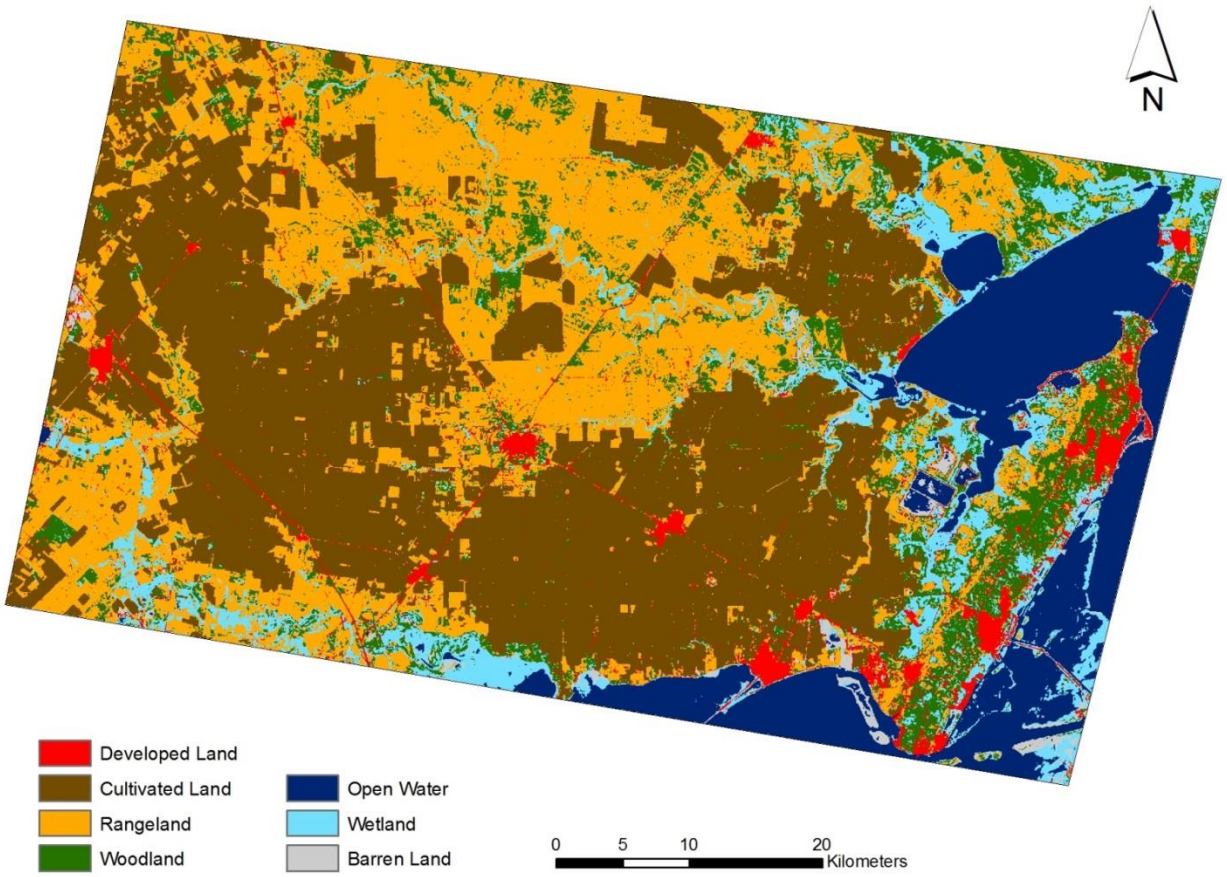

Figure II-4. Map of land use/land cover (LULC) for Mission-Aransas Coastal Region (MACR) for 1990.

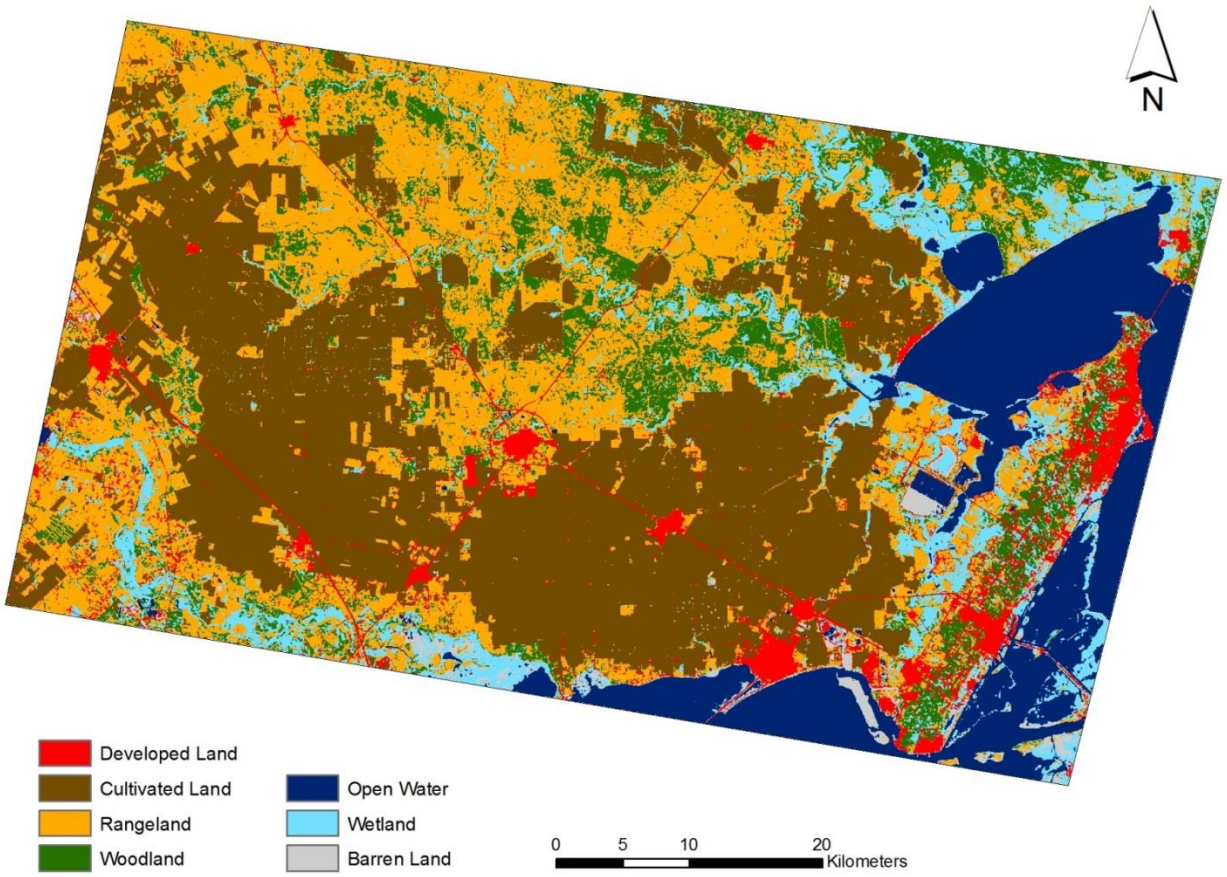

Figure II-5. Map of land use/land cover (LULC) for Mission-Aransas Coastal Region (MACR) for 2010.

2.4.2.1 Lower Aransas River Basin (LARB)

As work in other chapters of this thesis will be focusing on the LARB, maps of LULC for 1990 and 2010 within the LARB were constructed as well (Figures II-6 and II-7). In 1990 and 2010, developed land is mostly represented by the cities of Sinton and Taft in the south-central and southeastern portions of the LARB (Figure II-2). Cultivated land dominates much of the southern, western, and eastern portions. Rangeland is mostly found in the northern and central parts of the LARB. Woodland is found in areas near riverine and semi-coastal water bodies and in patches around Sinton. Wetland is found along streams/rivers within the basin and near the outlet. Open water and barren land have minimal coverage with the largest patches found at in the vicinity of rivers and near the basin outlet.

Similar to the MACR, cultivated land and rangeland are the dominant LULC classes within the LARB as they represent 59.1% and 29.6% of the total area in 1990 (Table II-17), respectively. Barren land (0.4%) and developed land (2.0%) are the two classes in 1990 that occupy the lowest proportion of area within the LARB. For 2010, cultivated land and rangeland remain the dominant classes in the LARB, but the proportions that they represent declined to 56.8% and 26.1%, respectively. Additionally, barren and developed lands remained the classes that encompass the smallest proportion of the MACR, but the proportion encompassed by developed land increased to 2.5% with barren land remaining at 0.4%.

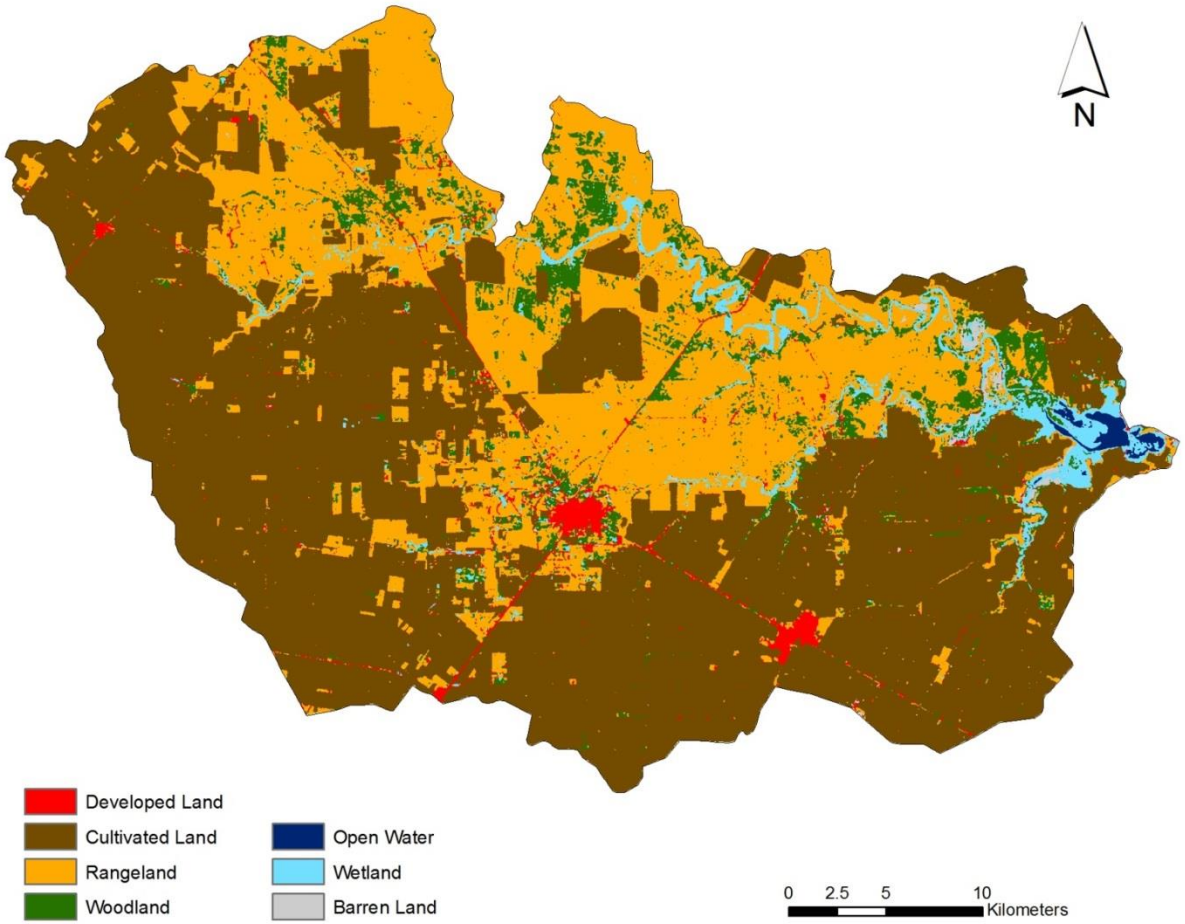

Figure II-6. Map of land use/land cover (LULC) for 1990 within the Lower Aransas River Basin (LARB).

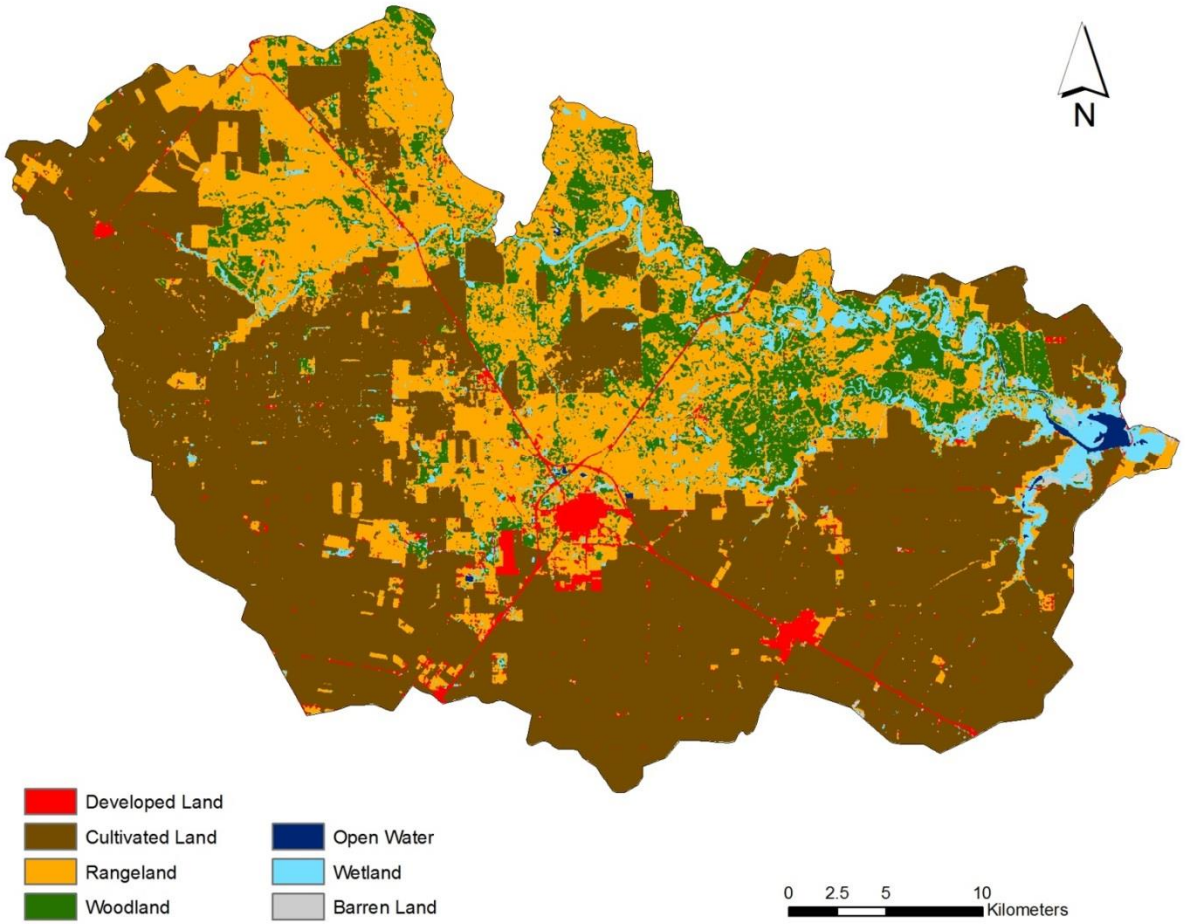

Figure II-7. Map of land use/land cover (LULC) for 2010 within the Lower Aransas River Basin (LARB).

The most recognizable differences between the 1990 and 2010 LULC maps is an expansion of woodland in areas near the Aransas River and an expansion developed land around Sinton and Taft.

2.4.3 LULC Change

2.4.3.1 Mission-Aransas Coastal Region (MACR)

The LULC maps for 1990 and 2010 were used to construct change matrices to understand the quantity and type of LULC change that occurred within the MACR. Table II-18 is a change matrix of LULC from 1990 to 2010 for the MACR. Developed land increased by 59.7 km^2 from 1990 to 2010 with most gains coming from rangeland (46.5 km^2) and woodland (33.5 km^2), although it is surprising to note that a fair amount of developed land was lost to rangeland (21.4 km^2). It is generally assumed that development does not transition back to vegetated land surface, but this disagreement could be due to abandonment and mapping error. Cultivated land decreased by 99.3 km^2 with most losses going to rangeland (127.8 km^2), but it is interesting to note that cultivated land gained some land from rangeland (42.5 km^2) for a net loss of 85.3 km^2 to rangeland. Rangeland decreased by 44.7 km^2 with the greatest loss going to woodland (195.7 km^2), but with a gain from woodland (112.1 km^2) that made for a net loss to woodland of 83.6 km^2. These large transitions between rangeland and woodland might be due to an overall greening of the MACR over the twenty year period and map error associated the difficulty in separating these similar LULC classes using imagery at 30 m resolution. Woodland increased by 34.5 km^2, but as noted above, there was a large amount of transition between woodland and rangeland. Open water increased by 6.7 km^2

with most of the net gains coming from wetland (6.6 km^2), which is appropriate as these LULC classes are generally found near each other. Wetland increased by 27.8 km^2 with most net gains coming from rangeland (21.3 km^2) and woodland (15.4 km^2), and a general net loss to other classes. Barren land increased by 16.1 km^2 with the largest net gain coming from wetland (9.9 km^2).

Table II-18. Change matrix of land use/land cover (LULC) change from 1990 to 2010 for the Mission-Aransas Coastal Region (MACR).

		2010 LULC (km^2)							
		Developed	**Cultivated**	**Rangeland**	**Woodland**	**Water**	**Wetland**	**Barren**	**Total**
1990 LULC (km^2)	**Developed**	82.6	6.2	21.4	9.1	0.7	6.9	4.7	131.7
	Cultivated	15.4	1218.1	127.8	5.9	0.5	10.9	3.5	1382.1
	Rangeland	46.5	42.5	734.0	195.7	1.2	57.2	4.7	1081.9
	Woodland	33.5	11.3	112.1	150.1	0.8	49.4	4.4	361.5
	Water	0.1	0.0	0.1	0.0	437.8	5.8	7.8	451.6
	Wetland	7.2	3.0	35.9	34.0	12.4	177.4	18.3	288.3
	Barren	5.4	1.7	5.7	1.2	4.8	8.4	20.5	47.8
	Total	190.8	1282.8	1037.0	396.0	458.3	316.1	63.9	3744.9

Various forms of change are occurring throughout the MACR with some classes responsible for most of the change occurring (rangeland, woodland, cultivated land) and some that contribute little in relative terms to the total amount of change (open water and barren land). This analysis is not only interested in the amount of LULC change that occurred, but also on the spatial distribution of change throughout the MACR. Figure II-8 is a Boolean change map of the MACR that identifies locations where a LULC class in 1990 changed to another class in 2010. Within the entire MACR, 24.7% of the pixels

experienced LULC change, which includes the open water class that experiences change on a limited basis. Excluding changes and non-changes that involve the open water class, 27.1% of the total land surface experienced some form of LULC change. Areas that experienced change are littered throughout the MACR, but clusters of areas with the most change are near water bodies (streams/rivers, estuaries, and bays) and urban centers. Clusters of areas that did not experience change are found in the eastern-southeastern portions (bays and estuaries) and the south-central potions (cultivated areas) as these areas are not expected to change much over a 20-year period.

To better understand the patterns of change occurring within the MACR, maps that depict the LULC class in 1990 before it changed (Figure II-9a) and the class to which the pixel changed to 2010 (Figure II-9b) were developed. In terms of patterns of LULC change, there are numerous clusters of rangeland that change to woodland in the north-central portions of the MACR. Cultivated land that changed to rangeland is scattered around the edges of the large patch of cultivated land in the south-central portions. Areas that changed to developed land are mostly found along the coast and outside urban areas such as Sinton and Portland. Clusters of areas that didn't experience change are those associated with large patches of cultivated land and water bodies.

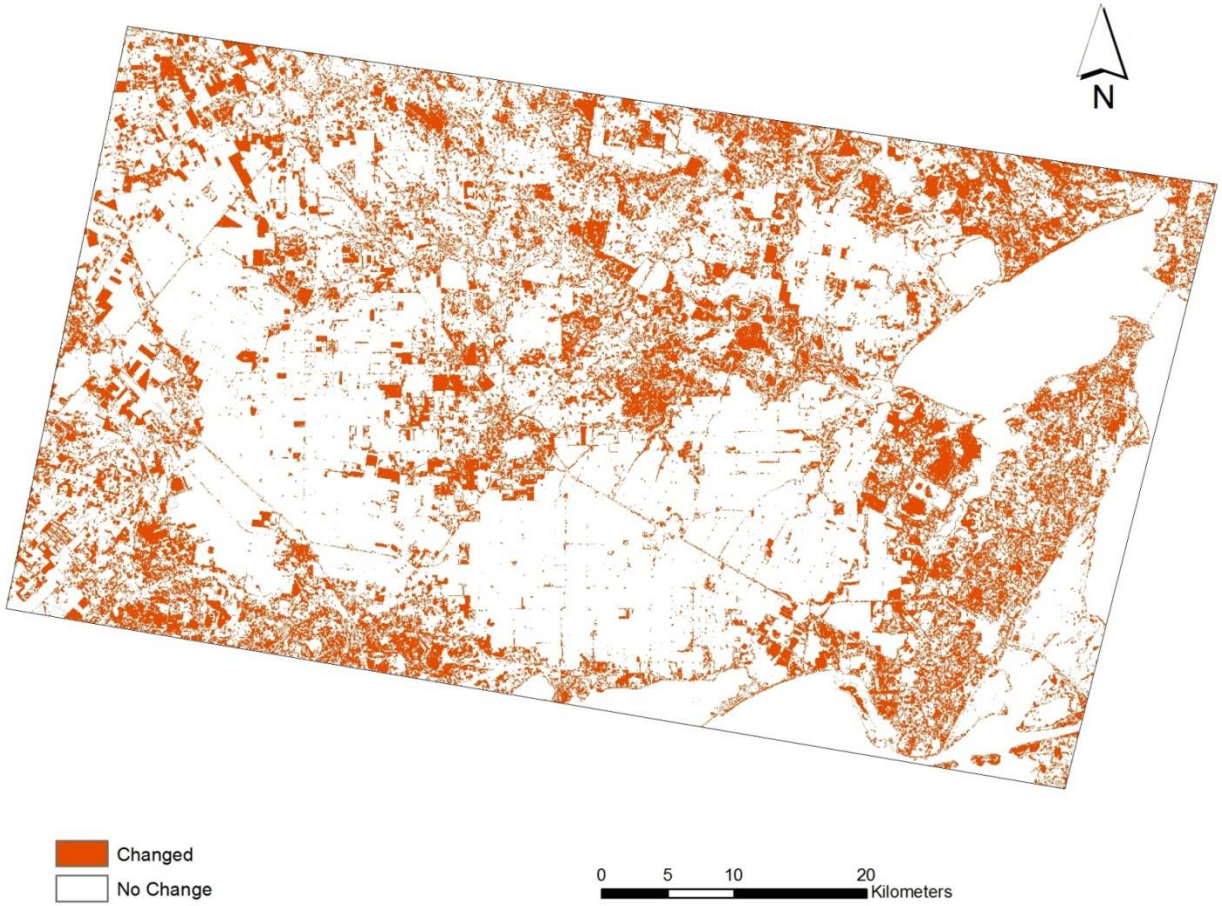

Figure II-8. Map of land use/land cover (LULC) change from 1990 to 2010 within the Mission-Aransas Coastal Region (MACR).

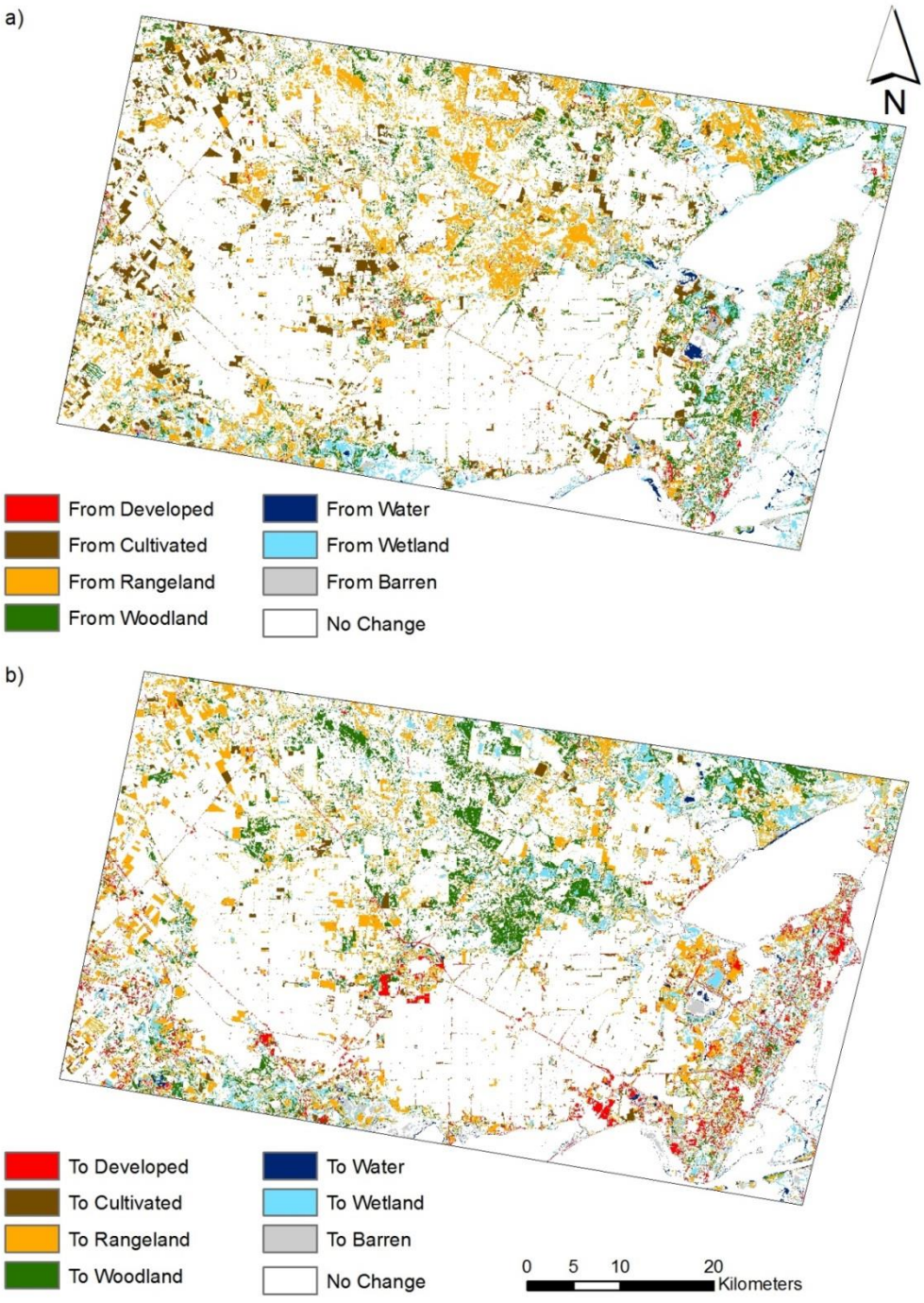

Figure II-9. Land use/land cover (LULC) changes from 1990 to 2010 within the Mission-Aransas Coastal Region (MACR). a) LULC classes in 1990 that experienced change. b) LULC classes that previous classes changed to in 2010.

A variety of LULC change has occurred within the MACR, but many of these types of change contribute little in terms of the total amount of area they encompass. Figure II-10 is a map of the LULC changes that represent the greatest amount of coverage within the MACR. Six out of the seven dominant types of LULC change involve rangeland and they are mostly situated in the northern half of the MACR in areas with the least amount of human disturbance.

The MACR experienced a relatively large amount of LULC change from 1990 to 2010. Rangeland is the LULC class that has been involved with the greatest proportion of change during this 20-year period. This makes intuitive sense because rangeland is the class with the second greatest amount of coverage within the MACR. Furthermore, the similarities between rangeland and woodland make for some of the change to be attributed to potential error in the misclassification of areas that have a mixture of the two classes. Additionally, this analysis is particularly interested in the expansion of developed land. While developed land encompasses a relatively small proportion of the MACR area (3.5% and 5.1% for 1990 and 2010, respectively), developed land experienced a percent change of 44.9% (Table II-19), making it the class that experienced the greatest amount of change using the percent change metric. The MACR has no large urban centers and it has a relatively sparse population, nonetheless the amount of developed land has been increasing over time.

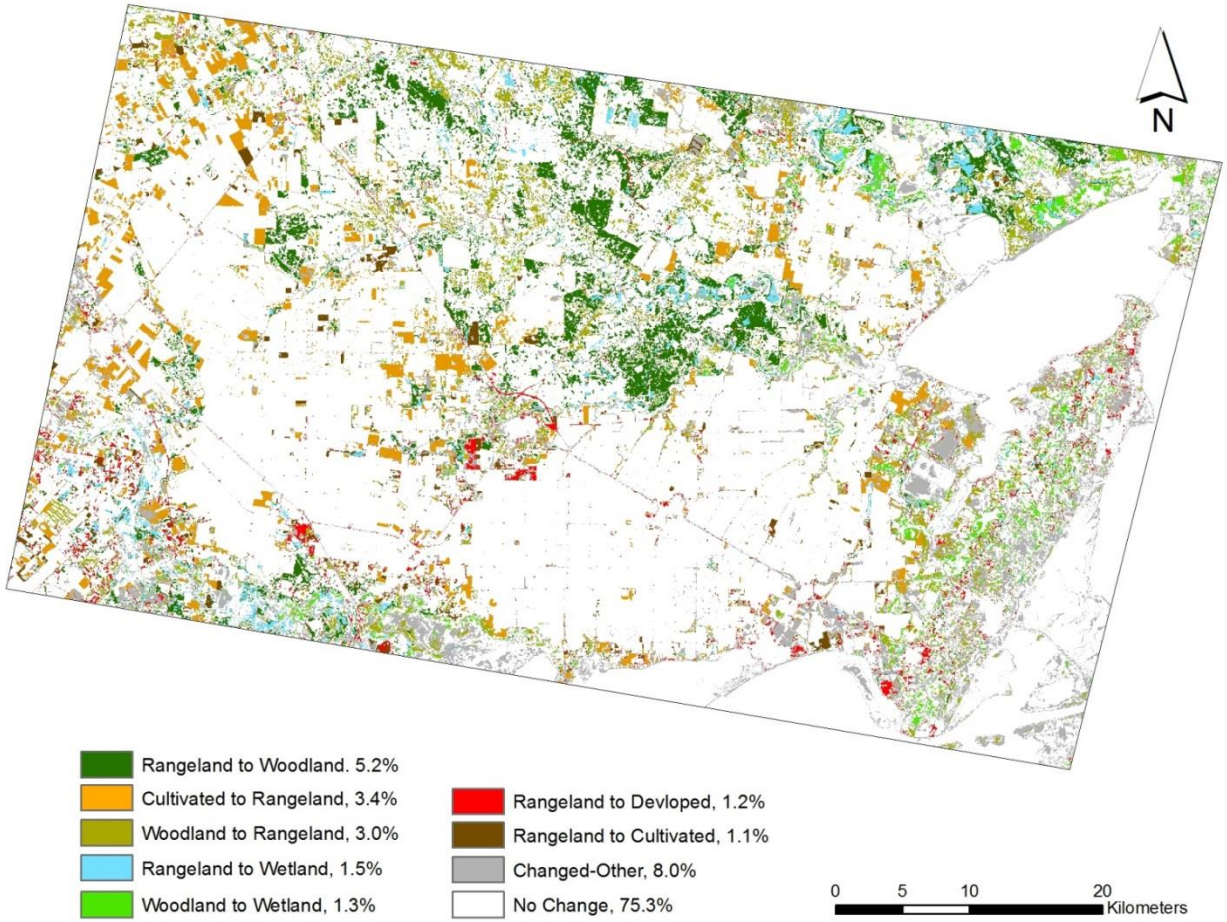

Figure II-10. Map of land use/land cover (LULC) classes that represent the highest percentage of total area (percentage listed on legend) within the Mission-Aransas Coastal Region (MACR).

Table II-19. Percent change for each land use/land cover (LULC) class from 1990 to 2010 for the Mission-Aransas Coastal Region (MACR) and the Lower Aransas River Basin (LARB).

LULC Class	Percent Change from 1990 to 2010	
	MACR	LARB
Developed Land	44.9%	24.6%
Cultivated Land	-7.2%	-3.8%
Rangeland	-4.1%	-11.9%
Woodland	9.5%	76.0%
Open Water	1.5%	-6.9%
Wetland	9.6%	36.2%
Barren Land	33.8%	-10.1%

2.4.3.2 Lower Aransas River Basin (LARB)

As the LARB is the focus for later chapters in this thesis, the LULC maps for 1990 and 2010 were used to construct change matrices to understand the quantity and type of LULC change that occurred within the LARB. Table II-20 is a change matrix of LULC change from 1990 to 2010 for the LARB. Developed land increased by 6.8 km^2 from 1990 to 2010 with most gains coming from rangeland (10.7 km^2) and cultivated land (5.5 km^2), although similarly to the MACR, a fair amount of developed land was lost to rangeland (6.9 km^2) and woodland (2.0 km^2). Cultivated land decreased by 31.9 km^2 with the majority of losses going to rangeland (45.7 km^2), but cultivated land also gained some land from rangeland (17.8 km^2) for a net loss of 27.9 km^2 to rangeland. Rangeland land decreased by 49.7 km^2 with the greatest loss going to woodland (91.8 km^2), but with a gain from woodland of 27.9 km^2 that made for a net loss to woodland of 63.9 km^2. As noted above, the large transitions between rangeland and woodland might be due to a greening of the region and errors in image classification. Woodland increased

by 60.9 km^2, but much of the transition is between woodland and rangeland. Open water encompasses a small proportion of the LARB area and decreased by a seemingly negligible amount (0.3 km^2). Wetland increased by 14.7 km^2 with the greatest net gain coming from rangeland (9.8 km^2). Similarly to open water, barren land represents a small proportion of the LARB area, but it experienced a net decrease of 0.5 km^2.

Table II-20. Change matrix of land use/land cover (LULC) change from 1990 to 2010 for the Lower Aransas River Basin (LARB).

		2010 LULC (km^2)							
		Developed	**Cultivated**	**Rangeland**	**Woodland**	**Water**	**Wetland**	**Barren**	**Total**
1990 LULC (km^2)	**Developed**	14.6	2.8	6.9	2.0	0.0	1.5	0.4	28.2
	Cultivated	5.5	772.8	45.7	2.7	0.1	3.0	0.8	830.6
	Rangeland	10.7	17.8	280.0	91.8	0.3	14.6	0.9	416.1
	Woodland	3.5	4.3	27.9	37.6	0.1	6.4	0.3	80.1
	Water	0.0	0.0	0.0	0.0	3.0	1.4	0.5	4.9
	Wetland	0.4	0.6	4.8	6.5	1.0	25.8	1.1	40.2
	Barren	0.3	0.4	1.1	0.4	0.1	2.2	1.1	5.6
	Total	35.0	798.7	366.4	141.0	4.6	54.9	5.1	1405.7

In a similar fashion to the MACR, rangeland and woodland are the classes responsible for most of the changes occurring within the LARB, with open water and barren land experiencing very little change. To gain insight on the spatial distribution of change throughout the LARB, change maps for the LARB were constructed. Figure II-11 is a Boolean change map of the LARB that identifies locations where a pixel changed from one LULC class in 1990 to another class in 2010. Within the entire LARB, 19.3% of the pixels experienced LULC change. Areas that experienced change are generally

found in the northern and central portions of the LARB. Dense clusters of areas that experienced change are generally found in areas surrounding Sinton and in areas near the basin outlet (northeastern portions). Clusters of areas that did not experience change are generally associated with cultivated lands and they are found in the southern portions and along the western edge of the LARB.

To visualize the patterns of land-change within the LARB, maps that depict the LULC class in 1990 before a pixel changed (Figure II-12a) and the class to which the pixel changed to in 2010 (Figure II-12b) were developed. Clusters of rangeland that changed to woodland are found in the northern portions of the LARB, with a relatively large cluster near the basin outlet. Patches of cultivated land that changed to rangeland are scattered within the western portions of cultivated land that dominate much of the LARB. Areas that changed to developed land are mostly found outside of Sinton and in areas where roads were constructed and/or expanded. Clusters of areas that didn't experience change are those associated with large patches of cultivated land in the southern and western parts of the LARB.

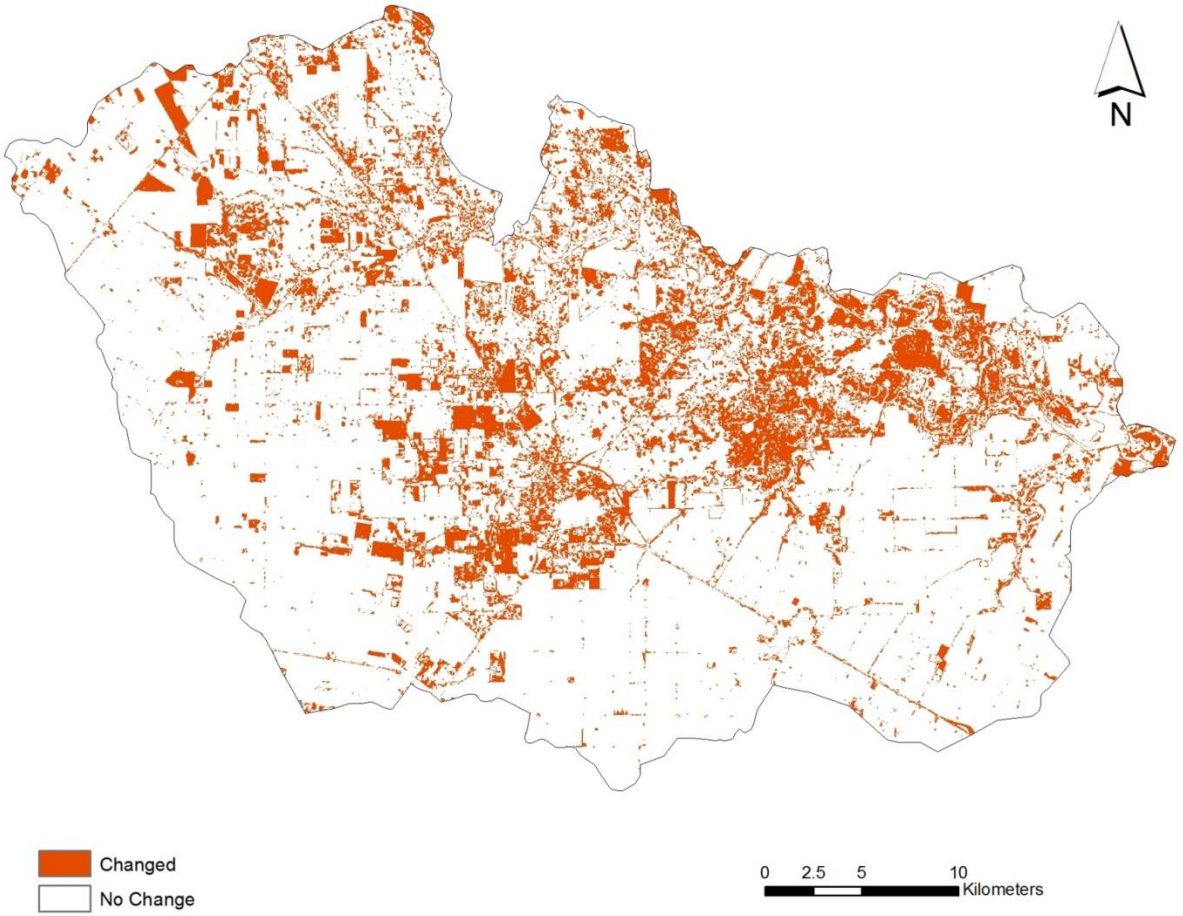

Figure II-11. Map of land use/land cover (LULC) change from 1990 to 2010 within the Lower Aransas River Basin.

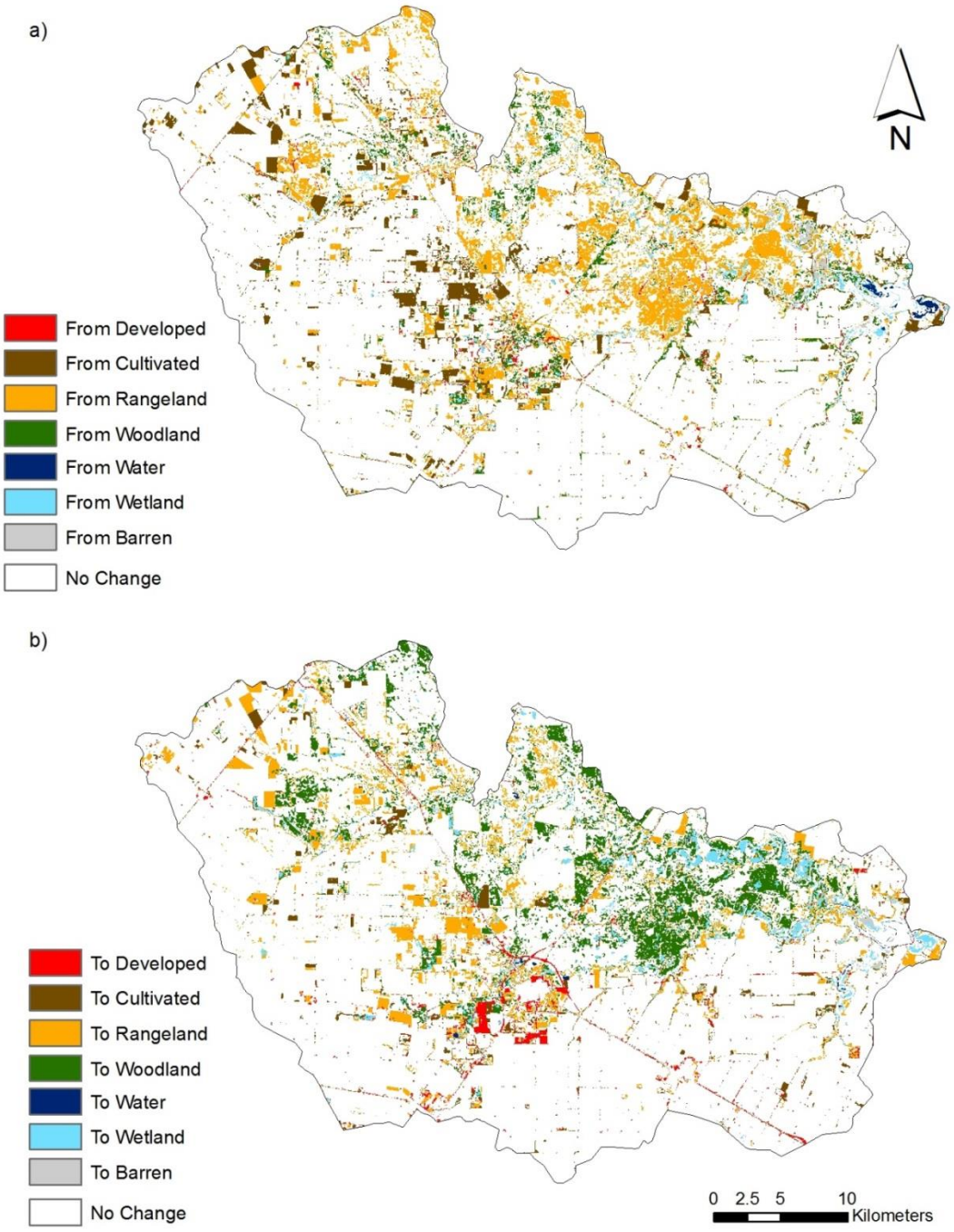

Figure II-12. Land use/land cover (LULC) changes from 1990 to 2010 within the Lower Aransas River Basin (LARB). a) LULC classes in 1990 that experienced change. b) LULC classes that previous classes changed to in 2010.

Various forms of LULC change has occurred within the LARB, but only a handful of the types of change contributed a significant proportion to the overall area. Figure II-13 is a map of the LULC changes that represent the greatest amount of coverage within the LARB. All of the seven dominant types of LULC change involve rangeland and these areas are mostly situated in the northern and central portions of the LARB. The northern areas that experienced change are generally where there is relatively little human disturbance and the central areas are situated around Sinton.

The LARB experienced a relatively large amount of change from 1990 to 2010, but the proportions were slightly less than for the entire MACR. Again, rangeland is the LULC class that is involved with the greatest proportion of change. This is due to the large amount of rangeland coverage within the LARB and potential classification error for the LULC images. Woodland expanded dramatically from 1990 to 2010 because it had a percent change of 76.0% (Table II-19), but again this proportion could be skewed due to similarities with the rangeland class. Wetland also experienced a relatively large amount of expansion because it had a percent change of 36.2% (Table II-19), and most of the expansion occurred in riparian areas near the Aransas River and the basin outlet. Developed land contributes a relatively small proportion of the LARB area (2.0% and 2.5% for 1990 and 2010, respectively), but developed land experienced a percent change of 24.6% (Table II-19), which makes it the class that experienced the third greatest amount of change using the percent change metric. Similarly to the rest of the MACR, developed land is expanding within the LARB.

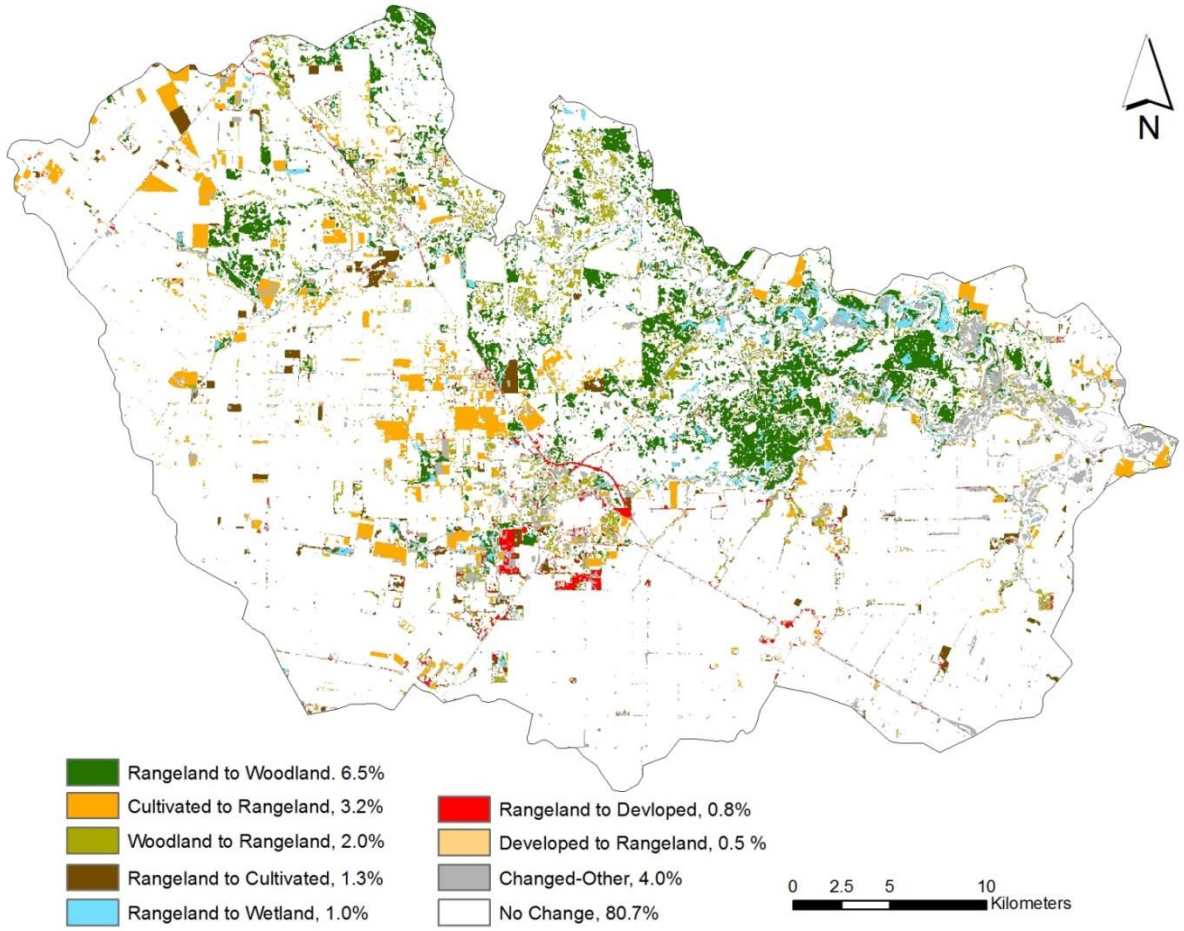

Figure II-13. Map of land use/land cover (LULC) classes that represent the highest percentage of total area (percentage listed on legend) within the Lower Aransas River Basin (LARB).

2.5 Conclusion

To gain an understanding of the quantity and spatial distribution of LULC change within the MACR and LARB over the last two decades was the principal goal of this analysis. This was accomplished by classifying LTM imagery, describing the LULC within the MACR and LARB, and conducting a LULC change analysis for both areas.

The northwestern corner of LTM images (Path: 26 and Row: 41) for 1990 and 2010 were classified to a modified Anderson Level I classification (Anderson et al. 1976) using the ML classification procedure in ENVI. An accuracy assessment was conducted on each image where 50 samples/sites were generated for each LULC class (350 samples per image) using a stratified random sample and compared to various reference images. The samples were used to estimate the overall accuracy, a standard Kappa index, and the quantity and allocation disagreement for each image. The 1990 and 2010 classified imagery had an overall accuracy of 88% and 84%, a Kappa estimate of 0.86 and 0.82, a quantity disagreement of 3% and 4%, and an allocation disagreement of 4% and 7%, respectively. While the classified 1990 image has a higher degree of accuracy, the statistics for both images indicate a strong level of agreement between the classified and reference imagery.

The dominant LULC classes within the MACR and LARB are cultivated land and rangeland. For the MACR, cultivated land and rangeland represent an average of 35.6% and 28.3%, respectively, of the total area for the 20-year period from 1990 to 2010. As for the LARB, cultivated land and rangeland make up an average of 58.0% and

27.9%, respectively, of the total area during the same time period. Developed land represents a modest proportion of the total area within MACR and LARB, as it makes up an average of 4.3% and 2.3%, respectively, of the total area. The MACR and LARB are predominantly rural areas, but much of the LULC is influenced by anthropogenic disturbance.

A relatively large degree of LULC change occurred within the MACR and LARB from 1990 to 2010. In terms of land area that experienced change, 27.1% and 19.3% of the MACR and LARB, respectively, experienced some form of LULC change. Rangeland is the class that experienced the greatest degree of LULC change, but some of this change is potentially attributed to errors in the classification procedure. The proportion of total coverage for developed land did not differ dramatically from 1990 to 2010, but developed land experienced a percent change/increase of 44.9% and 24.6% within the MACR and LARB, respectively. This shows that some of the LULC change that has occurred is due to anthropogenic disturbance along with a natural succession of LULC.

Results from this analysis will help understand how LULC are potentially disrupting watershed hydrology for the LARB. Also, the LULC data generated in this analysis will serve as a vital input for a hydrologic model that will be utilized in work presented in later chapters. Additionally, this work will increase the level of understanding associated with the types of changes occurring in coastal and estuarine environments of Texas; and it can be used to inform land and other resource management decisions within the greater Mission-Aransas and Nueces region.

CHAPTER III

CALIBRATION OF SWAT MODEL FOR THE LOWER ARANSAS RIVER BASIN

3.1 Introduction

The hydrologic cycle controls the volume and timing of freshwater delivery and its chemical and sediment load to coastal ecosystems (Scavia et al. 2002). Estuaries and other systems are largely dependent on the quantity and quality of freshwater inflows. Freshwater inflows can be defined as inputs of freshwater from streams draining into estuaries/bays. These inflows are important factors in the overall health of estuarine environments because they are major drivers of salinity gradients, sedimentation rates, and nutrient delivery. The Mission-Aransas (M-A) estuarine system on the Coastal Bend of Texas is no exception.

In Texas, the importance of freshwater inflows to estuaries has been recognized (Estevez 2002, Powell, Matsumoto, and Brock 2002). As estuaries provide habitat for several species of fish and shellfish of economic and recreational value, Texas has mandated the study of freshwater inflows to its bays and estuaries (Chen 2010, Schoenbaechler and Guthrie 2011). For the M-A estuarine system, freshwater inflows has been estimated by the Texas Water Development Board (TWDB) using data from U.S. Geological Survey (USGS) stream gages and the Texas Rainfall-Runoff (TxRR) model that is based on the Soil Conservation Service's curve number method to estimate direct runoff from a precipitation event for ungagged watersheds (Schoenbaechler and

Guthrie 2011). While estimates of freshwater inflows to the M-A estuarine system have been established, publicly available estimates are lumped into regional values with no information regarding individual freshwater inflows from lower portions of the Aransas River Basin (ARB). Furthermore, these estimates lack information regarding sediment and nutrient delivery to the estuary.

Generalized hydrologic models, such as the Soil and Water Assessment Tool (SWAT), are well-suited for simulating hydrology and water quality within watersheds with complex mosaics of land use/land cover (LULC), soil types, and topographic features. SWAT and other similar models can perform operations and provide results at various scales including watershed, subwatershed, and reaches that is useful in hydrologic modeling as these are the scales that should be included in any surface water analysis (Praskievicz and Chang 2009).

SWAT has become one of the most widely used watershed-scale computer simulation models (Arnold et al. 2012). The general nature and computationally efficiency of SWAT has allowed it to be widely applied in watersheds of various sizes with different hydrologic, geologic, and climatic conditions (Borah and Bera 2004, Arnold et al. 2012). Applications of SWAT have been reported in rural (Kirsch, Kirsch, and Arnold 2002, Saleh et al. 2000), more urbanized (Franczyk and Chang 2009), and coastal (Wu and Xu 2006, Lee et al. 2011) watersheds. Furthermore, SWAT has been successfully applied by Lee et al. (2011) in the estimation of freshwater inflows for the coastal watersheds of Matagorda Bay and Galveston Bay in Texas. This suggests that

SWAT can be applied to estimate freshwater inflows to the M-A estuary, as well as the delivery of sediment and nutrients to the coast.

While the usefulness of SWAT and other watershed-scale models is unquestionable, the uncertainty associated with model predictions has been widely recognized in the literature (Legates and McCabe Jr 1999, Engel et al. 2007, Gassman et al. 2007, Moriasi et al. 2007, Praskievicz and Chang 2009, Arnold et al. 2012, Duda et al. 2012, Moriasi et al. 2012). The provision of information regarding the uncertainty of model predictions and observed data used in model evaluation will better inform scientific assessments and decision-making that is conducted using the model (Harmel, Smith, and Migliaccio 2010).

Engel et al. (2007) defines models as "a simplification of the processes they are intended to represent (pg. 1230)." This simplification can add a significant amount of uncertainty to model predictions. Additionally, when applying a hydrologic model for a specific area, site specific parameters will need to be calibrated. The data needed to accurately estimate these parameters is often time consuming and expensive to acquire; that can result in imperfect parameter estimation. Uncertainty estimates for model predictions will provide important information regarding the sensitivity and reliability of the model.

The calibration process often involves comparing model predictions with observed data. In general, modelers will attempt to fit model predictions to trends in the observed data. Graphical procedures and goodness-of-fit (GOF) indicators are used to assess the agreement between observed and predicted variables. While this type of

procedure is considered common practice when conducting model calibration, observed data can also exhibit various levels of uncertainty. Harmel et al. (2006) identified four procedural categories (streamflow measurement, sample collection, sample preservation/storage, and laboratory analysis) that can potentially add large degrees of measurement uncertainty. To incorporate uncertainty in observed data used for model evaluation; Harmel, Smith, and Migliaccio (2010) derived a correction factor that modifies the deviation calculation used by several GOF indicators (Nash-Sutcliffe coefficient of efficiency, index of agreement, root mean square error, and mean absolute error). The incorporation of the correction factor can add to the degree of confidence in a model's predictive ability.

Thus, the use of standard and modified GOF indicators in SWAT model evaluation will give a better idea of the degree of uncertainty associated with estimates of freshwater inflows and the delivery of sediment and nutrient loads to the M-A estuarine system. This is important because uncertainty should always be considered in any management implications that are potentially induced by model predictions.

3.2 Objectives

The main objective of this chapter is to assess the capabilities of a SWAT model developed for the lower portions of the Aransas River Basin to predict freshwater inflows and the delivery of associated sediment and nutrient loads to the Mission-Aransas estuarine system. To address this objective, the work presented here was divided into three tasks:

1. Calibration and validation of SWAT for streamflow using observed data from a stream gage; along with adjustment of model parameters to make predictions of sediment and nutrient delivery comparable to published estimates in the literature and agency reports.
2. Incorporation of correction factors as described by Harmel, Smith, and Migliaccio (2010) to common goodness-of-fit indicators used in pair-wise comparisons for model evaluation of streamflow predictions.
3. Describe predictions of freshwater inflow and delivered loads of sediment and nutrients to the Mission-Aransas estuarine system from lower portion of the Aransas River Basin using the calibrated SWAT model.

3.3 Materials and Methodology

3.3.1 Study Area

The Lower Aransas River Basin (LARB) has an area of 1383 km^2 and it lies on the Coastal Bend of Texas just north of Corpus Christi (Figure III-1). This subbasin makes up the lower portions of the Aransas River Basin (ARB) and it occupies about 62% of the total ARB area. Streams in the region drain into Copano Bay that is part of the M-A estuarine system. The LARB includes the lower reach of the Aransas River (~73 km); that is the principle stream in the drainage basin and one of the few rivers in Texas not obstructed by dams. The Aransas River is relatively short, but it has a highly meandering course within the flat coastal plain. Major tributaries to the Aransas River within the LARB include Chiltipin and Papalote Creeks.

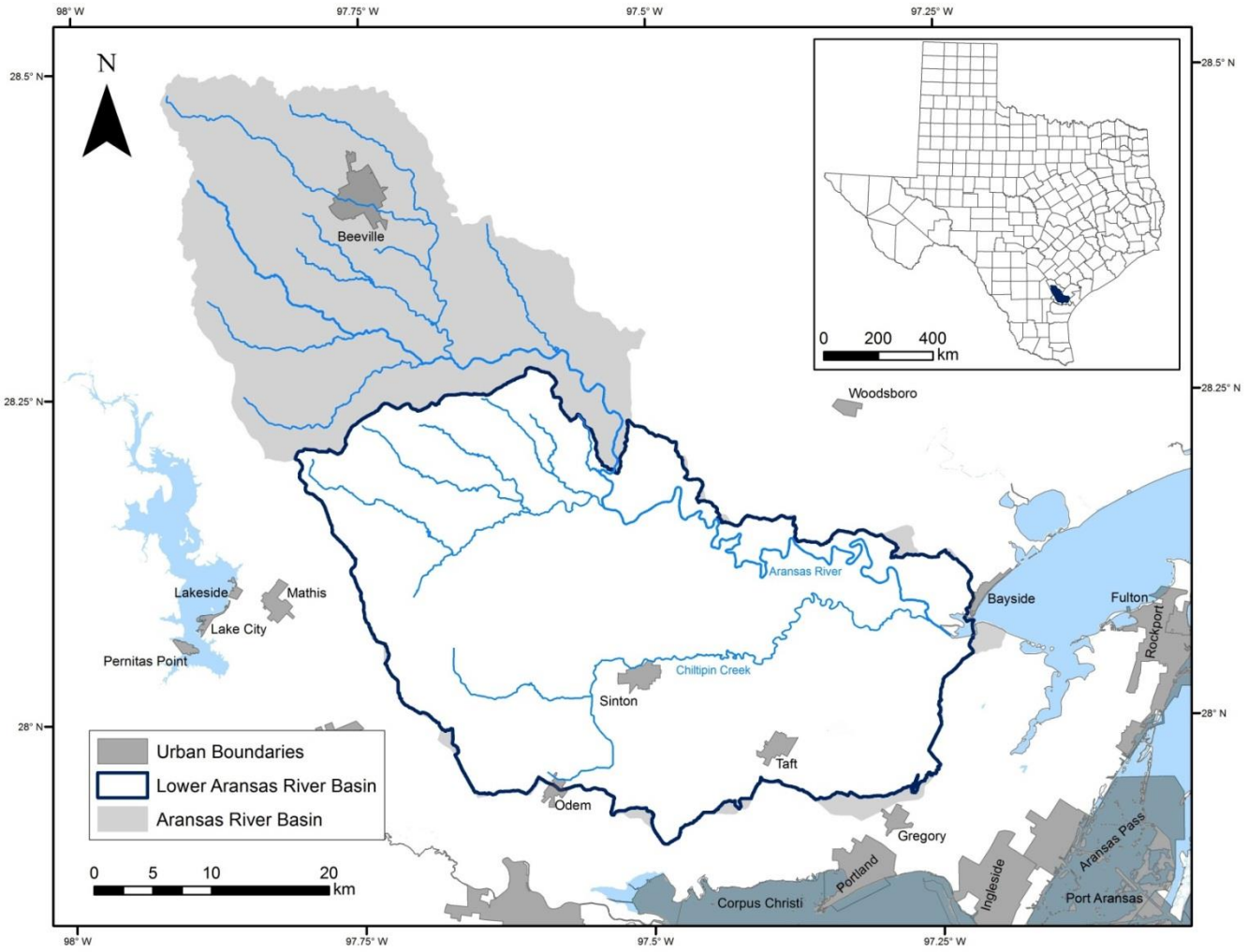

Figure III-1. Location map of the Lower Aransas River Basin (LARB) (delineated with ArcSWAT); Aransas River Basin (ARB) (HUC: 12100407); and city boundaries (Texas Natural Resources Information System: StratMap. Note: blue polylines are streams.

The region has a semi-arid climate with mean annual precipitation of 864 mm and a mean temperature of 21.8 °C. However, the distribution of annual precipitation is skewed by seasonal tropical storms that occasionally bring large amounts of rainfall in late-summer and early-fall. Dominant LULC includes: agriculture, shrub/scrub, and pasture. The LARB region is predominantly rural with no large urban centers (Morehead, Beyer, and Dunton 2007). Within the LARB, the only prominent urban areas are Sinton and Taft that lie in the central and southeastern portions of the watershed (Figure III-1).

3.3.2 SWAT

SWAT is a semi-distributed physically-based continuous simulation model that runs on a daily time-step and it was developed in the early 1990s for conducting assessments regarding water balance and pollutant loadings for various land use practices within agricultural watersheds (Neitsch et al. 2011). Over time the capabilities of SWAT have been continuously upgraded and later versions of SWAT can be used to model mosaics of different land uses (agriculture, forest, urban, etc.) within large watersheds (Neitsch et al. 2011). SWAT divides watersheds into hydrologic response units (HRUs) based on LULC, soil, and slope allowing for hydrology to be modeled within each respective HRU. Hydrologic modeling within SWAT is divided into a land phase and a channel routing phase (Franczyk and Chang 2009). The land phase of the simulation is governed by runoff and the modeling procedures are based on the curve number (CN) method (Neitsch et al. 2011). The CN method calculates a CN for a given area using soil and land cover characteristics that predicts when soil will become

saturated and thus allowing surface runoff to occur (Neitsch et al. 2011). Soil erosion within the land phase is modeled empirically using the modified universal soil loss equation (MUSLE) (Neitsch et al. 2011). The channel routing phase models flow within the main channel of each HRU. SWAT uses Manning's equation to define the rate of flow. Water is routed through the network using the variable storage routing method that utilizes mass balance within channel segments (Neitsch et al. 2011). Sediment transport within the channel is modeled using the Simplified Bagnold Equation that models the maximum amount of sediment that can be transported as a function of stream power and peak channel velocity (Neitsch et al. 2011). Nutrient (nitrogen and phosphorus) transport in streams is modeled using a loading function developed by McElroy et al. (1976) and modified by Williams and Hann (1978).

SWAT requires a large number of input files and the construction of these input files is aided by using the ArcSWAT graphical user interface that runs as an extension in ArcGIS (Winchell et al. 2010). ArcSWAT can be used to delineate the watershed; as well as process the land use, soil, slope data that are used to define the HRUs. In this study, ArcSWAT version 2009.93.7b that runs in ArcGIS 9.3 (ESRI 2009) was used.

3.3.3 Data

A digital elevation model (DEM) from the National Elevation Dataset (NED) at 10 meter resolution was obtained from the National Oceanic and Atmospheric Administration (NOAA)'s Digital Coast website (NOAA 2012). Slope characterization and delineation of the watershed (LARB) boundary and channel networks was conducted in ArcSWAT using the DEM. Attempts were made to delineate the watershed

using a 30 meter DEM from NED, but ArcSWAT was unable to accurately accomplish this task due to the flatness of the region. Elevation in this region ranges from 0 to 67 meters with most relief occurring in the northwestern portions of the basin. Slope ranges from 0 to 65% with an average slope of 0.57%.

Soil was defined using a 30 meter grid of the U.S. General Soil Map (STATSGO) that was resampled to a resolution of 10 meters. Dominant soil types within the LARB are Victoria (clay loam) and Papalote (clay loam) with coverage of 57.7% and 33.1%, respectively, of the total watershed area.

Land use/land cover (LULC) was for 1990 at 30 meter resolution (resampled to 10 meter resolution) and it was developed by classifying a Landsat Thematic Mapper image (Path: 26 Row: 41). Dominant LULC classes were cultivated land (58.0%) and rangeland (30.7%) (Table III-1). LULC data had seven classes (Table III-1) and it was matched to built-in land use classes within ArcSWAT (Table III-2). The pairing between LULC classes from the Landsat imagery and SWAT land use makes intuitive sense with the exception of the barren land and urban-industrial pair. SWAT does not have a barren land use, but since barren land has very little coverage and much of it is from mining facilities, the urban-industrial land use was considered as an appropriate approximation.

Daily precipitation and temperature (maximum and minimum) data for the time period from 1950 to 2010 from six weather stations (GHCND: USC00410302, USW00012925, USC00415661, USW00012972, USC00418354, and USC00419559) (Figure III-2) was obtained from the National Climatic Data Center (NCDC) website (NCDC 2012). As expected, there were numerous holes in the time-series' and data from

the nearest weather station with available data was used in order to have continuous datasets for each weather station.

Streamflow data (mean daily streamflow) from two U.S. Geological Survey (USGS) stream gages (08189700 and 08189800) was obtained from the USGS National Water Information System (NWIS) (NWIS 2012). As the LARB doesn't include the entire stretch of the Aransas River, streamflow data for 1964 to 2010 from a gage on the Aransas River above Skidmore, TX (08189700) is used as a point source inlet to the portion of the Aransas River that lies within the watershed boundary (Figure III-2). Gage 08189700 is located approximately 21 river km upstream of the LARB boundary, but as this area is not being modeled, the inlet was placed at the location where the Aransas River crosses the watershed boundary. Within the LARB boundary, lies gage 08189800 on Chiltipin Creek (tributary of the Aransas River) at Sinton, TX (Figure III-2). Streamflow records exist from Aug-1970 to Sep-1991and this data was used for the calibration and validation of SWAT.

Table III-1. Areal coverage of each land use/land cover class for the Lower Aransas River Basin.

	Areal Coverage	
LULC class	**km2**	**%**
Developed Land	28.0	2.0
Cultivated Land	801.6	58.0
Rangeland	424.6	30.7
Woodland	81.0	5.9
Open Water	3.4	0.2
Wetland	39.0	2.8
Barren Land	5.5	0.4
Total	**1383.0**	**100.0**

Table III-2. Pairing of land use/land cover class from Landsat image classification to SWAT land use classes.

LULC class	SWAT land use
Developed Land	Urban - Mixed
Cultivated Land	Agricultural - Row Crops
Rangeland	Rangeland - Mixed
Woodland	Forest - Mixed
Open Water	Water
Wetland	Wetland - Mixed
Barren Land	Urban - Industrial

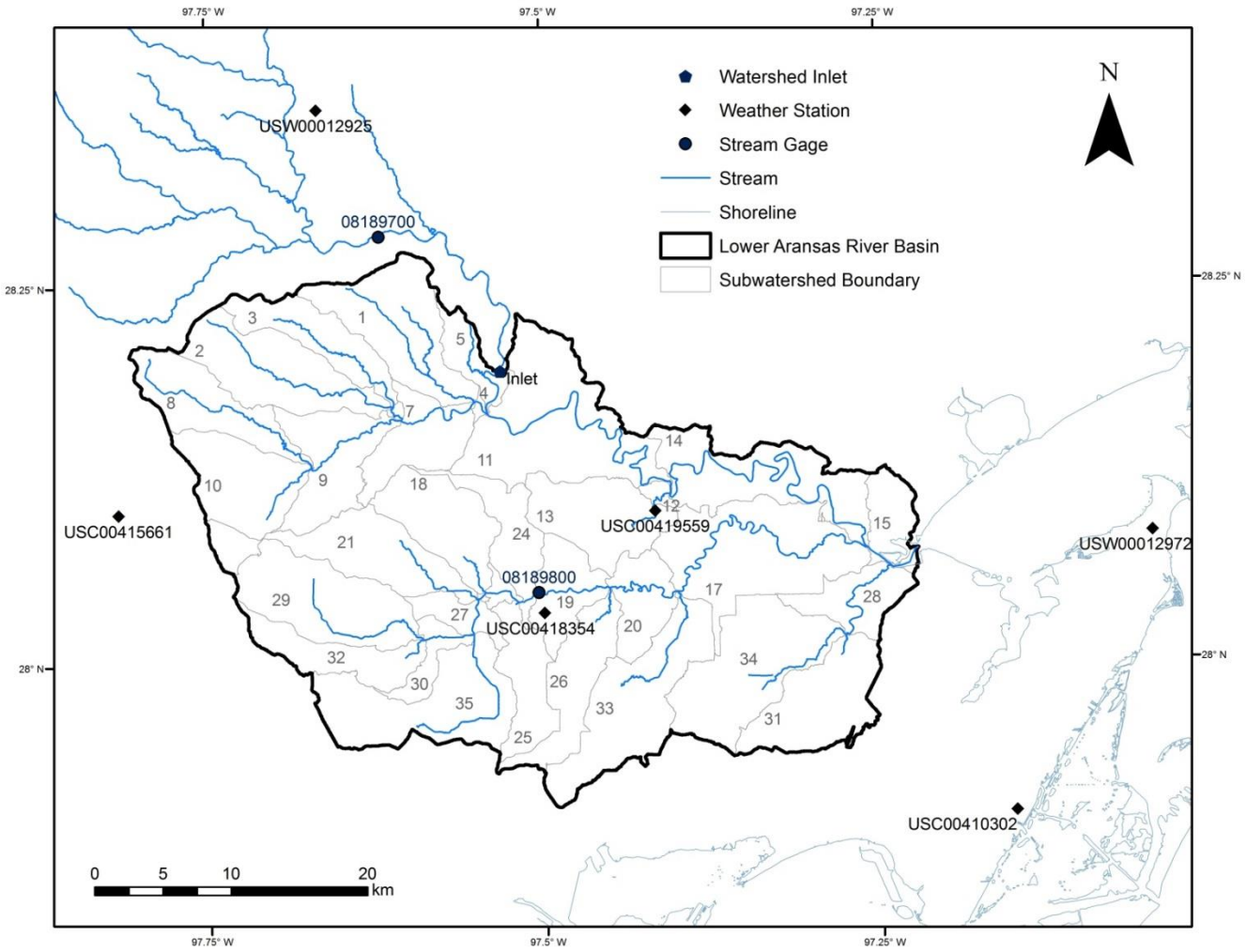

Figure III-2. Map of Lower Aransas River Basin (LARB) (delineated with ArcSWAT); stream network (stream network within the LARB delineated using ArSWAT); U.S, Geological Survey (USGS) stream gages used as watershed inlets (08189700) and for SWAT calibration (08189800); and National Climatic Data Center (NCDC) weather stations used as precipitation and temperature inputs.

3.3.4 SWAT Model Setup

Watershed and subwatershed boundaries were delineated using ArcSWAT. The location of gage 08189800 was specified in the delineation of subwatersheds in order to make this location a subwatershed outlet and allow appropriate model evaluations to be conducted. A maximum drainage area threshold of 1100 hectares was used to delineate 35 subwatersheds within the LARB. Within each subwatershed, HRUs were generated on the basis of slope, soil, and land use. Three slope classes (0 to 1%, 1 to 2%, and greater than 2%) were used in the generation of HRUs. A threshold of 5% for slope class and soil type was used to limit the number of HRUs; meaning that slope classes and soil types that covered more than 5% of a subwatershed area would become their own HRU.

Water diversions and return flows from waste water treatment plants were not incorporated in the SWAT model. While there is an unknown amount of water diversion within the LARB, there are seven point-source return flows (Schoenbaechler and Guthrie 2011). These anthropogenic modifications can impact the fluvial system, but return flows account for only a small percent of freshwater inflow to the M-A estuarine system (Schoenbaechler and Guthrie 2011), and the incorporation of these components was beyond the scope of this study.

3.3.5 Model Calibration and Validation

Monthly mean daily stream flows estimated by SWAT from Jan-1972 to Sep-1991 (18.75 years) were manually calibrated and validated against streamflow data from the gage on Chiltipin Creek (08189800). Estimated and measured monthly mean daily streamflow were divided into a calibration period (Jan-1972 to Dec-1981) and a

validation period (Jan-1982 to Sep-1991); with a model warm-up period from Jan-1960 to Dec-1971 (12 years). The latter years were chosen for validation because work presented in later chapters will focus on using the model to predict hydrologic and water quality impacts from various land-use/land-cover change scenarios that could occur in the future.

For the evaluation of model performance, pair-wise GOF indicators and graphical techniques were employed. The primary GOF indicators used in this analysis were the Nash-Sutcliffe model efficiency coefficient (NS) (Nash and Sutcliffe 1970), the coefficient of determination (R^2), and the percent difference between average observed and estimated monthly mean daily streamflow (PD). The Nash-Sutcliffe model efficiency coefficient has a range of $-\infty$ to 1 with values closer to 1 indicating a better predictive ability for the model. Negative values for the NS indicate that the mean for the observed variable of interest is a more reliable predictor than the model being evaluated (Legates and McCabe Jr 1999). An $NS \geq 0.5$ is considered satisfactory for most model applications (Engel et al. 2007, Moriasi et al. 2007, Arnold et al. 2012) and it will be the target NS value used in this analysis. R^2 and PD are traditional indicators used in model evaluation and values of $R^2 \geq 0.6$ and $PD \leq 15\%$ for streamflow indicate acceptable model performance for most applications (Santhi et al. 2001, Engel et al. 2007, Arnold et al. 2012). To further evaluate model performance, the index of agreement (d), root mean square error (RMSE), and mean absolute error (MAE) were also computed. Similar to R^2, the index of agreement (d) has a range of 0 to 1 with values closer to 1 indicating better agreement between observed and predicted values.

The RMSE and MAE are measures of the difference between modeled output and measured data with lower values indicating better agreement. Equations for each of these GOF indicators are presented in Table III-3. The graphical methods used in model evaluation were plotting observed and predicted streamflow on time-series and one-to-one plots.

Table III-3. Goodness-of-fit indicators used in pairwise comparison of measured and predicted values (adapted from Table 1 from Harmel, Smith, and Migliaccio (2010)). Note: O_i is the observed value; P_i is the predicted values; $\bar{O}$ is the mean for observed values; P_{bar} is the mean for predicted values.

Indicator	Equation	Eq. No.
NS	$NS = 1 - \frac{\sum_{i=1}^{N}(O_i - P_i)^2}{\sum_{i=1}^{N}(O_i - \bar{O})^2}$	(III-1)
R^2	$R^2 = 1 - \frac{\sum_{i=1}^{N}(P_i - \bar{O})^2}{\sum_{i=1}^{N} O_i^{\,2}}$	(III-2)
PD	$PD = \left[\frac{(\bar{P} - \bar{O})}{\bar{O}}\right] * 100\%$	(III-3)
d	$d = 1 - \frac{\sum_{i=1}^{N}(O_i - P_i)^2}{\sum_{i=1}^{N}(\lvert P_i - \bar{O}\rvert + \lvert O_i + \bar{O}\rvert)^2}$	(III-4)
RMSE	$RMSE = \sqrt{N^{-1}\sum_{i=1}^{N}(O_i - P_i)^2}$	(III-5)
MAE	$MAE = N^{-1}\sum_{i=1}^{N}\lvert O_i - P_i\rvert$	(III-6)

Parameter values that influence streamflow were adjusted manually (Table III-4) following guidelines specified by Santhi et al. (2001), Arnold et al. (2011), and Arnold et al. (2012); as well as parameter estimates from Wu and Xu (2006) and Lee et al. (2011).

Due to a lack of available data, SWAT predictions could not evaluated using a pair-wise statistical approach for sediment and nutrient loading. Estimates of annual total suspended sediment (TSS) loads and yields for the Aransas River above Skidmore, TX for 1966 to 1974 have been calculated by Welborn and Bezant (1978) and Brock et al. (2008) using field samples and sediment-transport curves. As for nutrient loading, Rebich et al. (2011) utilized a SPAtially Referenced Regressions on Watershed attributes (SPARROW) model to estimate delivered loads of total nitrogen (TP) and total phosphorus (TP) to the coast from the Aransas River in 2002. Parameter values that influence sediment and nutrient loading were adjusted (Table III-4) following guidelines from Santhi et al. (2001), Arnold et al. (2011), and Arnold et al. (2012) to get estimates that fall in the same "ball-park" as values calculated by Welborn and Bezant (1978) and Rebich et al. (2011), respectively.

Table III-4. SWAT parameters that were adjusted in model calibration.

Parameter	Description	Process	Default Value	Recommended Range	Input Value	Units
CN2	Curve number for soil moisture condition II	Streamflow	60 - 95	30 - 100	63 - 93	n/a
SOL_AWC	Available water capacity	Streamflow	0.08 - 0.15	0.00 - 1.00	0.08	mm H_2O/mm soil
ESCO	Soil evaporation compensation factor	Streamflow	0.95	0.01 - 1.00	0.05	n/a
GW_REVAP	Groundwater "revap" coefficient	Streamflow	0.05	0.02 - 0.20	0.20	n/a
REVAPMN	Threshold depth of water in the shallow aquifer for revap	Streamflow	0.000	n/a	0.100	mm H_2O
GWQMN	Threshold depth of water in the shallow aquifer for return flow to occur	Streamflow	0.00	n/a	0.01	mm H_2O
ALPHA_BF	Baseflow alpha factor	Streamflow	0.048	0.100 - 1.000	0.300	days
CH_K2	Effective hydraulic conductivity in main channel alluvium	Streamflow	-1.000	0.0250 - 2.500	0.025	mm/hr
USLE_C	USLE equation support practice factor	Sediment	0.0	0 -1	0.8	n/a
CH_EROD	Channel erodibility factor	Sediment	0.0000	0.0000 - 1.0000	0.0001	n/a
NPERCO	Nitrate percolation coefficient	Nutrients	0.20	0.1 - 1.0	0.01	n/a
PPERCO	Phosphorus percolation coefficient	Nutrients	10.0	10.0 - 17.5	15.0	10 m^3 /Mg
PHOSKD	Phosphorus soil partitioning coefficient	Nutrients	175	n/a	125	m^3/Mg

3.3.6 Incorporation of Correction Factor

The correction factor developed by Harmel, Smith, and Migliaccio (2010) was designed to be applied to GOF indicators that utilize the deviation calculation, that is the difference between each pair of observed and predicted values (Equation III-7):

$$e_i = O_i - P_i \tag{III-7}$$

where e_i is the deviation between paired observed and predicted data, O_i observed value, and P_i is the predicted value. As indicated by Harmel, Smith, and Migliaccio (2010), this error term is identical for four GOF indicators listed in Table III-3 (Equations III-1, III-4, III-5, and III-6) and they argue that the assumed uncertainty distributions for observed and predicted data should be incorporated when analyzing the deviation between pairs. This incorporation involves calculating the degree of overlap (*DO*) between the respective assumed probability density functions (pdfs). Making the assumption that observed and predicted values are independent, the degree of overlap can be calculated using Equation III-8 (Harmel, Smith, and Migliaccio 2010):

$$DO_i = \int_{P_1\,min}^{P_1\,max} p_O(o_i)do \,.\int_{O_i\,min}^{O_1\,max} p_P(p_i)dp$$

$$DO_i = [prob(o_i < P_{imax}) - prob(o_i < P_{imin})]$$
$$.\,[prob(p_i < O_{imax}) - prob(p_i < O_{imin})] \tag{III-8}$$

where DO_i is the degree of overlap for each pair; $p_O(o_i)$ and $p_p(p_i)$ are the pdfs for the observed and predicted values, respectively. The degree of overlap can then be used to calculate the correction factor using Equation III-9 (Harmel, Smith, and Migliaccio 2010):

$$CF(meas + pred)_i = 1 - DO_i \quad \text{(III-9)}$$

where $CF(meas + pred)_i$ is the correction factor for each observed and predicted pair. This correction factor will vary from 0 to 1 with values closer to 0 when there is a greater degree of overlap. With the correction factor, the modified error term that incorporates observed and predicted uncertainty can be calculated using Equation III-10 (Harmel, Smith, and Migliaccio 2010):

$$e(meas + pred)_i = CF(meas + pred)_i \,.\, (O_i - P_i) \quad \text{(III-10)}$$

where $e(meas + pred)_i$ is substituted for equation 7 in the GOF indicators (Table III-3).

Following the procedure used by Harmel, Smith, and Migliaccio (2010), three continuous probability distributions (normal, lognormal, and uniform) were used to calculate the degree of overlap (Equation III-8). For the normal and lognormal distributions, values for O_i and P_i were set as the means for their respective distributions with standard deviation being estimated using the coefficient of variation (Cv). Four Cv values were assumed (Cv = 0.026; Cv = 0.085; Cv = 0.192; and Cv = 0.256) with increasing levels of uncertainty used in the estimation of the standard deviation. The uncertainty boundaries (O_{imax}, O_{imin}, P_{imax}, and P_{imin}) were assumed to occur at the 0.0001 and 0.9999 probabilities in order to estimate the values for the uncertainty boundaries. For the uniform distribution, the parameters for the distribution (α and β) were estimated using Equation III-11:

$$\alpha = \bar{x} - \sqrt{3}s_x$$

$$\beta = \bar{x} + \sqrt{3}s_x \quad \text{(III-11)}$$

where α and β are the parameters of the uniform distribution.

These correction factors were only incorporated to model evaluations for monthly mean daily streamflow because continuous data for sediment and nutrient loadings/yields were unavailable.

3.3.7 Freshwater and Material Inflows

Once a desired level of model calibration had been reached, freshwater inflows and delivered loads of total suspended solids (TSS) and nutrients (TN and TP) from the LARB to the M-A estuarine system were estimated on a monthly basis. Time-series' and monthly averages of each variable of interest (fresh water inflows; and delivered loads of TSS, TN, and TP) were estimated for the time period from 1972 to 2010 using SWAT.

3.4 Results

3.4.1 Model Calibration and Validation

GOF indicators (NS, R^2, PD, d, RMSE, MAE) were used to evaluate model performance in predicting monthly mean daily streamflow. Model predictions were compared to measured streamflow at gage 08189800 on Chiltipin Creek for the calibration period (Jan-1972 to Dec-1981) and validation period (Jan-1982 to Sep-1991). Calculated values for the GOF indicators for streamflow at gage 08189800 are presented in Table III-5. For the calibration period, NS and R^2 had values of 0.66 and a PD of 5.58%, which meets the target specifications for each indicator. As for the validation period, NS and R^2 values are more promising with values of 0.76 and 0.78, respectively, and a PD of 40.69%. The PD for the validation period is the only indicator that did not meet target specifications.

Using graphical methods to evaluate model predictions of streamflow can help highlight time-periods where predicted and observed streamflow are significantly different. For the calibration and validation periods, peak flows do not always line-up in terms of magnitude and duration (Figures III-3 and III-4). Visually, the time-series for the calibration period seems to line up better, but this is not depicted in the GOF indicator values. Similarly, there is a smaller degree of variation between observed and predicted streamflow for the calibration period than the validation period (Figures III-5 and III-6). Contrary to the GOF indicators, the time-series (Figure III-3 and III-4) and one-to-one (Figures III-5 and III-6) plots indicate a better fit for the calibration period, but this might be due to the axis scaling in the plots.

Table III-5. Goodness-of-fit indicator scores for the calibration and validation periods. Note: NS = Nash-Sutcliffe model efficiency; R^2 = coefficient of determination; PD = percent difference between average observed and predicted streamflow; d = index of agreement; RMSE = root mean square error; MAE = mean absolute error.

Period	NS	R^2	PD (%)	d	RMSE	MAE
Calibration (Jan-72 to Dec-81)	0.66	0.66	5.57	0.89	57.38	26.82
Validation (Jan-82 to Sep-91)	0.76	0.78	40.68	0.94	50.67	20.96

Estimates of average annual TSS loads and yields for the Aransas River at Skidmore, TX for the years 1966-1974 were calculated by Welborn and Bezant (1978) and Brock et al. (2008), and their estimates were compared to estimates generated by SWAT at the LARB outlet (Table III-6). SWAT estimates of TSS load are much greater than both Welborn and Bezant (1978) and Brock et al. (2008) estimates (PD of 131%

and 127%, respectively), but TSS yields are much more similar as there is a percent difference of 6 and 3%, respectively.

Estimates of loads and yields of TN and TP for the Aransas River Basin have been reported by Rebich et al. (2011) for the year 2002. These estimates were compared to estimates generated by the calibrated SWAT model (Table III-7). SWAT estimates for load and yield of TN are greater by 44 and 567%, respectively, than the Rebich et al. (2011) estimates. The same trend is not the case for TP as SWAT estimates for load are lower by 35%, but the TP yield is greater by 204%.

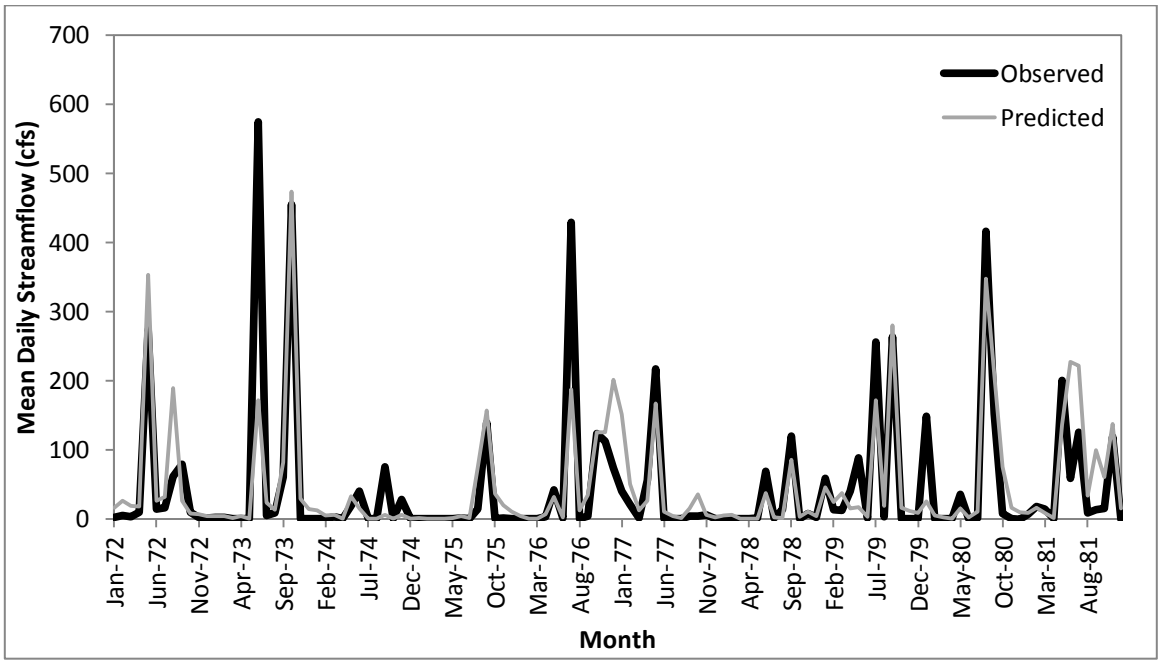

Figure III-3. Time-series of observed and predicted monthly mean daily streamflow for gage 08189800 on Chiltipin Creek during the calibration period (Jan-1972 to Dec-1981).

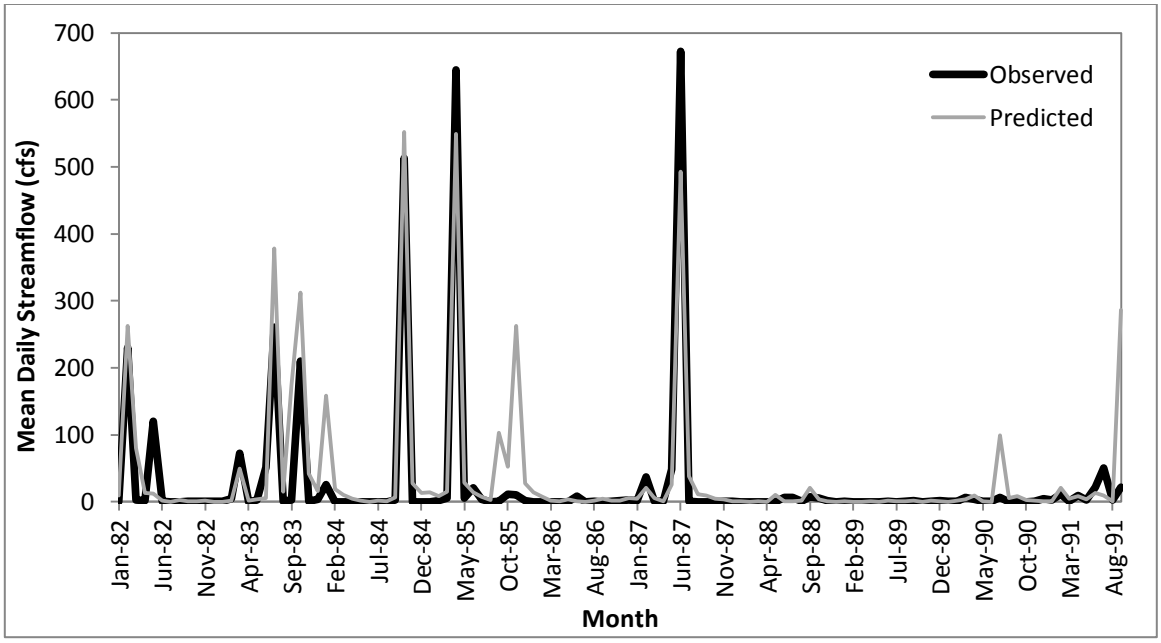

Figure III-4. Time-series of observed and predicted monthly mean daily streamflow for gage 08189800 on Chiltipin Creek during the validation period (Jan-1982 to Sep-1991).

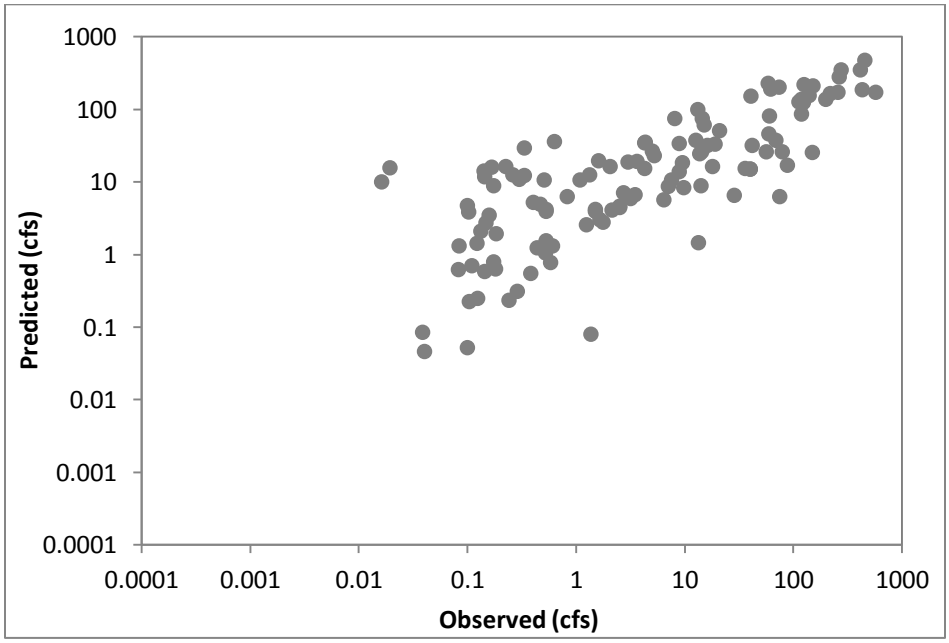

Figure III-5. One-to-one plot of observed vs. predicted streamflow for gage 08189800 on Chiltipin Creek during the calibration period (Jan-1972 to Dec-1981).

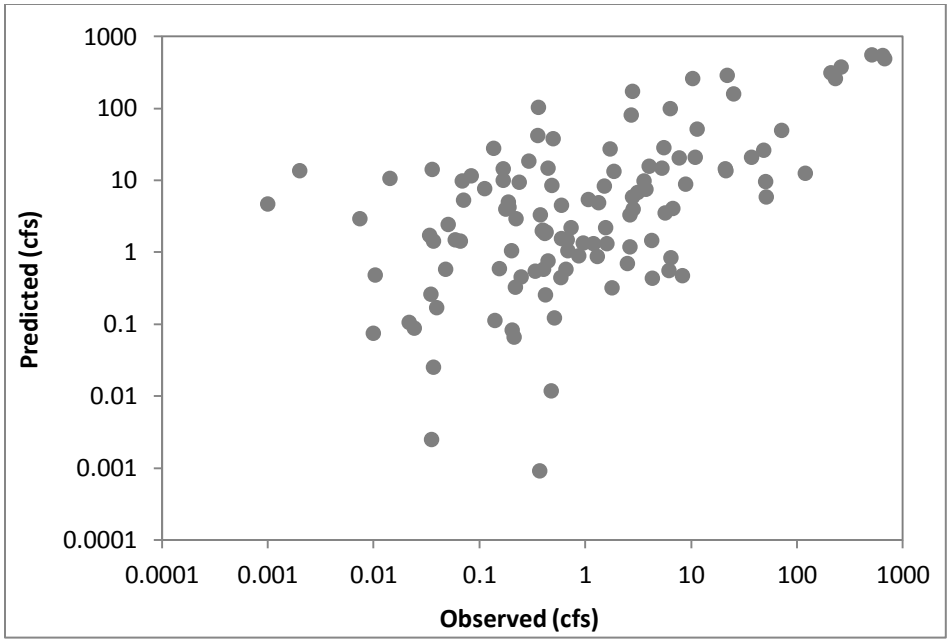

Figure III-6. One-to-one plot of observed vs. predicted streamflow for gage 08189800 on Chiltipin Creek during the validation period (Jan-1982 to Sep-1991).

Table III-6. Comparison of average annual total suspended sediment loads and yields in metric tons (mT) for the Aransas River during the 1966 to 1974 time period. SWAT estimates are for the outlet of Lower Aransas River Basin that were generated using the calibrated SWAT model. Estimates from Welborn and Bexant (1978) and Brock et al. (2008) are for a stream gage at Skidmore, TX (08189700). Note: Percent Difference was calculated by subtracting the published estimate from the SWAT estimate and dividing by the published estimate.

	Total Suspended Sediment	
Source	**Load (mT/year)**	**Yield (mT / km2/year)**
SWAT	51400	37
Welborn and Bexant (1978)	22226	35
Brock et al. (2008)	22680	36
Percent Difference (SWAT and Welborn and Bexant (1978))	131	6
Percent Difference (SWAT and Brock et al. (2008))	127	3

Table III-7. Comparison between estimates of loads and yields of total nitrogen and total phosphorus for the Aransas River in 2002. SWAT estimates are for the outlet of Lower Aransas River Basin that were generated using the calibrated SWAT model. Estimates from Rebich et al. (2011) are for the outlet of the entire Aransas River Basin. Note: Percent Difference was calculated by subtracting the Rebich et al. (2011) estimate from the SWAT estimate and dividing by the Rebich et al. (2011) estimate.

	Total Nitrogen		Total Phosphorus	
Source	Load (mT/year)	Yield (kg/km^2/year)	Load (mT/year)	Yield (kg/km^2/year)
SWAT	3976	2875	264	191
Rebich et al. (2011)	2760	431	404	63
Percent Difference	44	567	-35	204

3.4.2 Incorporation of Correction Factor

Correction factors were incorporated to four of the GOF indicators (NS, d, RMSE, and MAE) as described by Harmel, Smith, and Migliaccio (2010). The level of impact to each indicator is dependent on the Cv and distribution (Table III-8). Regardless of the distribution, indicator values improve as the Cv increases. The normal distribution is the most significant distribution in increasing the GOF between observed and predicted streamflow, with the uniform distribution being the least significant.

Table III-8. Values for standard and modified goodness-of-fit indicators for streamflow on Chiltipin Creek during the calibration (Jan-1972 to Dec-1981) and validation (Jan-1982 to Sep-1991) periods. A correction factor was incorporated the modified goodness-of-fit indicators that utilized statistical distributions (normal, log normal, or uniform) and an assumed coefficient of variation (Cv) as described by Harmel, Smith, and Migliaccio (2010). Note: NS = Nash-Sutcliffe model efficiency; NS(rat) is a model performance rating based on NS indicator with NS ≥ 0.5 considered satisfactory (Satis); R^2 = coefficient of determination; PD = percent difference between average observed and predicted streamflow; d = index of agreement; RMSE = root mean square error; MAE = mean absolute error.

		Calibration					Validation				
	Cv	**NS**	**NS (rat)**	**d**	**RMSE**	**MAE**	**NS**	**NS (rat)**	**d**	**RMSE**	**MAE**
Standard	N/A	0.66	Satis	0.89	57.38	26.83	0.76	Satis	0.94	50.68	20.96
Normal	0.026	0.66	Satis	0.89	57.33	26.53	0.76	Satis	0.94	50.56	20.74
Log Normal	0.026	0.66	Satis	0.89	57.33	26.53	0.76	Satis	0.94	50.56	20.74
Uniform	0.026	0.66	Satis	0.89	57.35	26.71	0.76	Satis	0.94	50.68	20.96
Normal	0.085	0.67	Satis	0.89	56.21	24.65	0.78	Satis	0.94	48.15	19.07
Log Normal	0.085	0.67	Satis	0.89	56.21	24.65	0.78	Satis	0.94	48.64	19.65
Uniform	0.085	0.66	Satis	0.89	57.34	26.62	0.76	Satis	0.94	50.53	20.65
Normal	0.192	0.70	Satis	0.90	53.54	21.40	0.81	Satis	0.95	44.57	16.14
Log Normal	0.192	0.70	Satis	0.90	53.54	21.40	0.80	Satis	0.95	45.49	17.26
Uniform	0.192	0.67	Satis	0.89	56.63	25.81	0.76	Satis	0.94	50.33	20.71
Normal	0.256	0.74	Satis	0.92	49.85	19.71	0.81	Satis	0.95	44.43	15.68
Log Normal	0.256	0.74	Satis	0.92	49.85	19.72	0.81	Satis	0.95	45.41	16.93
Uniform	0.256	0.67	Satis	0.89	56.61	25.74	0.78	Satis	0.94	48.41	20.05

3.4.3 SWAT Estimates of Freshwater and Material Inflows

Freshwater inflows to the M-A estuary from the Aransas River enter the estuarine system at the southwestern corner of Copano Bay (Figure III-1). For the time period from 1972 to 2010, mean monthly freshwater inflows from the Aransas River ranged from 7.68 million cubic meters in August to 33.96 million cubic meters in October (Table III-9). The fall months are the time of the year with the greatest freshwater inflows (especially September and October), which is not surprising as this is

tropical storm season for the Gulf of Mexico region. During the same time period (1972 to 2010), annual freshwater inflows from the Aransas River ranged from 1.39 to 583.21 million cubic meters; with a mean annual freshwater inflow volume of 188.93 million cubic meters (Table III-10).

Table III-9. Mean monthly freshwater inflows and delivered loads of total suspended solids (TSS), total nitrogen (TN), and total phosphorus (TP) from the Aransas River for 1972-2010. Values were estimated with SWAT.

Month	Freshwater Inflow (million m^3)	Delivered TSS Load (1000 mT)	Delivered TN Load (mT)	Delivered TP Load (mT)
Jan	8.62	1.03	76.61	3.67
Feb	10.16	1.59	65.63	4.48
Mar	8.56	1.20	42.96	5.07
Apr	7.77	1.29	51.40	5.62
May	14.45	2.53	71.73	5.45
Jun	16.18	3.07	64.97	6.62
Jul	18.67	3.67	69.71	8.22
Aug	7.68	0.77	24.49	2.05
Sep	32.29	5.76	170.67	19.13
Oct	33.96	7.51	229.80	22.27
Nov	20.32	3.43	165.75	9.00
Dec	10.26	1.41	77.32	2.89

Delivered material loads were also modeled using SWAT for the years 1972-2010 included TSS, TN, and TP. As surface water flows were the only transport mechanism considered in this study, the minimum and maximum mean monthly delivered loads occurred in the same respective month as freshwater inflows (August and September). Mean monthly delivered loads ranged from 0.77 to 7.51 thousand

metric tons for TSS, 24.49 to 229.90 metric tons for TN, and 2.05 to 22.27 metric tons for TP (Table III-9). Delivered mean annual material loads were 33.37 thousand metric tons for TSS, 1111.05 metric tons for TN, and 94.47 metric tons for TP.

Table III-10. Descriptive statistics of annual freshwater inflows and delivered loads of total suspended solids (TSS), total nitrogen (TN), and total phosphorus (TP) from the Aransas River for 1972-2010. Values were estimated with SWAT.

Statistic	Annual Freshwater Inflows (million m^3)	Annual Delivered TSS Load (1000 mT)	Annual Delivered TN Load (mT)	Annual Delivered TP Load (mT)
Mean	188.93	33.27	1111.05	94.47
Median	142.82	21.89	740.04	70.81
Maximum	583.21	138.23	4639.62	334.97
Minimum	1.39	0.03	14.99	0.93

3.5 Discussion

3.5.1 Model Calibration and Validation

Predicted monthly mean daily streamflow was evaluated by calculating GOF indicators (NS, R^2, PD, d, RMSE, MAE) (Table III-5) and plot comparisons (Figures III-3, III-4, III-5, and III-6) that utilized observed data for the calibration period (Jan-1972 to Dec-1981) and validation period (Jan-1982 to Sep-1991) from a stream gage on Chiltipin Creek (08189800). For the calibration period, the model has satisfactory performance as target specifications of $NS \geq 0.5$, $R^2 \geq 0.6$, and PD from Engel et al. (2007) were met (Table III-5). Peak flows are generally when there is the least amount of agreement between predicted and observed streamflow, but this partially might be due

to high sensitivities that NS and R^2 have to extreme values ((Legates and McCabe Jr 1999, Harmel, Smith, and Migliaccio 2010). This is part of the reason why the index of agreement (d) is often used in model evaluation, and a favorable value of 0.89 for the index of agreement was calculated for the calibration period. Furthermore, land use for 1990 was used in SWAT; meaning that land change between the calibration period and 1990 could influence the pair-wise comparisons.

For the validation period, there is generally more agreement between predicted and observed streamflow, as depicted by the GOF indicators (Table III-5). The percent difference (PD) is the only GOF indicator that does not meet the target specifications (PD $\leq$ 15%) as it has a value of 40.68%. This is largely due to differences in the magnitude of peak flows between observed and predicted values (Figure III-4). The better agreement between predicted and observed streamflow, is partially due to land use being from 1990; a year that is in the tail-end of the validation period.

Appropriate model calibration could not be conducted for material (TSS, TN, and TP) loadings due to a lack of observed data that could be used in pair-wise comparison. SWAT estimates were compared to published estimates in the literature and government agency reports. Annual TSS loading and yield estimates from SWAT were compared to estimates from Welborn and Bezant (1978) and Brock et al. (2008) that were estimated using field samples and sediment transport curves. Estimated TSS loads from SWAT are much greater than the published loads (>100%), while the yields are fairly similar (PD $\leq$ 6%). The published estimates are for the stream gage on the Aransas River at Skidmore, TX (08189700) that is in the upper portions of the ARB, upstream of the LARB.

Relative to the LARB, there is much less cultivated land in the upper portions of the ARB. For example, according to the 1992 National Land Cover Dataset, over 80% of the cultivated land found within the ARB, is found within the LARB. Greater amounts of cultivated land has the potential to dramatically increase sediment loads and thus make TSS load estimates to be much greater when they include the LARB. Additionally, this helps explain why estimated TSS yields from SWAT are slightly greater than the published estimates.

Predicted annual delivered nutrient (TN and TP) loads and yields from the Aransas River for 2002 were compared to estimates from Rebich et al. (2011) that predicted estimates using a SPARROW model. For TN, SWAT estimates were dramatically greater than the Rebich et al. (2011) (PD = 44% for load and PD = 567% for yield). It is difficult to determine why the SWAT TN load is much greater than the estimate from Rebich et al. (2011) as their estimates include TN delivered by surface water flows and atmospheric deposition. On the other hand, the dramatic difference in the yields could be due to errors in the watershed area used in the yield calculation by Rebich et al. (2011). The ARB has an area of 2221 km^2, but the Rebich et al. (2011) calculation depicts a watershed area of 6404 km^2. Contrary to the TN estimates, delivered TP load had a PD of -35%, but the PD for TP yield is 204%. Again, this is likely due to a much larger watershed area used in the yield calculations by Rebich et al. (2011). Estimates from Rebich et al. (2011) have not been validated, thus it is difficult to dismiss any potential errors in their estimates.

3.5.2 Incorporation of Correction Factor

Correction factors to common GOF indicators as described by Harmel, Smith, and Migliaccio (2010) that incorporate measured and modeled uncertainty were utilized in a secondary evaluation of predicted monthly mean daily streamflow from SWAT. Three uncertainty distributions (normal, lognormal, and uniform) along with a family of assumed coefficients of variation (Cv) was used to estimate the standard deviation for each observed or predicted value in the sample. The standard deviations were used to estimate the degree of overlap (DO) between the uncertainty distributions for each observed and predicted pair.

The level of agreement between observed and predicted streamflow increased as the Cv (uncertainty) increased for all three uncertainty distributions (Table III-8). For example, the RMSE ranged from 57.33 to 49.85 for calibration period with a Cv of 0.026 and 0.256, respectively, under the normal uncertainty distribution. In general, the normal distribution experienced the greatest increase in the level of agreement between observed and predicted streamflow for the calibration and validation periods.

The incorporation of the correction factor functioned in the matter described by Harmel, Smith, and Migliaccio (2010) because as the uncertainty increases, the degree of overlap between observed and predicted values increases, that consequently decreases the level of deviation between values. Furthermore, Harmel, Smith, and Migliaccio (2010) argue that the correction factor will have a least significant impact to datasets that have greater degree of agreement. This is evident when comparing NS values for the calibration and validation periods against each other. NS values for the calibration period

range from 0.66 to 0.74 (difference of 0.08), while the NS values for the validation period range from 0.76 to 0.81 (difference of 0.05).

Harmel, Smith, and Migliaccio (2010) also present a model evaluation matrix with four cases that is based on model accuracy (GOF) and precision. Based on the analysis presented here, it can be inferred that the SWAT model for the LARB falls into Case 3 because there is high uncertainty in model predictions due to the potential for imperfect parameter estimation, but the model has good accuracy (at least for monthly mean daily streamflow).

3.5.3 SWAT Estimates of Freshwater and Material Inflows

Estimated mean monthly freshwater inflows to the M-A estuarine system from the Aransas River ranged from 7.78 to 33.96 million cubic meters (Table III-9) for the years 1972-2010. The fact that the Aransas River has not been obstructed by dams allows for this relatively large degree of variation in mean monthly freshwater inflows. Mean annual freshwater inflows also exhibited a large degree of variation as they ranged from 1.39 to 583.21 million cubic meters for the same time period. This makes intuitive sense as the M-A region has a semi-arid climate that experiences regular droughts with the occasional tropical storm bringing large amounts of rainfall to the region.

As part of the Texas Water Development Board's Bays and Estuary Program, Schoenbaechler and Guthrie (2011) provide a regional estimate of freshwater inflows to the M-A estuarine system from basins that drain into the estuary. For the time period 1972-2010, SWAT estimates for the Aransas River follow a fairly similar trend to regional estimates from Schoenbaechler and Guthrie (2011) (Figure III-7). SWAT

estimates of freshwater inflows for the Aransas River represented an average of 24.7% of the freshwater inflows for the region; with a range of 1.2 to 62.0% of the total freshwater inflows for the years 1972-2010.

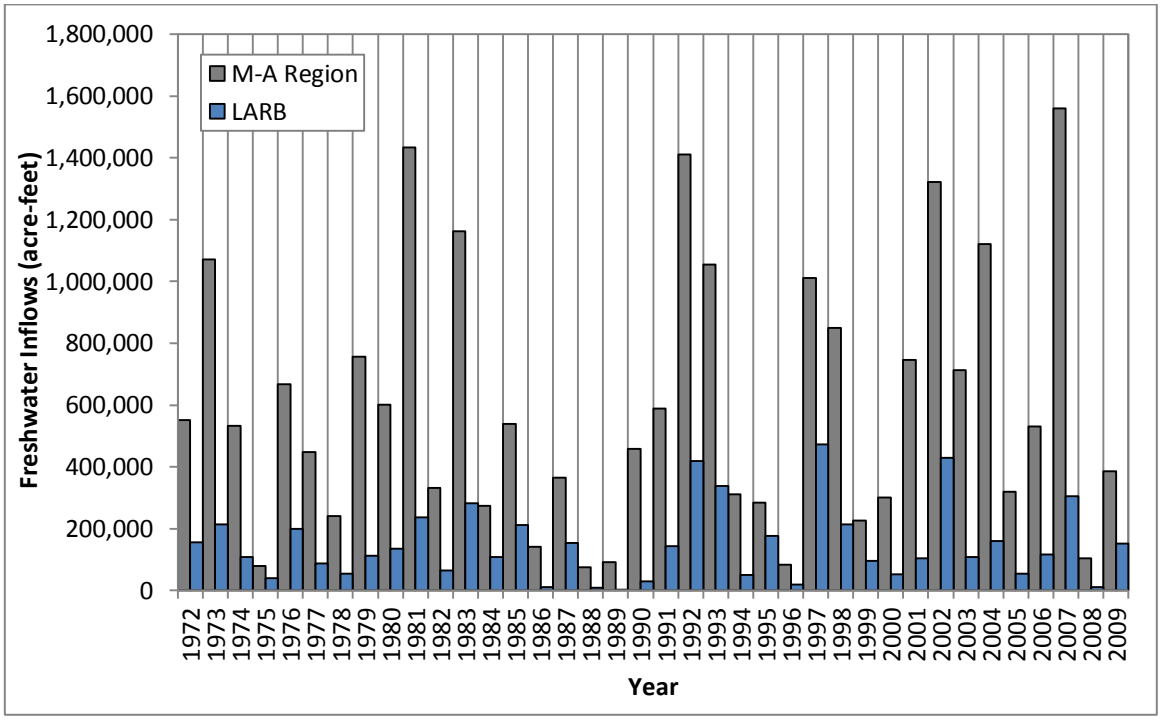

Figure III-7. Comparison between freshwater inflow estimates from the Texas Water Development Board (TWDB) for the Mission-Aransas (M-A) Region and SWAT estimates for the Lower Aransas River Basin. TWDB estimates are reported in Appendix B of Schoenbaechler and Guthrie (2011).

SWAT estimates of delivered TSS loads to the M-A estuarine system from the Aransas River very closely followed the trends in freshwater inflows with peak TSS loads occurring during times of peak flow (Figure III-8). This is expected as sediment transport from the flow of water was the only form of transport modeled in this study. Similarly, estimates of delivered loads of TN and TP tended to follow the freshwater

inflow trends (Figures III-9 and III-10, respectively), but not to the same degree as TSS. Peak loads of TP in particular deviated from the freshwater inflow trend with peak TP loads not occurring at time with peak freshwater inflows.

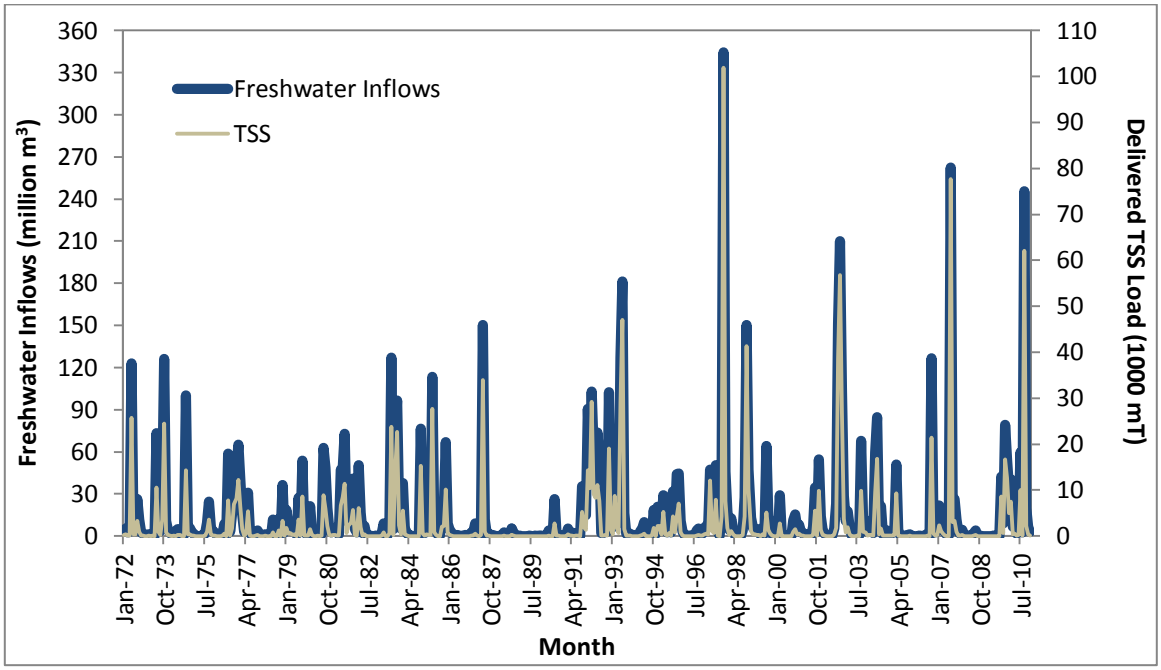

Figure III-8 Freshwater inflows and delivered total suspended solids (TSS) load to the Mission-Aransas estuarine system from the Aransas River for 1972-2010. Values were estimated using SWAT. Note: mT = metric ton.

When comparing delivered TSS loads with TN and TP loads, similar trends to those involving freshwater inflows and nutrients is found. Peak delivered loads of TSS and TN occur at the same points in time (Figure III-11), while peak TP loads occur at different times from the TSS loads (Figure III-12). The difference in these trends is likely due to aggregation of organic and inorganic nutrient into a total class. For

example, mineral phosphorus binds to soil and is transported along with TSS loads, but there is less organic phosphorus being transported during these times. As a final comparison, delivered loads of TN and TP were plotted together (Figure III-13). Once again, times of peak transport for the two nutrients do not occur during the same points in time.

Results from this analysis allow one to infer that SWAT estimates of delivered TSS and TN loads more closely follow freshwater inflow trends for the LARB.

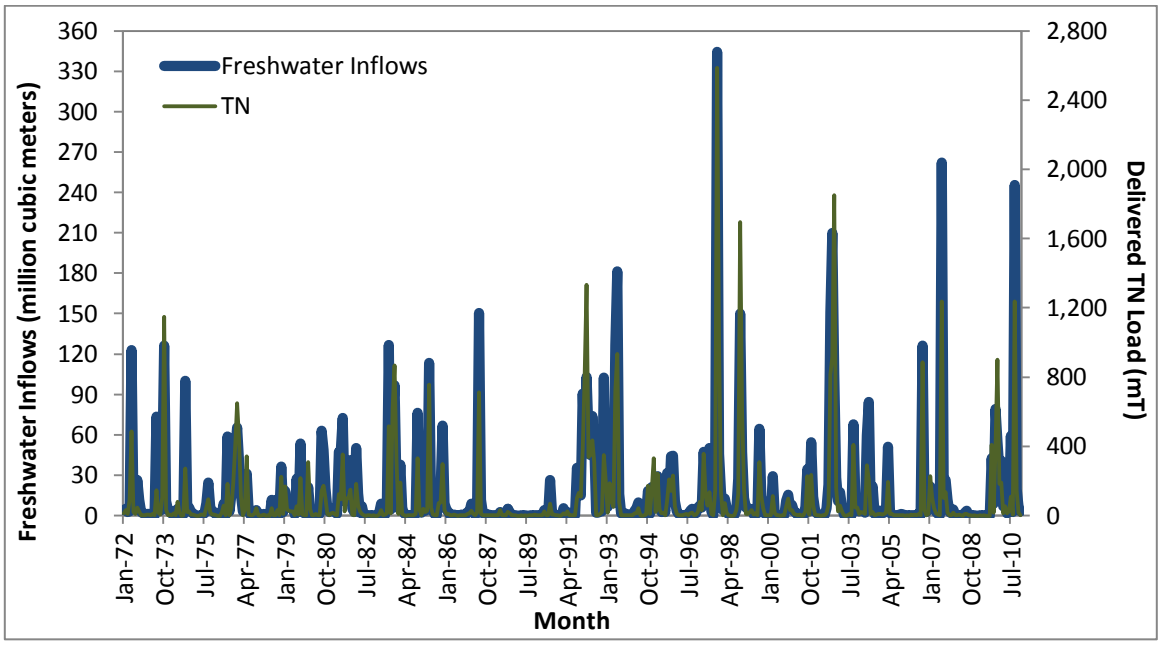

Figure III-9. Freshwater inflows and delivered total nitrogen (TN) load to the Mission-Aransas estuarine system from the Aransas River for 1972-2010. Values were estimated using SWAT. Note: mT = metric ton.

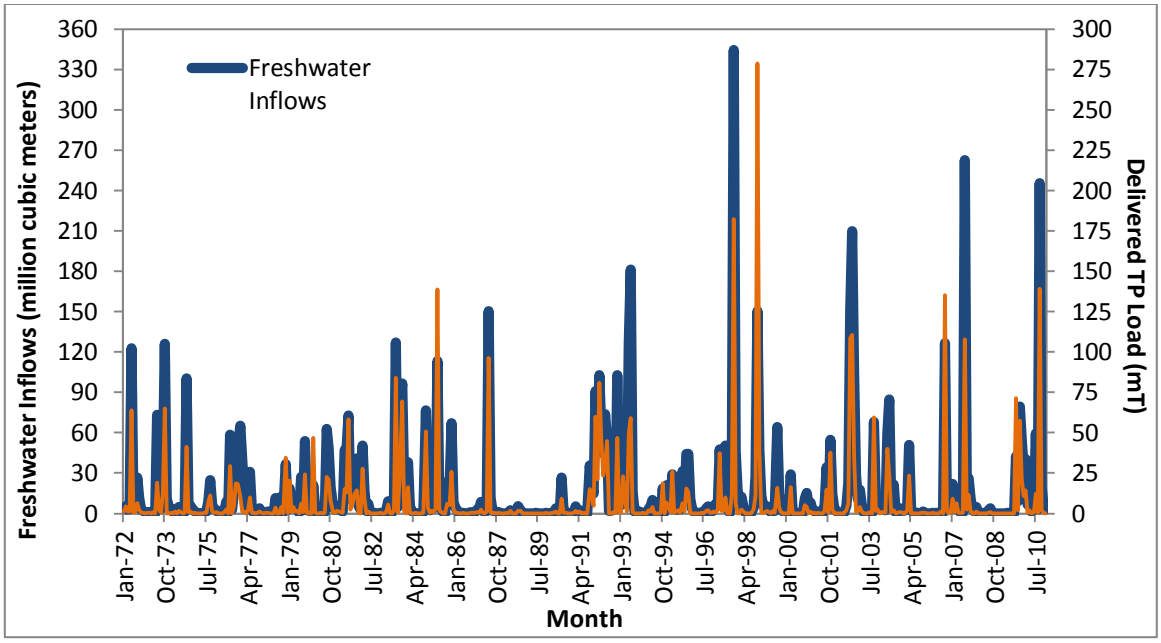

Figure III-10. Freshwater inflows and delivered total phosphorus (TP) load to the Mission-Aransas estuarine system from the Aransas River for 1972-2010. Values were estimated using SWAT. Note: mT = metric ton.

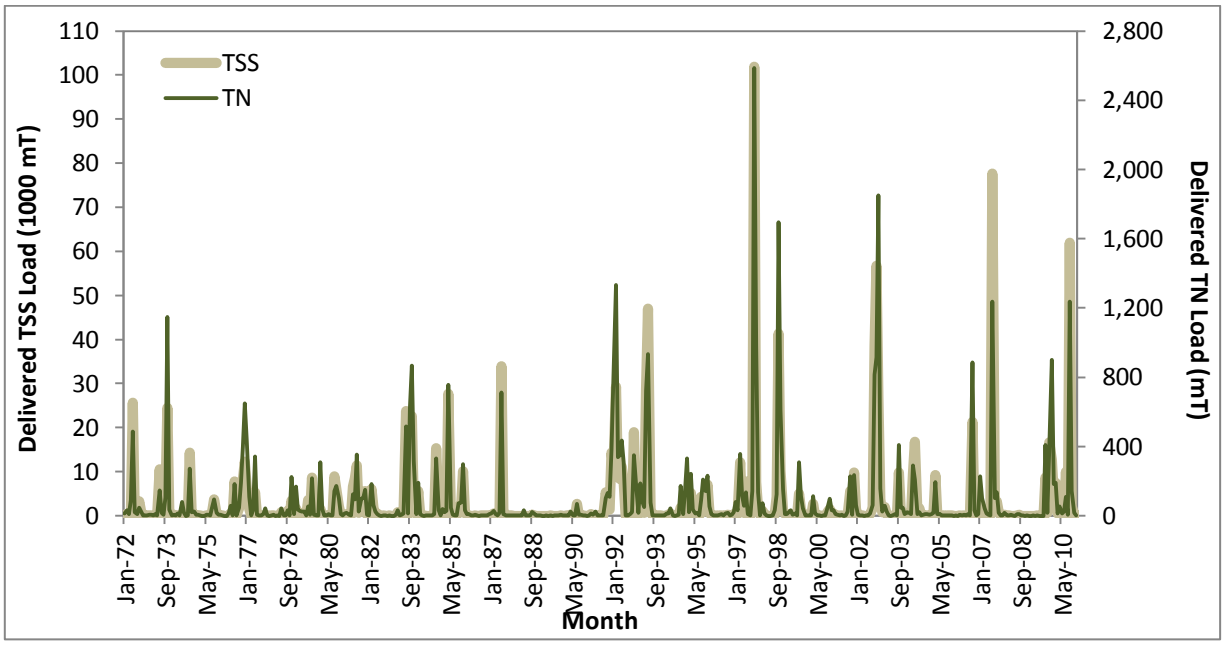

Figure III-11. Delivered total suspended solids (TSS) and total nitrogen (TN) loads to the Mission-Aransas estuarine system from the Aransas River for 1972-2010. Values were estimated using SWAT. Note: mT = metric ton.

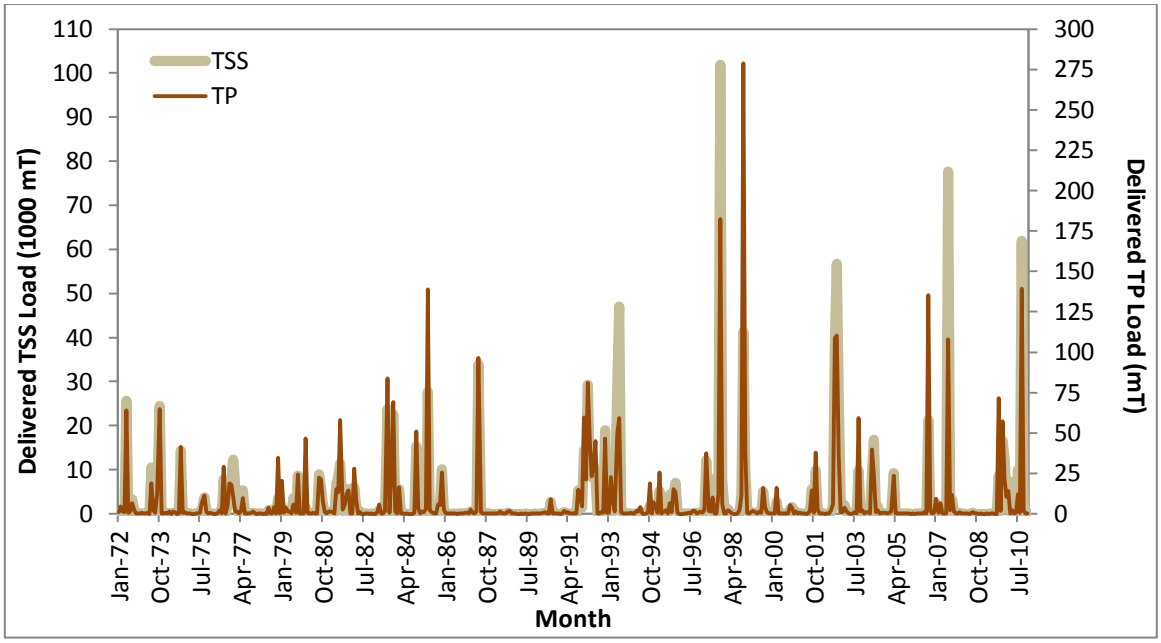

Figure III-12. Delivered total suspended solids (TSS) and total phosphorus (TP) loads to the Mission-Aransas estuarine system from the Aransas River for 1972-2010. Values were estimated using SWAT. Note: mT = metric ton.

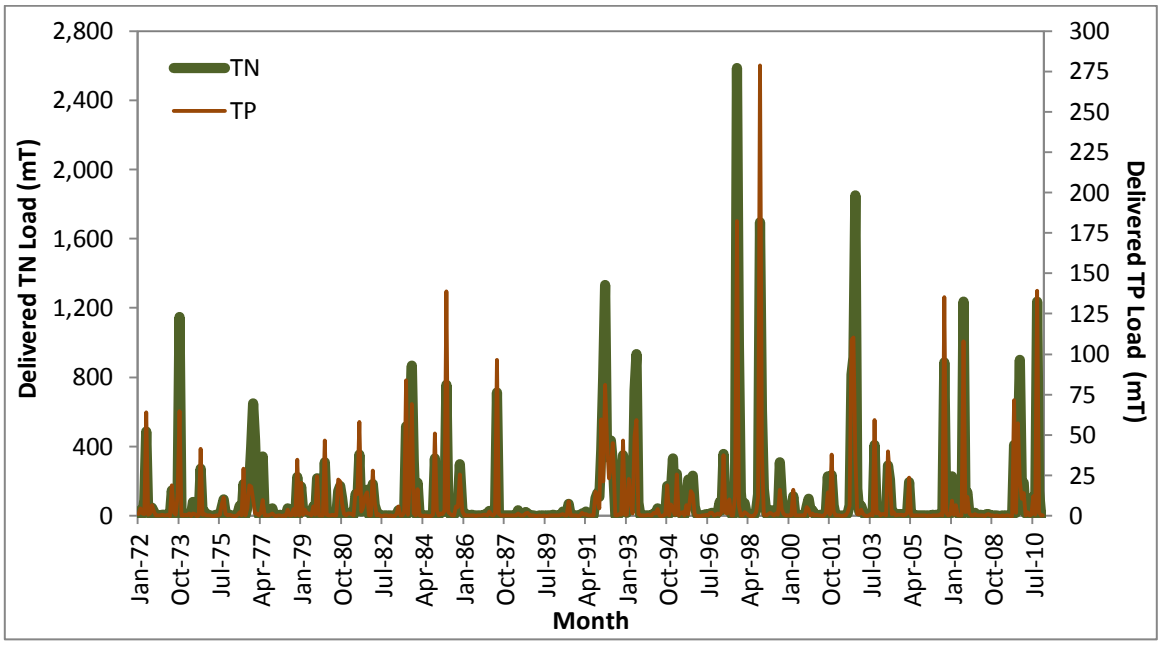

Figure III-13. Delivered total nitrogen (TN) and total phosphorus (TP) loads to the Mission-Aransas estuarine system from the Aransas River for 1972-2010. Values were estimated using SWAT. Note: mT = metric ton.

3.6 Conclusion

An assessment of the capabilities of SWAT to model freshwater inflows and loading of sediment and nutrients (TN and TP) was conducted. SWAT was calibrated for monthly mean daily streamflow using data from a USGS stream gage (08189800) on Chiltipin Creek. Evaluation of the calibrated model indicated that the model performed in a satisfactory fashion with an NS of 0.66, R^2 of 0.66, and PD of 5.57 for the calibration period (Jan-1972 to Dec-1981); and an NS of 0.76, R^2 of 0.78, and PD of 40.68 for the validation period (Jan-1982 to Sep-1991). Model parameters were also adjusted to try and match published estimates of sediment and nutrient loads, but SWAT estimates were very different.

In order to address the growing concern of uncertainty within the modeling community, a correction factor that incorporates measured and modeled uncertainty in common GOF indicators was computed for monthly mean daily streamflow. A family of correction factors was computed using three uncertainty distributions (normal, lognormal, and uniform) and four Cv values (0.026, 0.085, 0.192, and 0.256). The level of agreement generally increased as the Cv (uncertainty) increased with correction factors that utilized the normal distribution yielding the most promising results.

Using the calibrated model, freshwater inflows and loads of sediment and nutrients (TN and TP) to the M-A estuarine system from the Aransas River were estimated for the years 1972-2010. Mean annual freshwater inflows was 188.93 million cubic meters, with mean annual delivered loads of 33.27 thousand metric tons for TSS, 1111.05 metric tons for TN, and 94.47 metric tons for TP. With the exception of TP,

peak loads generally occurred during times of peak freshwater inflows, indicating that large flows are not the only factor influencing the delivery of TP to the coast.

The work presented here provided a successful application of SWAT to model freshwater inflows and associated sediment and nutrient loads. While more calibration is needed for more accurate results in sediment and nutrient loads, the model exhibits the behavior of the system fairly well. The incorporation of correction factors that considered measured and modeled uncertainty could prove very useful if this approach is used for management implications because there will be a greater degree of understanding the model's predictive abilities. Furthermore, the M-A National Estuarine Research Reserve is actively studying the effects of land use on the quantity and quality of freshwater inflows. SWAT was designed to model hydrologic impacts from various land use scenarios and this analysis has shown that SWAT can be a powerful tool in modeling hydrology within the Aransas River Basin.

CHAPTER IV

DEVELOPMENT OF LAND-USE/LAND-COVER CHANGE AND PRECIPITATION SCENARIOS

4.1 Introduction

Watershed hydrology is influenced by a number of factors that include climate, land use/land cover (LULC), soil characteristics, topography, geologic structure, and water resource management. Impacts to watershed hydrology from LULC change and variations in climate have gained a considerable amount of attention (Praskievicz and Chang 2011). The transformation of land for various uses can degrade water quality and disrupt the partitioning of precipitation into runoff, evapotranspiration, and groundwater flow (Foley et al. 2005). The characteristics of regional climate (e.g. precipitation, potential evapotranspiration, seasonality) are a major control of runoff volumes and timings (Praskievicz and Chang 2009). Furthermore, the type and intensity of precipitation can influence water quality (Howarth et al. 2011).

Coastal areas are not immune to potential issues associated with the transformation of land surfaces and climate change. In Texas, bays/estuaries and the drainage basins upstream from marine water bodies, are vital resources because these areas provide habitat for several fish and bird species of commercial and recreational value. Furthermore, development has continued to increase along the coast of Texas for industrial and municipal purposes. The Mission-Aransas (M-A) region on the Coastal Bend of Texas is an area with a complex mix of natural and anthropogenic land surfaces.

The bays and estuaries of the M-A region are especially sensitive to changes in LULC within drainage basins upstream because it can disrupt the volumes and timing of freshwater and material inputs that are vital in maintaining salinity gradients, sedimentation rates, and nutrient cycles within the system. Variations in climate within the M-A region can also disrupt ecological and anthropogenic systems. Extreme weather events such as tropical storms and flooding can dramatically alter the geometry of coastlines and disrupt the geomorphological characteristics of the coastal watershed that drain into the M-A system. On the other hand, times of drought reduce freshwater inflows and their associated sediment and chemical loads. These material inputs help sustain the ecological integrity of the estuary that is vital in sustaining fisheries and habit for endangered species, such as the whooping crane.

A hydrologic model (Soil and Water Assessment Tool (SWAT)) for the lower portions of the Aransas River Basin on the Coastal Bend of Texas was developed (Chapter III). This model utilizes historical weather data and LULC from 1990 and 2010 to simulate watershed hydrology. The SWAT model can be used to estimate freshwater inflows and the delivery of sediment and chemical loads to the M-A Estuary. The M-A National Estuarine Research Reserve (NERR) was established in 2006 with the primary mission of increasing the level of scientific knowledge and environmental stewardship associated with estuarine and coastal environments in Texas. One aspect of *Objective 1-7* of the M-A NERR management plan is aimed at understanding how changes in LULC and climate could impact the quantity and quality of freshwater inflows to the M-A estuarine system (NERRS 2006). A scenario analysis of how watershed hydrology and

water quality of the Lower Aransas River Basin could be impacted by changes in LULC and precipitation would provide useful information for adaptive management of the coastal and estuarine environment.

Coastal areas of the M-A region have recreational value that has driven urban development, especially in Aransas County (Morehead, Beyer, and Dunton 2007). Tourism and population has driven much of the increased concentration of urbanization along the coast. Most counties in the Aransas region have been experiencing population increases with communities becoming more densely populated (Morehead, Beyer, and Dunton 2007). The tourism industry and population dynamics are likely to cause increases in urban area. Furthermore, previous work has shown that developed land is expanding at fairly rapid rate. The expansion of developed land is characterized by the removal of permeable vegetative cover and the expansion of impervious surfaces that reduces infiltration; allowing greater amounts of rainfall to be converted to surface runoff that washes out sediment and pollutants stored on the surface to receiving water bodies. Thus, simulating SWAT with various scenarios of increasing development and precipitation within the Lower Aransas River Basin could provide some insight on how watershed hydrology could be impacted in the future.

4.2 Objectives

The work presented in this chapter is aimed at developing datasets of various scenarios of LULC change and precipitation that can be used as inputs to the Soil and Water Assessment Tool (SWAT) hydrological model. This research had two main tasks:

1. Develop three land use/land cover raster datasets that comprise three scenarios of the expansion of developed land (low, medium, and high) out to 2030 for the Lower Aransas River Basin (LARB).
2. Analyze and select daily weather data from records of climate stations in and around the LARB in order to have the continuous data that will encompass three precipitation scenarios (low, medium, and high) out to 2040 for the LARB.

4.3 Materials and Methodology

4.3.1 Study Area

The study area lies on the Coastal Bend of Texas just north of Corpus Christi. This area is part of the greater Mission-Aransas and Nueces river basin region; and it includes the lower portions of the Aransas River Basin (Figure IV-1) that will be referred to as the Lower Aransas River Basin (LARB). The boundary of the LARB was delineated using ArcSWAT procedures and it lies between 27.5 to 28.5 degrees north latitude and 98.0 to 97.0 degrees west longitude, with an area of 1384 km^2. The region has a semi-arid climate with mean annual precipitation of 864 mm and a mean temperature of 21.8 °C. However, the distribution of annual precipitation is skewed by seasonal tropical storms that occasionally bring large amounts of rainfall in late-summer and early-fall. Dominant LULC includes: cultivated land, rangeland, and woodland. The LARB region is predominantly rural with no large urban centers (Morehead, Beyer, and Dunton 2007). Within the LARB, the only prominent urban areas are Sinton and Taft that lie in the central and southeastern portions of the watershed (Figure IV-1).

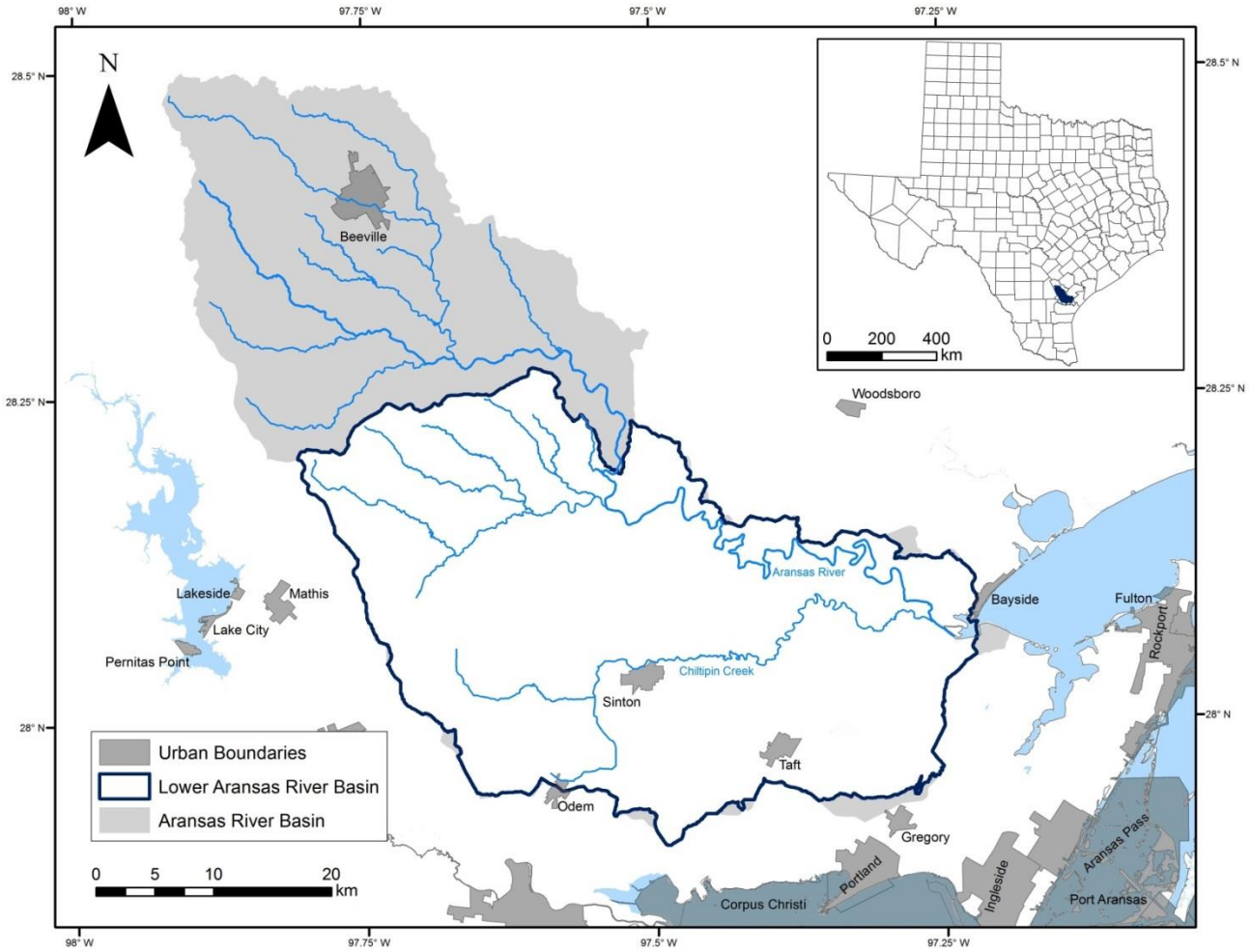

Figure IV-1. Location map of the Lower Aransas River Basin (LARB) (delineated with ArcSWAT); Aransas River Basin (ARB) (HUC: 12100407); and city boundaries (Texas Natural Resources Information System: StratMap. Note: blue polylines are streams. (Figure III-2 from Chapter III of Thesis).

4.3.2 Scenario Characterization

Three scenarios of LULC change with differing quantities in the expansion of developed land and three precipitation scenarios with differing amounts of average annual precipitation were developed (Table IV-1). The LULC change scenarios are differentiated and labeled with respective to relative differences in the predicted amounts of increased development within the LARB. Similarly, the precipitation scenarios are differentiated/labeled by relative differences in average annual precipitation.

Table IV-1. Description of land use/land cover and precipitation scenarios.

Scenario Code	Variable	Description
LD	Land Use/ Land Cover	Lower Expansion of Developed Land
MD	Land Use/ Land Cover	Medium Expansion of Developed Land
HD	Land Use/ Land Cover	Higher Expansion of Developed Land
LP	Precipitation	Lower amounts of Precipitation
MP	Precipitation	Medium Amounts of Precipitation
HP	Precipitation	Higher Amounts of Precipitation

4.3.3 LULC Change Scenarios

4.3.3.1 Data

The development of LULC change scenarios was conducted with a GIS land change model that called for variables to be in raster format, and the data used to generate these data is listed in Table IV-2. LULC for 1990 (Figure IV-2a) and 2010 (Figure IV-2b) were used to characterize historical LULC change within the study area and the coverage of each LULC for each year is described in Table IV-3. By

determining areas that transitioned to developed land from 1990 and 2010, the Variable Transformation Utility within the LCM can be used to calculate a predictor variable for the LCM that describes the relative frequency of a certain LULC class within an area that experienced change (Figure IV-3a). The expansion of developed land is more likely to occur in areas near development and major roads. LULC for 1990 was used to calculate the euclidean distance to developed land for every pixel (Figure IV-3b) and a roads shapefile was used to calculate the euclidean distance from farm-to-market roads and state, U.S., and interstate highways (Figure IV-3c). The proximity to surface water can have an influence on the location of developed land and a streams shapefile was used to calculate the euclidean distance to streams (Figure IV-3d). Areas with a higher concentration of people are also more likely to experience increased development and population data from 1990 for Census block-groups was used to calculate population density in 1990 for the study area (Figure IV-5e).

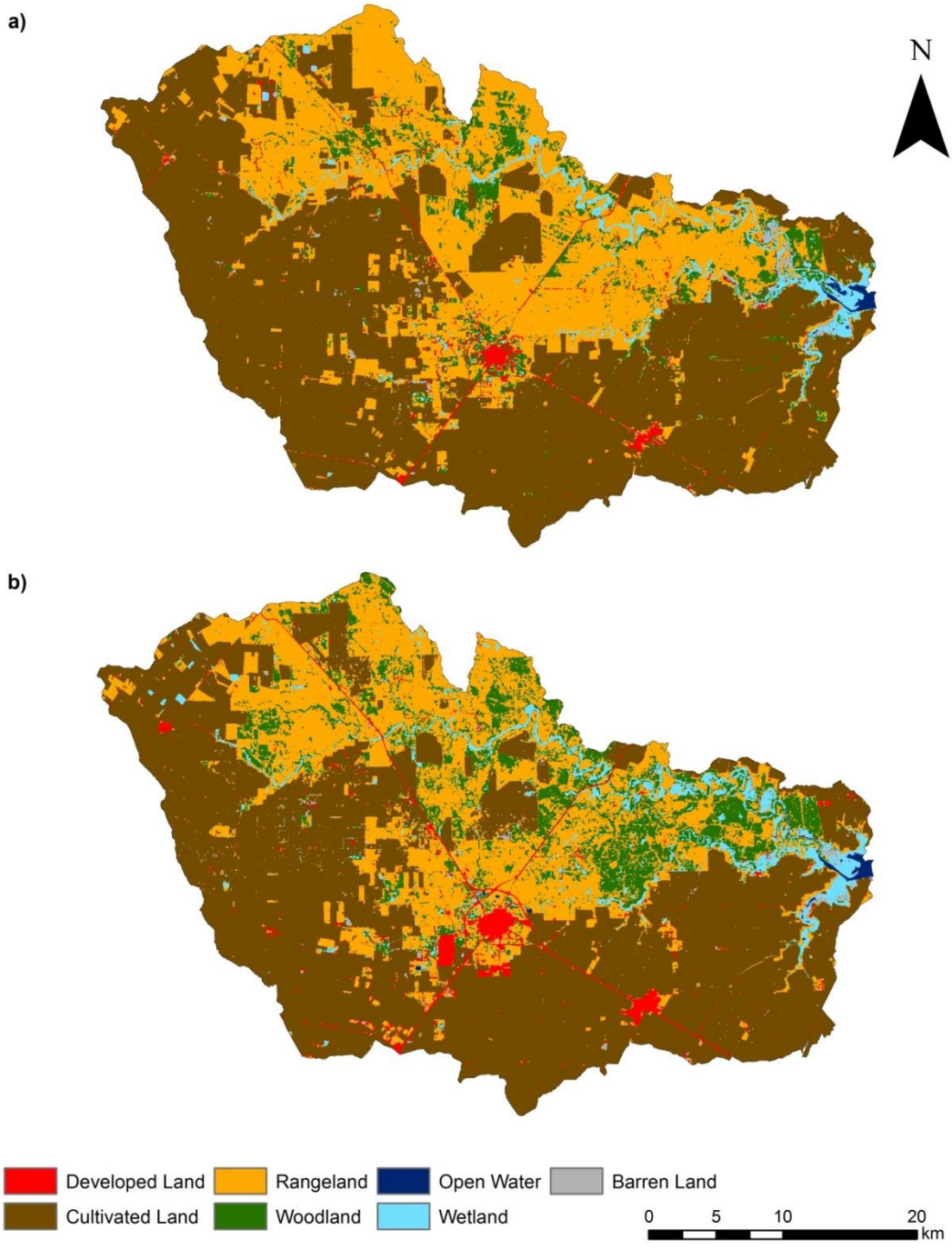

Figure IV-2. a) Land use/land cover for the Lower Aransas River Basin (LARB) in 1990. b) Land use/land cover for the LARB in 2010.

Table IV-2. Variables use in the land-use/land-cover (LULC) change modeling and the data used to generate/calculate these variables. Note: Thesis Chp. II refers to Chapter II in this Thesis.

Variable	Data used to generate/calculate variable	Data source
LULC for 1990	Landsat image	Thesis Obj. 1
LULC for 2010	Landsat image	Thesis Obj. 1
Likelihood of LULC class in area of change	LULC for 1990	Output from Variable Transformation Utility
Euclidean distance to development in 1990	LULC for 1990	Thesis Obj. 1
Euclidean distance to major roads	roads polyline shapefile	Texas Natural Resources Information Service: Strategic Mapping Program
Euclidean distance to streams	streams polyline shapefile	National Hydrography Dataset
Population density for 1990	Census block-group boundaries and population estimates	U.S. Census Bureau

Table IV-3. Coverage and percentage of total area for each land use/land cover class in the 1990 and 2010 LULC images.

	1990		2010	
Class	Coverage (km^2)	Percentage of Total Area (%)	Coverage (km^2)	Percentage of Total Area (%)
Developed Land	27.5	2.0	38.3	2.8
Cultivated Land	797.9	57.7	764.5	55.2
Rangeland	425.5	30.7	373.7	27.0
Woodland	82.2	5.9	141.6	10.2
Open Water	3.4	0.2	3.9	0.3
Wetland	40.5	2.9	54.5	3.9
Barren Land	6.7	0.5	7.2	0.5
Total	**1383.7**	**100.0**	**1383.7**	**100.0**

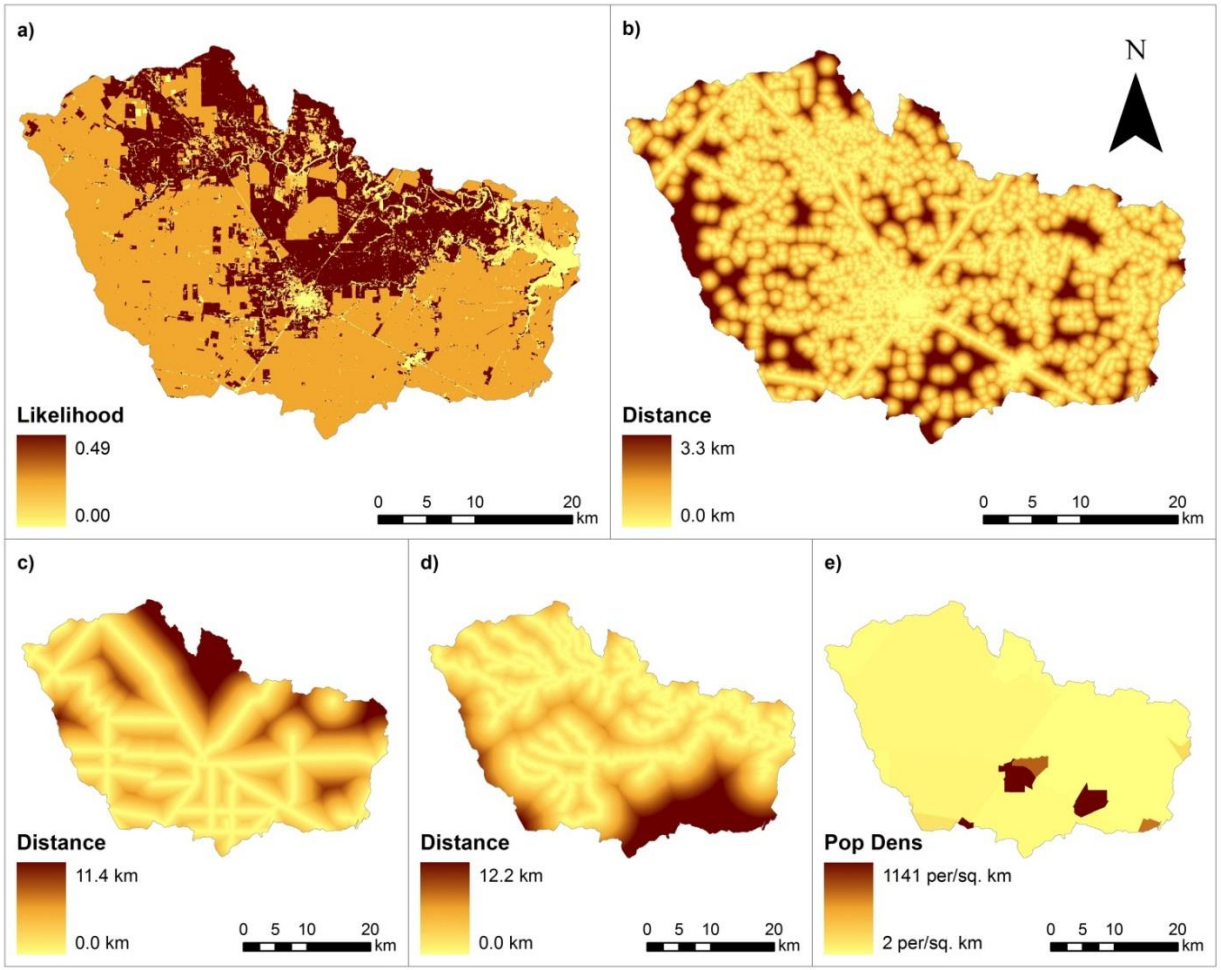

Figure IV-3. a) Output from Evidence Likelihood Transformation Utility. The likelihood of finding a particular land cover in an area where transition to developed land from 1990 to 2010 occurred. b) Euclidean distance to developed land use/land cover class. c) Euclidean distance to major roads. Major roads include farm-to-market roads and interstate, U.S., and state highways. d) Euclidean distance to streams. Location of streams is depicted by the National Hydrography Dataset. e) Population Density for Census Block-Groups in 1990.

4.3.3.2 Land Change Modeling

Three scenarios of the expansion of developed land (LD, MD, and HD) out to 2030 for the LARB were developed (Table IV-1). The Land Change Modeler (LCM) within the IDRISI Selva (Clark Labs 2012) GIS environment was employed to construct the raster data representing each LULC scenario. Within the LCM, three steps are necessary to develop each LULC scenario (Eastman 2012), and each step is described in the paragraphs below.

First, the base layers used to develop the LULC change scenarios were specified and they include: a before LULC dataset (1990; Figure IV-1a) and a later LULC dataset (2010; Figure IV-1b). Protected areas were masked out from the LULC datasets under the assumption that the expansion of developed land will not occur within these areas. After loading the LULC datasets, the LCM checks both datasets to ensure that they have identical attributes, projections, extents, and spatial resolution. Tools within the LCM (Harmonize) were used to process the LULC datasets to ensure that all criteria were met. Once all criteria are met, the Variable Transformation Utility within the LCM was used to construct the Evidence Likelihood predictor variable that computes the relative frequency of pixels from each LULC class within areas of LULC transition (Eastman 2012). The transition to developed land from 1990 to 2010 by other LULC classes was the type of LULC change of interest in this analysis, thus the output from the Variable Transformation Utility describes the likelihood of finding a particular LULC class in an area where the expansion of developed land occurred.

Second, the land transition potentials were established that defines the predictor variables and constraints that will be used to model LULC change. The LCM automatically detects the combinations of LULC change that occurred between the earlier (1990) and later (2010) images for all classes. For this analysis, the LULC transitions being modeled are: cultivated land-to-developed land; rangeland-to-developed land; woodland-to-developed land; wetland-to-developed land; and barren land-to-developed land. All transitions were modeled collectively using a common sub-model (function). A variety of different spatially explicit continuous variables for each pixel in the study area were tested as potential predictor variables with the final combination being: evidence likelihood of finding a particular LULC in an area where transition to developed land from 1990 to 2010 occurred (Figure IV-3a), euclidean distance to developed land in 1990 (Figure IV-3b), euclidean distance to major roads (Figure IV-3c), euclidean distance to streams (Figure IV-3b), and population density for 1990 by Census block-group (Figure IV-3e). Predictor variables can be specified as static or dynamic over time; all predictor variables other than distance to developed land in 1990 were specified as static. The LCM provides three methods for fitting a function that model LULC change and they include logistic regression, a SimWeight procedure, and the Multi-Layer Perceptron (MLP) neural network; the MLP was employed here because it allows multiple LULC classes to be modeled in a single run. The MLP conducts a training procedure over a user specified number of iterations that models pixels that transitioned and those that persisted from the earlier and later LULC raster datasets, while adjusting the function over each iteration by trying to minimize the root

mean square error from a sampling of pixels that checks the prediction accuracy of changed and persisted pixels. The MLP was run using automatic training, a dynamic learning rate, and a variety of parameter specifications. Ultimately, default parameter specifications yielded the best results and they are listed in Table IV-4. Once the MLP training procedure was complete, a transition potential image for each LULC class was generated. A transition potential assigns a value from 0 to 1 to every pixel for that class that describes the likelihood of that pixel transitioning to developed land with values closer to 1 being more likely to transition.

Table IV-4. Parameter specifications for the Multi-Layer Perceptron (MLP) neural network.

Parameter	Value
Start Learning Rate	0.01
End Learning Rate	0.001
Momentum Factor	0.5
Sigmoid Constant a	1.0
Input Layer nodes	5
Iterations	10000
Samples Per Class	564

Third, the LCM allows two types of LULC change predictions (soft and hard) to be made. A soft prediction identifies pixels that are most vulnerable to change using the transition potentials, while a hard prediction makes a prediction of the amount of change that occurs and generates a new LULC image/map using a multi-objective land allocation algorithm with quantities of change determined using a Markov chain procedure (Eastman 2012). As the earlier (1990) and later (2010) images used to model

LULC change comprised two decades worth of data, it made logical sense to make a prediction out to 2030. A Markov matrix that assigns a transition probability to each LULC class is used to adjust the amount of change that will occur over the prediction time-line. The Markov matrix generated by the transition potentials was originally making predictions of fairly high expansion of developed land (development increased by over 70%). To avoid the cumbersome trial and error task of modifying the Markov matrix, a different approach was utilized. When generating a prediction using the Markov process, the LCM gives the option of setting the number of recalculation stages/steps for dynamic variables (distance to developed land in this case). A recalculation stage of 1 is the default, but by increasing the number of recalculation stages, the total amount of change is divided linearly to each stage in the allocation of LULC change (Eastman 2012). By increasing the recalculation stages to 2 or 3, the number of pixels that transition to developed land is one half or one third, respectively, of what it would be with one recalculation stage. Three predictions of the expansion of developed land (low, medium, and high) out to 2030 were run using a recalculation stage of 1 (HD), 2 (MD), and 3 (LD).

4.3.4 Precipitation Scenarios

4.3.4.1 Data

Daily precipitation data from 1950 to 2012 was analyzed to identify wetter and drier time periods. Data from eight weather stations with differing periods of record were downloaded from the National Climatic Data Center (Table IV-5). To have a continuous time-series of precipitation data from 1950 to 2012 for each weather station,

available data from the nearest weather station was utilized when data was unavailable for each respective weather station.

Table IV-5. Weather in and around the Lower Aransas River Basin (LARB). Data downloaded from the National Climatic Data Center website.

Station GHCND	Name	Elevation (m)	Latitude (DD)	Longitude (DD)	Period of Record
USC00410302	Aransas Pass 2 TX US	3.0	27.90	-97.17	01/01/1950 - 07/31/1971
USC00410639	Beeville 5 NE TX US	67.1	28.45	-97.70	01/01/1950 - 12/31/2012
USW00012925	Beeville Chase NAAS TX US	20.1	28.37	-97.67	08/02/1954 - 09/30/1992
USC00415661	Mathis 4 SSW TX US	24.1	28.10	-97.82	07/01/1964 - 12/31/2012
USW00012972	Rockport Aransas CO Airport TX US	6.7	28.08	-97.05	07/01/1996 - 12/31/2012
USC00417704	Rockport TX US	2.1	28.02	-97.05	01/01/1959 - 12/31/2012
USC00418354	Sinton 3 NW TX US	14.9	28.03	-97.52	02/04/1950 - 12/31/2012
USC00419559	Welder W Life Found TX US	14.9	28.10	-97.42	10/01/1964 - 12/31/2012

4.3.4.2 Precipitation Data Selection

Three precipitation scenarios (low, medium, and high) of continuous daily precipitation and temperature data out to 2040 were developed (Table IV-1). Data from each of the eight weather stations was used to calculate an aerial weighted average time-series of daily precipitation for the LARB. This daily precipitation time-series was aggregated to an annual time-scale (Figure IV-4).

Given that a continuous time-series of daily precipitation out to 2040 was needed, 28 years of data needed to be selected for each scenario. A 14-year moving

average of annual precipitation from 1950 to 2012 was calculated (Figure IV-5), in order to select two 14-year time-periods (28 years) of weather data. For example, the 14-year average annual precipitation for 2012 calculates the average annual precipitation for the time-period from 1999 to 2012. The two non-overlapping 14-year periods with the lowest average annual precipitation, as depicted by the moving average, were selected for the low precipitation (LP) scenario. Similarly, two non-overlapping 14-year periods with average annual precipitation closest to the median value were selected for the medium precipitation scenario (MP); and two 14-year non-overlapping periods with the greatest average annual precipitation were selected for the high precipitation (HP) scenario

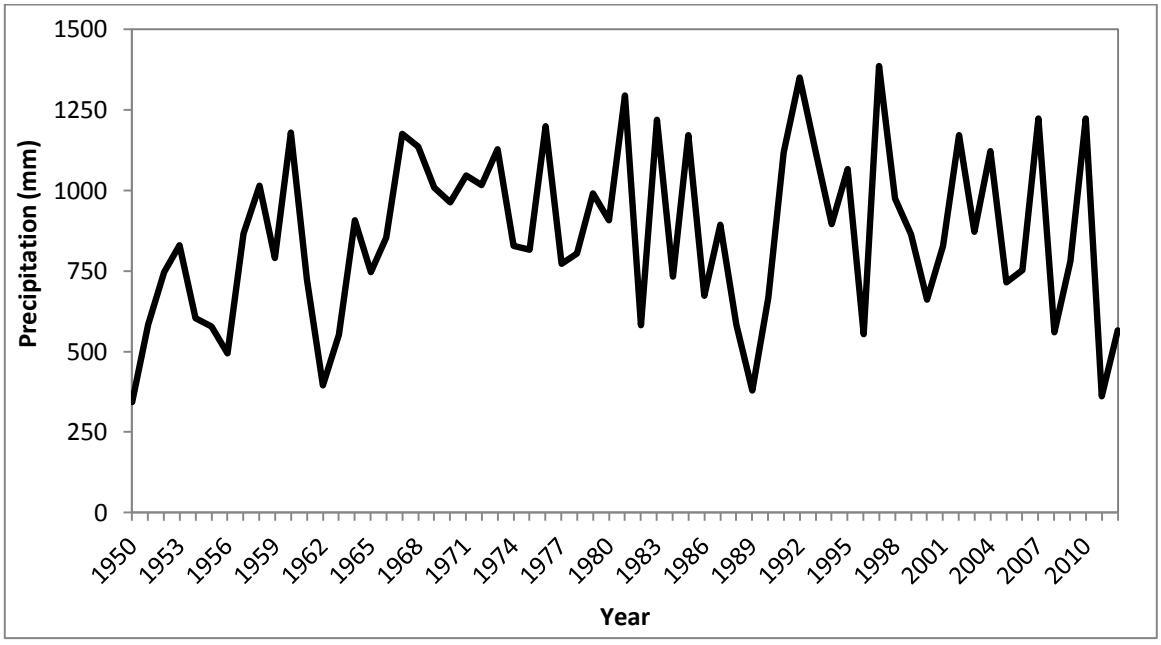

Figure IV-4. Aerially weighted time-series of annual precipitation for the Lower Aransas River Basin (LARB) for the time-period 1950-2012.

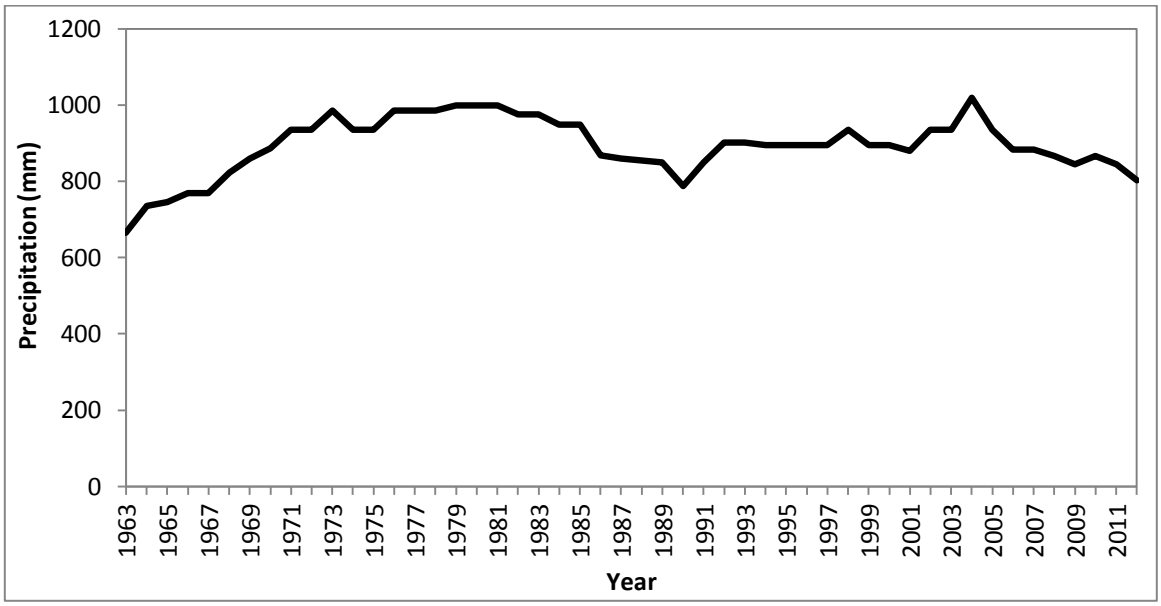

Figure IV-5. Moving average (14-year) of annual precipitation for the Lower Aransas River Bains (LARB). Precipitation data from 1950 to 2012 was used to calculate the 14-year moving average.

4.4 Results

4.4.1 LULC Change Scenarios

4.4.1.1 LCM-MLP Training

The MLP training procedure develops a neural network between an input layer, a hidden layer, and the output layer. Communication between each layer in the neural net is passed through a number of nodes in each layer. While conducting the training procedure, the MLP uses the user specified number of input nodes to determine the number of nodes in the hidden and output layers to most accurately predict the LULC changes being modeled. The final number of nodes for the hidden and output layers was 14 and 10, respectively (Table IV-6). A dynamic learning rate for the training procedure

was utilized with a final learning rate of 0.003. In terms of the overall accuracy of the predictive abilities of the MLP, estimates of the training and testing root mean square error (RMS) (Table IV-6) were used to calculate an accuracy rate of 63.72% for the prediction. These statistics were used by the LCM to determine that the model had a skill measure of 0.5968 in predicting LULC change between 1990 and 2010 (Table IV-6).

Table IV-6. Performance of Multi-Layer Perceptron (MLP) neural network training procedure for predicting land use/land cover (LULC) change between the earlier (1990) and later (2010) LULC images. Note: RMS = root mean square error.

Parameter	Value
Input Layer Nodes	5
Hidden Layer Nodes	14
Output Layer Nodes	10
Final Learning Rate	0.0003
Training RMS	0.2129
Testing RMS	0.2165
Accuracy Rate	63.72%
Skill Measure	0.5968

4.4.1.2 LULC Change Predictions

Three scenarios of increased development going out to 2030 were generated using the LCM (Figure IV-6). For the LD scenario (Figure IV-1a), most of the transition to developed land occurs in the vicinity of urban areas (Sinton and Taft). There is a similar trend for the MD scenario, but there is also an increased amount of change occurring in areas near major roads (Figure IV-2a). Much more transition to developed land occurs in urban areas and along roads under the HD scenario (Figure IV-3a).

Increases in the coverage of developed land ranged from 9 to 27 km^2 between the LD and HD scenarios (Table IV-7). The use of 1, 2, and 3 recalculation stages in the Markov chain process allowed for the LD and MD scenarios to predict one-third and one-half, respectively, of the LULC change predicted by the HD scenario (Table IV-7).

Table IV-7. Comparison between the aerial coverage of developed land for successive time-periods. Land use/land cover change scenarios for 2030 include low expansion of developed land (LD), medium expansion of developed land (MD), and high expansion of developed land (HD). Note: Values for 2010 are compared to values for 1990 and values for 2030 are compared to values from 2010.

Year/Scenario	Coverage (km^2)	Increase in Coverage (km^2)	Percent Difference (%)
1990	27.5	na	na
2010	38.3	10.8	39.4
2030-LD	47.3	9.0	23.5
2030-MD	51.8	13.5	35.3
2030-HD	65.3	27.0	70.6

Output from the Markov chain process yielded a distinct map of LULC in 2030 for each LULC change scenario (Figure IV-7). Each map differs in the quantity of land comprised by each LULC class (Table IV-8). With the exception of developed land comprising a higher proportion of the LARB than wetlands under the HD scenario, there are no major changes in the proportions comprised by each LULC class for the other LULC change scenarios.

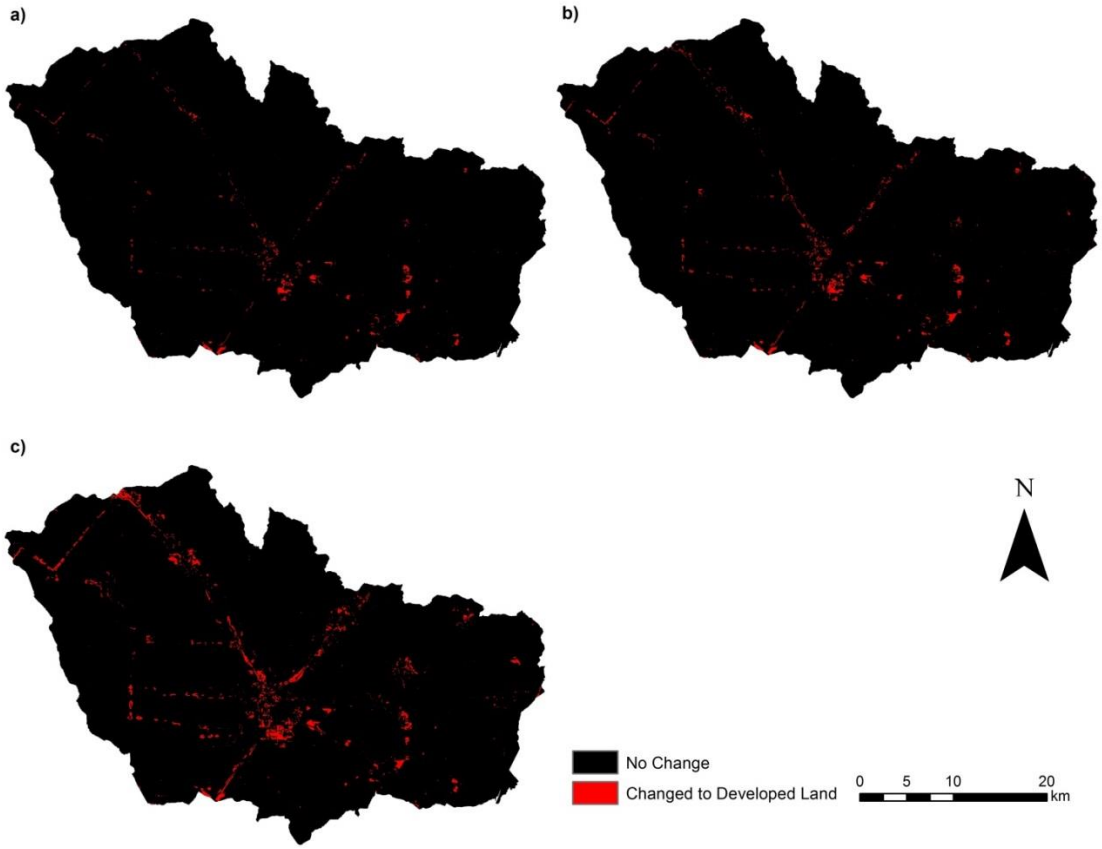

Figure IV-6. a) Land use/land cover change between 2010 and 2030 for the low expansion of developed land (LD) scenario. Three recalculation stages for distance to developed land were used in the Markov Chain process. b) Land use/land cover change between 2010 and 2030 for the medium expansion of developed land (MD) scenario. Two recalculation stages for distance to developed land were used in the Markov Chain process. c) Land use/land cover change between 2010 and 2030 for the high expansion of developed land (HD) scenario. One recalculation stage for distance to developed land was used was used in the Markov Chain process. Note: All expansion of developed land scenarios were generated using the Land Change Modeler in the Idrisi Selva GIS environment.

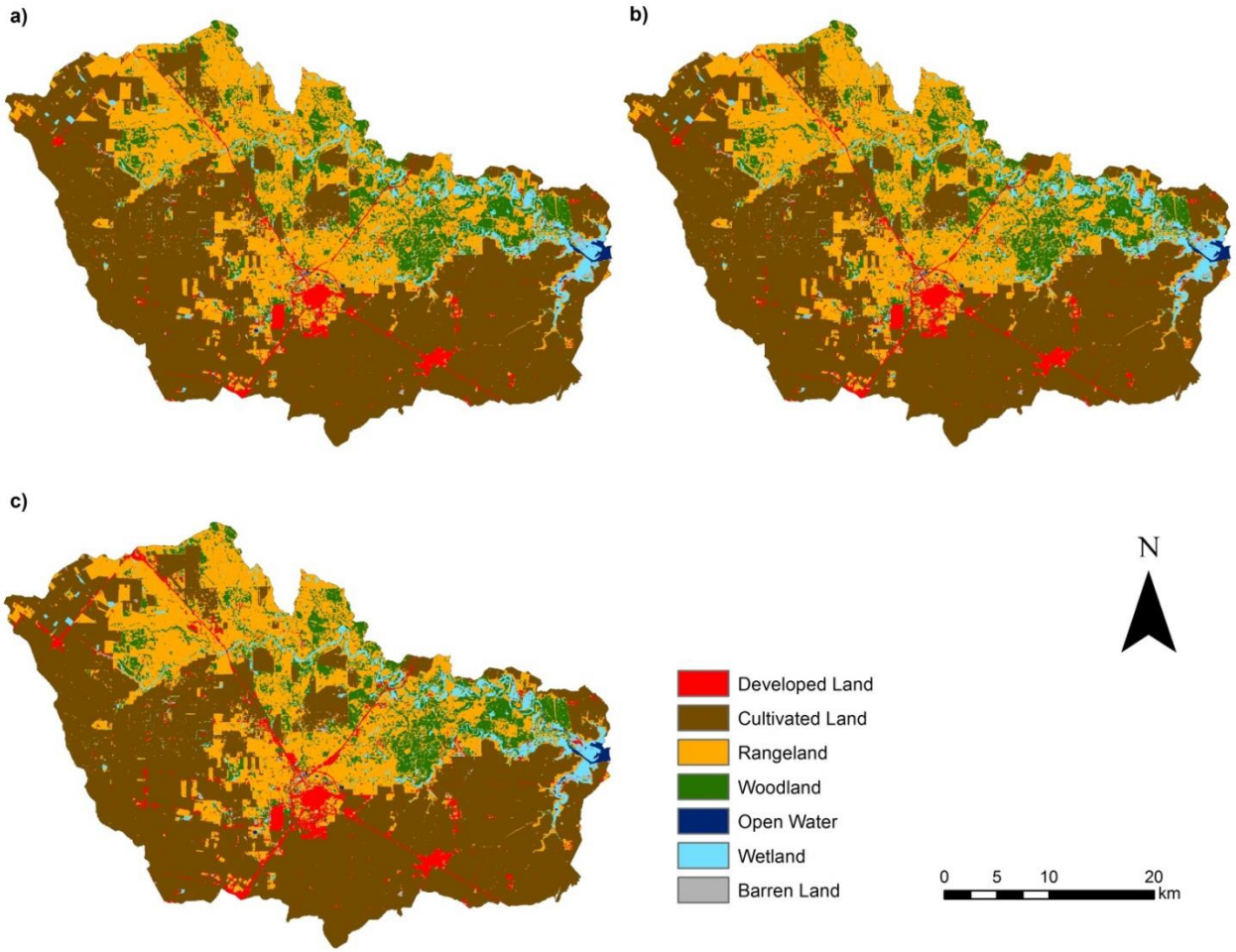

Figure IV-7. a) Land use/land cover in 2030 for the low expansion of developed land (LD) scenario. b) Land use/land cover in 2030 for the medium expansion of developed land (MD) scenario. c) Land use/land cover in 2030 for the high expansion of developed land (HD) scenario.. Note: All land use/land cover scenarios were generated using the Land Change Modeler in the Idrisi Selva GIS environment.

Table IV-8. The coverage and percentage of total area for the lower expansion of developed land (LD), medium expansion of developed land (MD), and high expansion of developed land (HD) scenarios of LULC for 2030.

	2030					
	LD		MD		HD	
Class	Coverage (km^2)	Percentage of Total Area (%)	Coverage (km^2)	Percentage of Total Area (%)	Coverage (km^2)	Percentage of Total Area (%)
Developed Land	47.3	3.4	51.8	3.7	65.3	4.7
Cultivated Land	762.2	55.1	761.0	55.0	757.6	54.7
Rangeland	370.1	26.7	368.2	26.6	362.7	26.2
Woodland	139.0	10.0	137.7	10.0	133.8	9.7
Open Water	3.9	0.3	3.9	0.3	3.9	0.3
Wetland	54.3	3.9	54.2	3.9	53.8	3.9
Barren Land	7.0	0.5	6.9	0.5	6.6	0.5
Total	**1383.7**	**100.0**	**1383.7**	**100.0**	**1383.7**	**100.0**

4.4.2 Precipitation Scenarios

Precipitation data from 1950 to 2012 was analyzed using a 14-year moving average to identify time periods that had lower, medium, and higher amounts of annual precipitation. The 14-year periods selected for each precipitation scenario are listed on Table IV-9. Average annual precipitation for the LP, MP, and HP scenarios is 763, 907, and 996 mm, respectively.

The weather data selected for these scenarios was combined with historical data to have three time-series from 1950 to 2040 for each precipitation scenario (Figure IV-8). As historical data was used, there are no significant differences between the data for 2013-2040 and the historical record. By viewing the entire record of precipitation data (1950-2040), it is a little difficult to notice the differences in the overall trend of

synthetic precipitation data, but the trends are more apparent when only focusing on the time-period from 2013 to 2040 (Figure IV-9). The LP scenario displays a decreasing linear trend going out to the future that is well below the MP trend line. The MP and HP scenario trends remain fairly constant, but the HP trend line is greater by ~100 mm throughout the time-period.

Table IV-9. Assignment of historical weather data to dates in the future dates and the corresponding precipitation scenario. Note: LP = lower precipitation; MP = medium precipitation; higher precipitation.

Scenario	Assigned Time Period	Historical Time Period	Average Annual Precipitation (mm)
LP	2013 - 2026	1977 - 1990	833
LP	2027 - 2040	1950 - 1963	693
MP	2013 - 2026	1985 - 2008	903
MP	2027 - 2040	1975 - 1988	910
HP	2013 - 2026	1968 - 1981	993
HP	2027 - 2040	1991 - 2004	998

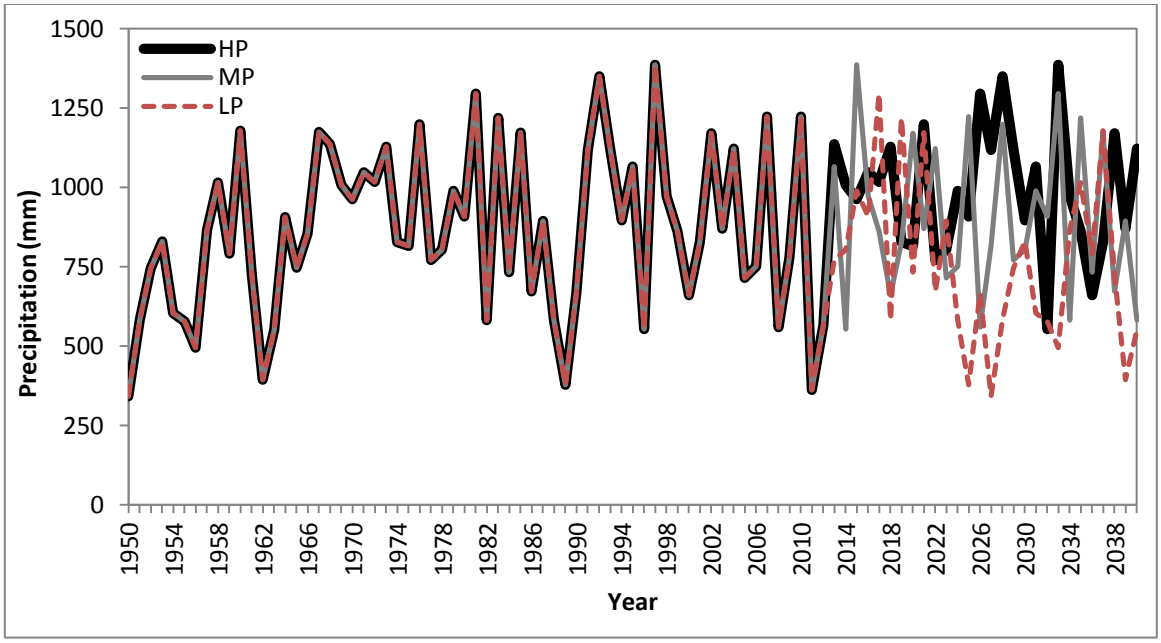

Figure IV-8. Time-series' of annual precipitation for 1950 - 2040 for the lower precipitation (LP), medium precipitation (MP), and higher precipitation scenarios.

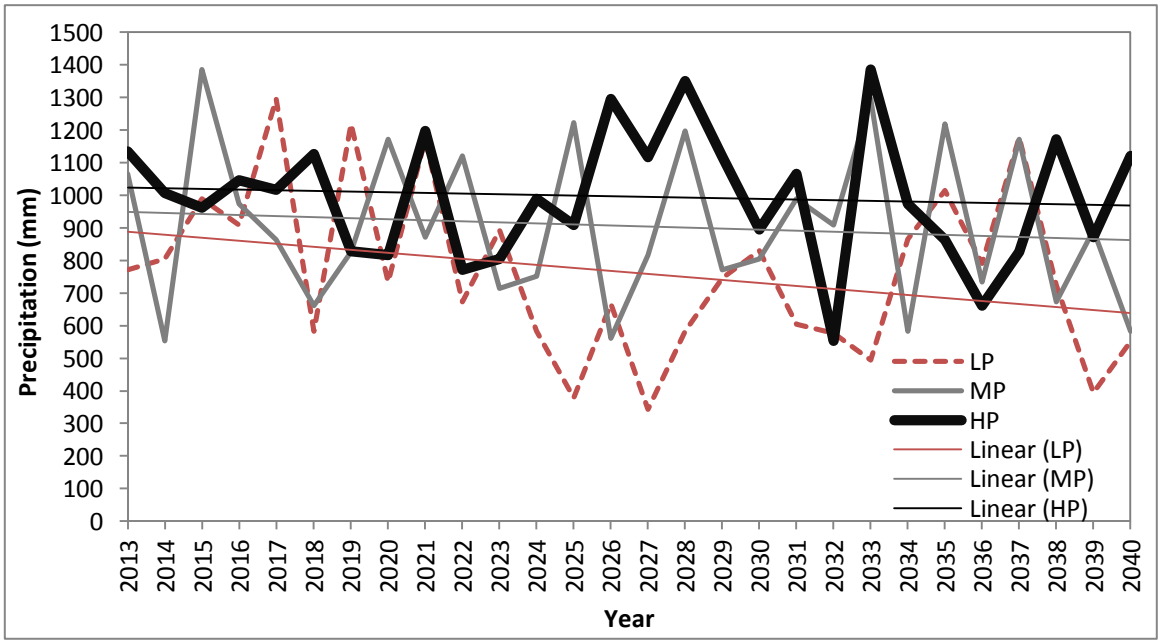

Figure IV-9. Time-series' of annual precipitation and linear trend line for each scenario for the time-period from 2013 to 2040.

4.5 Discussion

4.5.1 LULC Change Scenarios

The MLP training procedure had a fairly low accuracy rate of 63.7%. While barren land comprised the least amount of area within the LARB, the MLP performed very poorly in modeling the persistence or transition of barren land to developed land. For example, under the HD scenario (Figure IV-3c), the LCM predicted a transition from the barren land to developed at the mouth of the Aransas River in an area completely surrounded by wetlands and open water. Nonetheless, the LCM performed reasonably well with most expansion of developed land occurring near urban areas and major roads.

It is difficult say which LULC change scenario is a more realistic prediction of LULC change for the LARB out to 2030. There is a large degree of uncertainty associated with LULC change predictions. Given the rural character of the LARB, it can be assumed that the LD and MD scenarios are more realistic because the rates of LULC change are more similar to the historical trend. Nonetheless, it will be interesting to examine how the HD scenario affects the watershed hydrology and water quality of the LARB.

4.5.2 Precipitation Scenarios

Annual precipitation varied significantly from 1950 to 2012 (Figure IV-4). The minimum annual precipitation occurred in 1950 (342 mm) and the maximum occurred in 1997 (1384 mm). Oscillations between wet and dry years are abrupt and occur regularly throughout the time period, but especially over the last 3 decades. The only visible trend

in annual precipitation is the area gradually becoming wetter as it comes out from the drought of record in the 1950s.

Observed precipitation for the LARB was analyzed at an annual scale. Extreme weather events, such as tropical storms, can skew annual statistics and potentially make a relatively dry year seem like a wet year. The utilization of a different time-scale (e.g. seasonal or monthly) would likely have called for the selection of different time-series' of precipitation. Furthermore, an average was used as the analyzing statistic for the 14-year window, using a different statistic such as the median could have yielded different results.

To avoid the time consuming effort of statistically downscaling a climate change prediction, observed data was used to develop the precipitation scenarios. Any climatological forecast carries a large degree of uncertainty, whether it was developed using a climate model or observed data. As this analysis is not attempting to make a climate prediction for the LARB, it seems reasonable to use observed data in developing the precipitation scenarios.

4.6 Conclusion

Three LULC change scenarios and three precipitation scenarios were developed to be used in a SWAT hydrological model calibrated to conditions for the LARB. The LULC change scenarios each represent a different amount of increasing development within the LARB and they were generated using the LCM in the Idrisi Selva GIS environment. The MLP neural network within the LCM was used to conduct a training procedure that modeled LULC change using historical LULC images (for1990 and

2010) and predictor variables (e.g. distance to major roads, distance to developed land in 1990). The training procedure yielded an accuracy rate of 63.7%. A Markov chain process was used to generate three scenarios of increased development (low: 23.5%, medium: 35.3%, and high: 70.6%) within the LARB.

Precipitation data from 1950 to 2012 was analyzed at an annual scale to select 28 years of weather data that comprised each precipitation scenario (low, medium, and high). A 14-year moving average was used to select two 14-year periods for each precipitation scenario. Average annual precipitation for the low, medium, and high scenarios is 763, 907, and 996 mm, respectively.

These scenarios will be used to gain insight into how these types of changes could impact watershed hydrology and water quality for the LARB. Furthermore, they will be used to assess how freshwater inflows and delivered loads of sediment and nutrients to the Mission-Aransas estuary could potentially be impacted. This type of information will be useful for the overall management Mission-Aransas estuary and the surrounding drainage basins.

CHAPTER V

SCENARIO ANALYSIS OF IMPACTS TO WATERSHED HYDROLOGY AND WATER QUALITY

5.1 Introduction

The hydrologic cycle controls the volume and timing of freshwater delivery and its chemical and sediment load to coastal ecosystems (Scavia et al. 2002). Estuaries and other systems are largely dependent on the quantity and quality of freshwater inflows. Freshwater inflows can be defined as inputs of freshwater from streams draining into estuaries/bays. These inflows are important factors in the overall health of estuarine environments because they are major drivers of salinity gradients, sedimentation rates, and nutrient delivery.

Regional climate and land use interact in complex ways to modify hydrology and water quality. Chang (2004) simulated hydrologic impacts in southeastern Pennsylvania from climate change and land-use change individually and interactively and found the climate (mostly precipitation) signal to be the dominant driver of surface water flows and nutrient loadings. Similar studies conducted by Franczyk and Chang (2009) and Praskievicz and Chang (2009) noted similar sensitivities to amounts of precipitation within a set of watersheds in northwest Oregon. Changes to seasonal precipitation are inferred to be the principal factor of hydrologic impacts within rainfed basins (Chang 2004, Franczyk and Chang 2009, Praskievicz and Chang 2011). Wetter time periods

coupled with urban development increase surface water flows and the transport of pollutants and other materials within watersheds.

The pursuit of more informed and adaptive watershed management strategies has driven the use of modeling techniques that evaluate a variety of climate and LULC change scenarios. Climate and LULC change scenarios carry a large degree of uncertainty, due to the prediction/modeling methods (Praskievicz and Chang 2011) and data availability (Breuer, Huisman, and Frede 2006). Nonetheless, scenario analysis can provide insight into how hydrologic variables can change in direction and magnitude (Praskievicz and Chang 2011). Generalized hydrologic models, such as the Soil and Water Assessment Tool (SWAT), used to simulate hydrologic impacts give results at the basin and subbasin scale, as these are the natural boundaries for any surface water analysis (Praskievicz and Chang 2011). These models allow a range of scenarios to be analyzed individually and in combination in order to infer whether precipitation or LULC can be considered the dominant signal of the hydrological and water quality characteristics of a watershed.

Coastal areas are not immune to potential issues associated with the transformation of land surfaces and climate change. In Texas, bays/estuaries and the drainage basins upstream from marine water bodies, are vital resources because these areas provide habitat for several fish and bird species of commercial and recreational value. Furthermore, development has continued to increase along the coast of Texas for industrial and municipal purposes. The Mission-Aransas (M-A) region on the Coastal Bend of Texas is an area with a complex mix of natural and anthropogenic land surfaces.

The bays and estuaries of the M-A region are especially sensitive to changes in LULC within drainage basins upstream because it can disrupt inputs of freshwater and material that are vital in maintaining salinity gradients, sedimentation rates, and nutrient cycles within the system. Variations in climate within the M-A region can also disrupt ecological and anthropogenic systems. Extreme weather events such as tropical storms and flooding can dramatically alter the geometry of coastlines and disrupt the geomorphological characteristics of coastal watersheds that drain into the M-A system. On the other hand, times of drought reduce freshwater inflows and their associated sediment and chemical loads. These material inputs help sustain the ecological integrity of the M-A estuary that is vital in sustaining fisheries and habit for endangered species, such as whooping crane.

Watershed-based computer simulation systems are powerful tools when analyzing potential hydrologic impacts under LULC and precipitation scenarios. SWAT in particular, is very powerful in that it allows hydrology, sediment transport, and other water quality constituents to be simulated simultaneously within the same modeling system. Additionally, SWAT is computationally efficient and it has been widely applied in watersheds of various sizes with different hydrologic, geologic, climatic, and land management conditions (Borah and Bera 2004, Arnold et al. 2012). Furthermore, SWAT was successfully applied by Lee et al. (2011) for the coastal Matagorda Bay Watershed in Texas in order to estimate freshwater inflows for Matagorda Bay. This suggests that SWAT, and the graphical user interface ArcSWAT, can be applied to understand hydrologic impacts under various scenarios to freshwater inflows in the M-A region.

5.2 Objectives

The research presented in this chapter is aimed at understanding how SWAT simulations of the watershed hydrology and water quality for the Lower Aransas River Basin (LARB) are impacted under various scenarios of LULC change (increased development) and precipitation. The research presented here had two objectives:

1. Incorporation of LULC change and precipitation scenarios into a SWAT hydrological model that was calibrated to conditions within the LARB.
2. Analyze how stream/channel flow and loads of sediment, total nitrogen (TN), and total phosphorus (TP) for the LARB are impacted under the LULC change and precipitation scenarios at the subbasin and basin scales by comparing the scenarios to each other and a historical baseline.

5.3 Materials and Methodology

5.3.1 Study Area

The Lower Aransas River Basin (LARB) has an area of 1383 km^2 and it lies on the Coastal Bend of Texas just north of Corpus Christi (Figure V-1). This subbasin makes up the lower portions of the Aransas River Basin (ARB) and it occupies about 62% of the total ARB area. Streams in the region drain into Copano Bay that is part of the M-A estuarine system. The LARB includes the lower reach of the Aransas River (~73 km); that is the principle stream in the drainage basin and one of the few rivers in Texas not obstructed by dams. The Aransas River is relatively short, but it has a highly meandering course within the flat coastal plain. Major tributaries to the Aransas River within the LARB include Chiltipin and Papalote creeks.

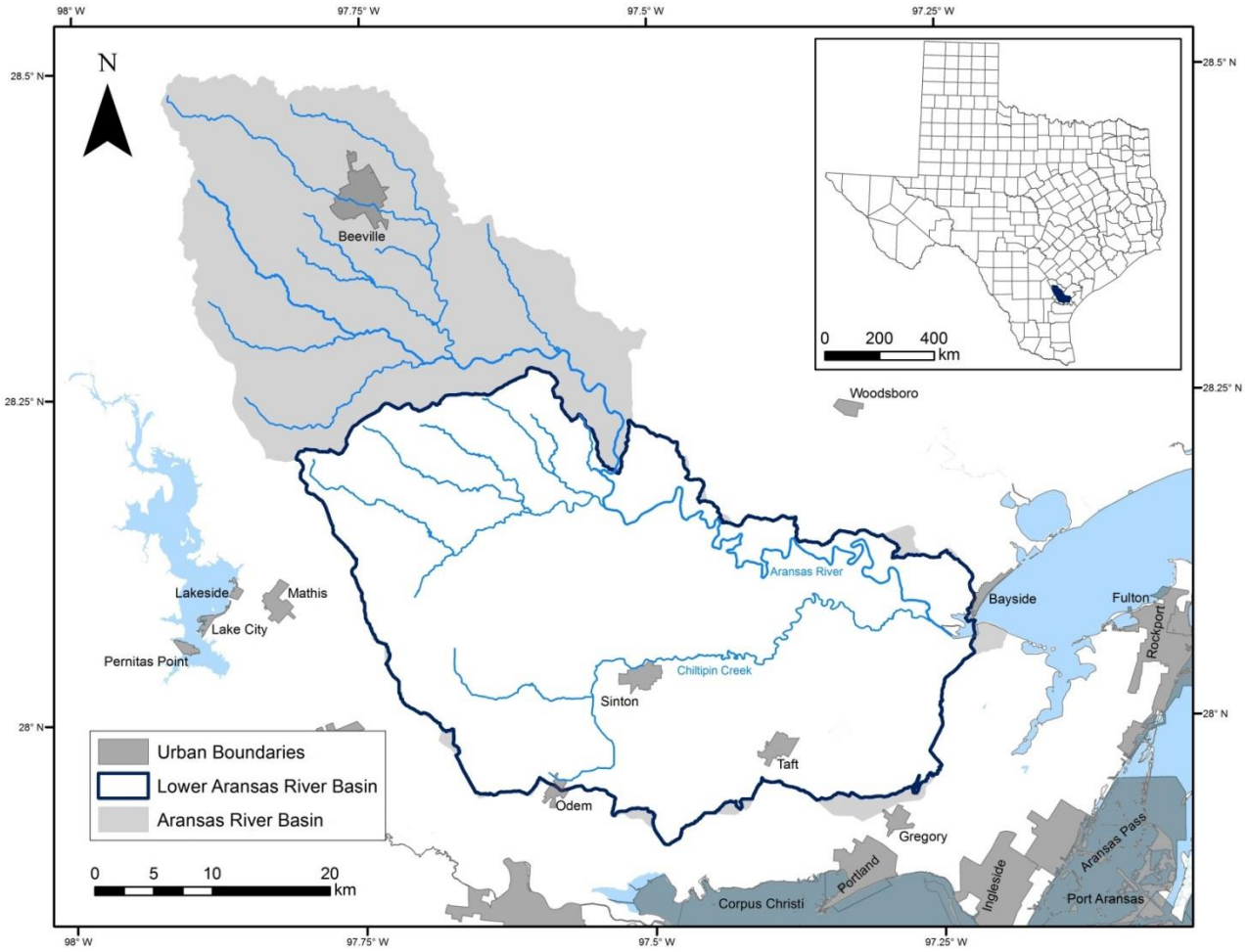

Figure V-1. Location map of the Lower Aransas River Basin (LARB) (delineated with ArcSWAT); Aransas River Basin (ARB) (HUC: 12100407); and city boundaries (Texas Natural Resources Information System: StratMap. Note: blue polylines are streams. (Figure III-2 from Chapter III and Figure IV-1 from Chapter IV from this Thesis).

The region has a semi-arid climate with mean annual precipitation of 864 mm and a mean temperature of 21.8 °C. However, the distribution of annual precipitation is skewed by seasonal tropical storms that occasionally bring large amounts of rainfall in late-summer and early-fall. Dominant LULC includes: cultivated land, rangeland, and woodland. The LARB region is predominantly rural with no large urban centers (Morehead, Beyer, and Dunton 2007). Within the LARB, the only prominent urban areas are Sinton and Taft that lie in the central and southeastern portions of the watershed (Figure V-1).

5.3.2 Scenario Characterization

Three scenarios of increased development, along with three precipitation scenarios were developed for the LARB (Chp. IV). The LULC change scenarios predict various amounts of increased development within the LARB going out to the year 2030, while the precipitation scenarios represent differing amounts of precipitation going out to 2040 for the area. Each individual LULC change scenario was combined with a precipitation scenario to have a total of 9 scenarios (Table V-1). Each scenario is a hypothetical future LULC and climatological (precipitation and temperature) condition for the LARB; and from this point each scenario will be addressed by its respective scenario code (e.g. scenario 1: S1, scenario 2: S2, etc.) (Table V-1).

SWAT outputs (stream/channel flow, sediment loads, TN loads, and TP loads) are compared to each other using a scenario and historical baseline to analyze how the LULC change and precipitation are impacted. Decadal (2030-2039) annual averages for each output variable are used as the basis for comparing how hydrology and water

quality are affected. Eight of the nine scenarios are compared to model outputs from S5 (MD + MP) that was specified as the scenario baseline. The historical baseline (HB) is comprised of annual, seasonal, and monthly averages of each output variable for the years 1990-1999.

Table V-1. Description of scenario combinations of land use/land cover and precipitation used as inputs in SWAT.

Scenario Code	Scenario	Land Use/Land Cover	Precipitation
S1	LU + LP	Lower amounts of Developed Land	Lower Amounts of Precipitation
S2	MU+LP	Medium Amounts of Developed Land	Lower Amounts of Precipitation
S3	HU+LP	Higher Amounts of Developed Land	Lower Amounts of Precipitation
S4	LU+MP	Lower Amounts of Developed Land	Medium Amounts of Precipitation
S5	MU+MP	Medium Amounts of Developed Land	Medium Amounts of Precipitation
S6	MU+HP	Higher Amounts of Developed Land	Medium Amounts of Precipitation
S7	LU+HP	Lower amounts of Developed Land	Higher Amounts of Precipitation
S8	MU+MP	Medium Amounts of Developed Land	Higher Amounts of Precipitation
S9	HU+HP	Higher Amounts of Developed Land	Higher Amounts of Precipitation

5.3.3 Data

A digital elevation model (DEM) with 10-meter spatial resolution from the National Elevation Dataset depicts the topography for the LARB. Elevation in this region ranges from 0 to 67 meters with most relief occurring in the northwestern portions of the basin. Slope ranges from 0 to 65%, with an average slope of 0.57%. Historical LULC (1990 and 2010) is represented by Landsat imagery classified to a modified Anderson Level I classification (Anderson et al. 1976). Cultivated land and rangeland are the dominant LULC classes for 1990 and 2010 (Table V-2). Soil is

characterized using the U.S. General Soil Map (STATSGO) with dominant soil types being Victoria (clay loam) and Papalote (clay loam) each with coverage of 57.7 and 33.1%, respectively, of the LARB. Daily precipitation and temperature (maximum and minimum) data from six National Climatic Data Center weather stations (GHCND: USC00410302, USW00012925, USC00415661, USW00012972, USC00418354, and USC00419559) for the time-period 1950-2012 depicts the historical climate. Temperature ranges from 13 to 30 °C throughout the year with the fall and summer months being the wettest times of the year (Figure V-2). Streamflow records (mean daily discharge from 1964 to 2012) from a U.S. Geological Survey (USGS) gage on the Aransas River, above Skidmore, TX (08189700) are used as a point source inlet to the LARB to represent streamflow not being modeled by SWAT.

Table V-2. Areal coverage and percentage of total area for each land use/land cover class for each historical (1990 and 2010) and scenario (2030 – LD, 2030 – MD, and 2030 – HD) image.

	1990		2010		2030 - LD		2030 - MD		2030 - HD	
Class	Area (km^2)	% of Total Area (%)	Area (km^2)	% of Total Area (%)	Area (km^2)	% of Total Area (%)	Area (km^2)	% of Total Area (%)	Area (km^2)	% of Total Area (%)
Developed Land	27.5	2.0	38.3	2.8	47.3	3.4	51.8	3.7	65.3	4.7
Cultivated Land	797.9	57.7	764.5	55.2	762.2	55.1	761.0	55.0	757.6	54.7
Rangeland	425.5	30.7	373.7	27.0	370.1	26.7	368.2	26.6	362.7	26.2
Woodland	82.2	5.9	141.6	10.2	139.0	10.0	137.7	10.0	133.8	9.7
Open Water	3.4	0.2	3.9	0.3	3.9	0.3	3.9	0.3	3.9	0.3
Wetland	40.5	2.9	54.5	3.9	54.3	3.9	54.2	3.9	53.8	3.9
Barren Land	6.7	0.5	7.2	0.5	7.0	0.5	6.9	0.5	6.6	0.5
Total	**1383.7**	**100.0**	**1383.7**	**100.0**	**1383.7**	**100.0**	**1383.7**	**100.0**	**1383.7**	**100.0**

The three LULC change scenarios are represented by raster files developed using the Land Change Modeler in the Idrisi Selva GIS environment (Clark Labs 2012). Each LULC change scenario predicts a differing amount of developed land within the LARB when compared to the HB (1990 LULC). The proportion of the LARB occupied by developed land in 1990 is 2.0% (Table V-2 and Figure V-3a); while developed land comprises 3.4, 3.7, and 4.7% of the LARB for the low development (LD) (Table V-2 and Figure V-3b), medium development (MD) (Table V-2 and Figure V-3c), and high development (HD) (Table V-2 and Figure V-3d) scenarios, respectively. Most development is situated in areas near Sinton, Taft, and major roads for each LULC scenario and the HB.

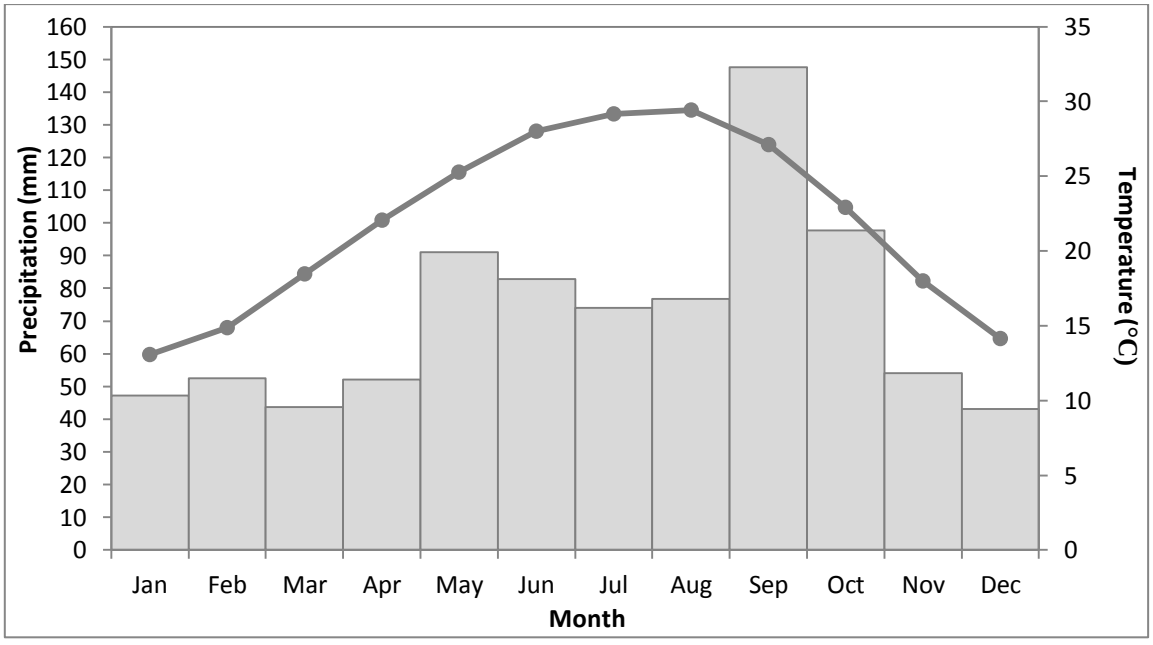

Figure V-2. Mean monthly precipitation and temperature for the Lower Aransas River Basin for the time-period from 1950 to 2012.

Three time-series' of daily precipitation and temperature (maximum and minimum) were selected from the historical record (1950-2012) to represent climate data for each precipitation scenario. Each scenario depicts differing amounts of precipitation from 2013 to 2040 for rain gages in and around the LARB (Figure V-4). Average annual precipitation for the low precipitation (LP), medium precipitation (MP), and high precipitation (HP) scenarios is 763, 907, and 996 mm, respectively. The fall and summer months are the wetter times of the year with winter being the driest (Figure V-5). The average annual precipitation by each subbasin for the HB (Figure V-6a), LP (Figure V-6b), MP (Figure V-6c), and HP (Figure V-6d) scenarios is mapped in Figure V-6. Interestingly, the HB predicts a greater amount of precipitation than those predicted by each precipitation scenario with a spatial distribution similar to the HP scenario. This is because some of the weather data from the 1990s (1991-1999) was used for the development of the HP scenario, but the alignment of the time-series made it so that only weather data from 1995-1999 was used in the comparisons. In general, subbasins in the vicinity of the Aransas River (northern edge) receive higher amounts of precipitation.

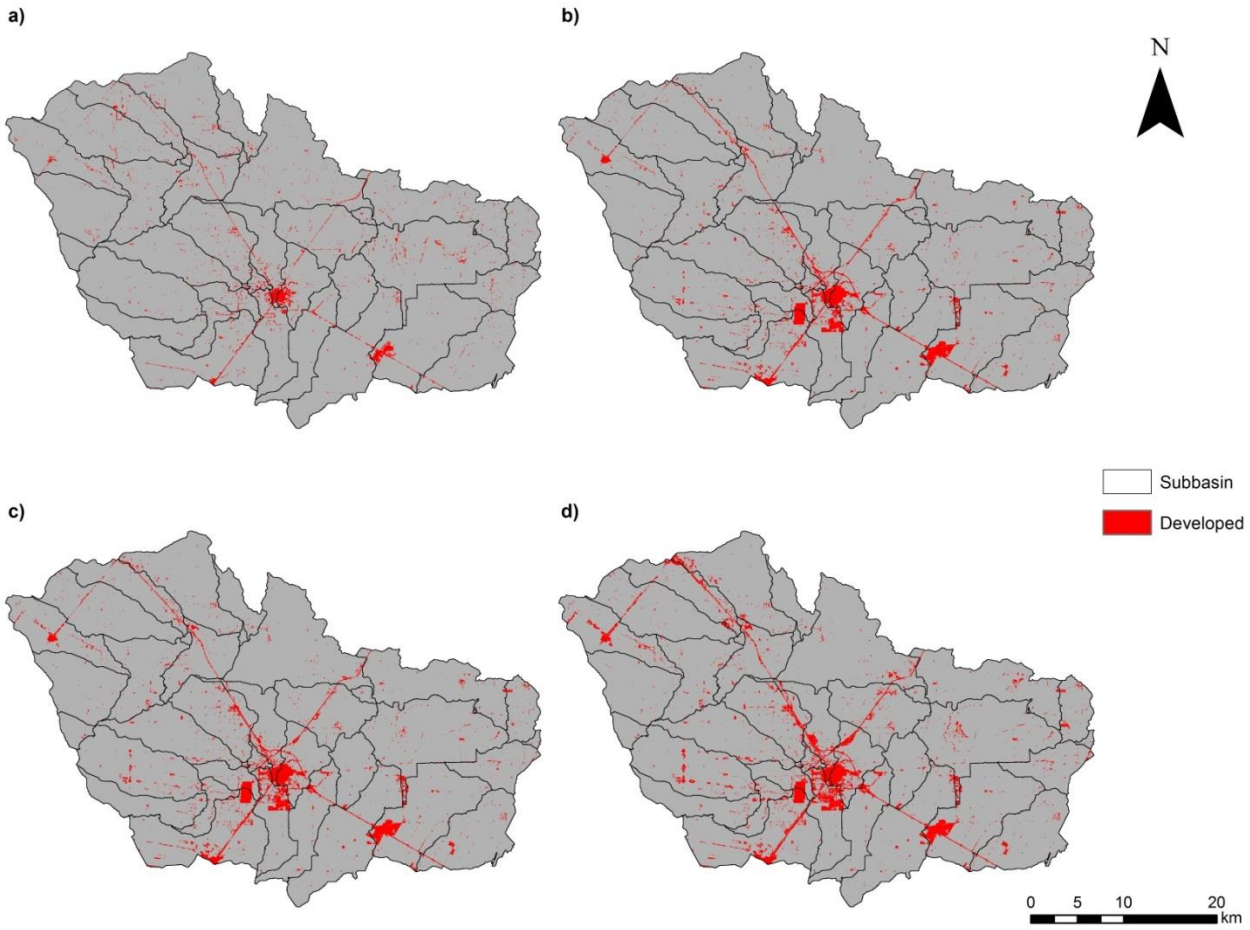

Figure V-3. a) Spatial configuration of developed land within the LARB for the historical baseline (1990-1999). b) Spatial configuration of developed land for the low expansion of developed land scenario (2030-2039). c) Spatial configuration of developed land for the medium expansion of developed land scenario (2030-2039). d) Spatial configuraiton of developed land for the high expansion of developed land scenario (2030-2039).

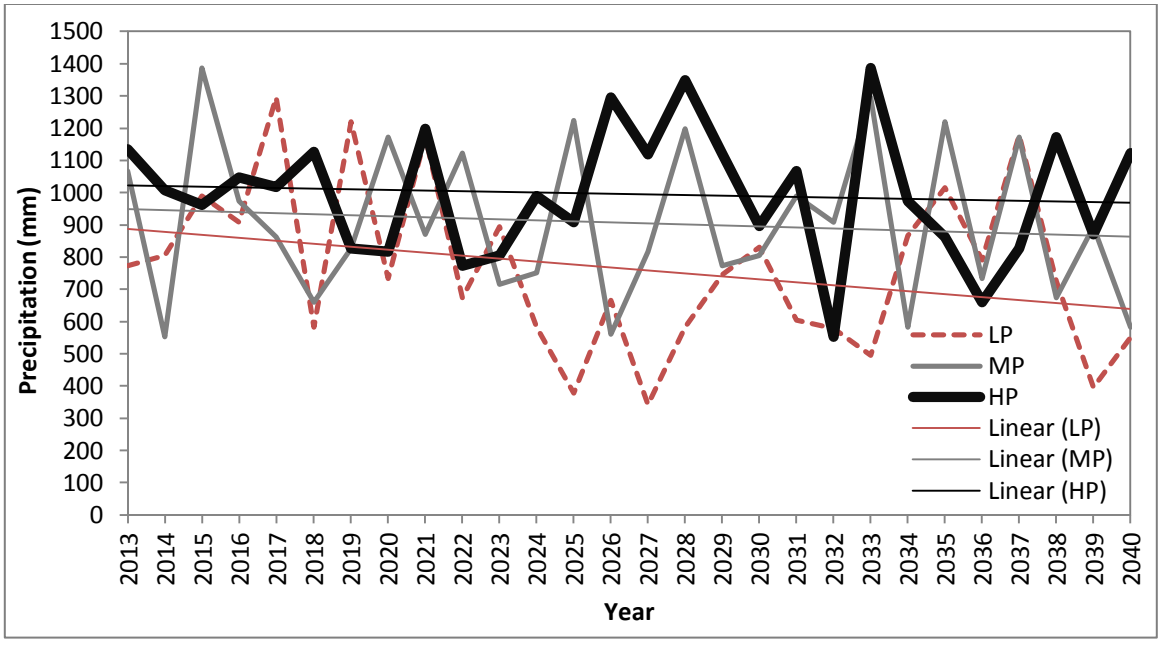

Figure V-4. Time-series' of annual precipitation and linear trend line for the low precipitation (LP), medium precipitation (MP), and high precipitation (HP) scenarios for the time-period from 2013 to 2040. (Figure IV-9 from Chapter IV of this Thesis).

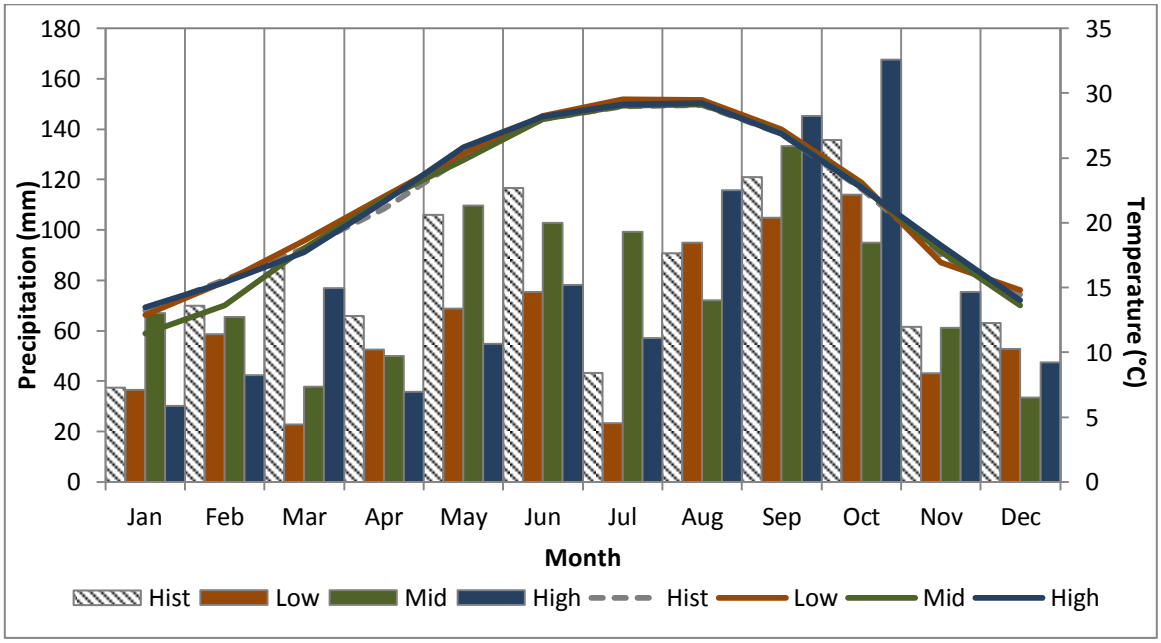

Figure V-5. Climagraph of mean monthly precipitation and temperature for the LARB for the historical baseline and each precipitation scenario.

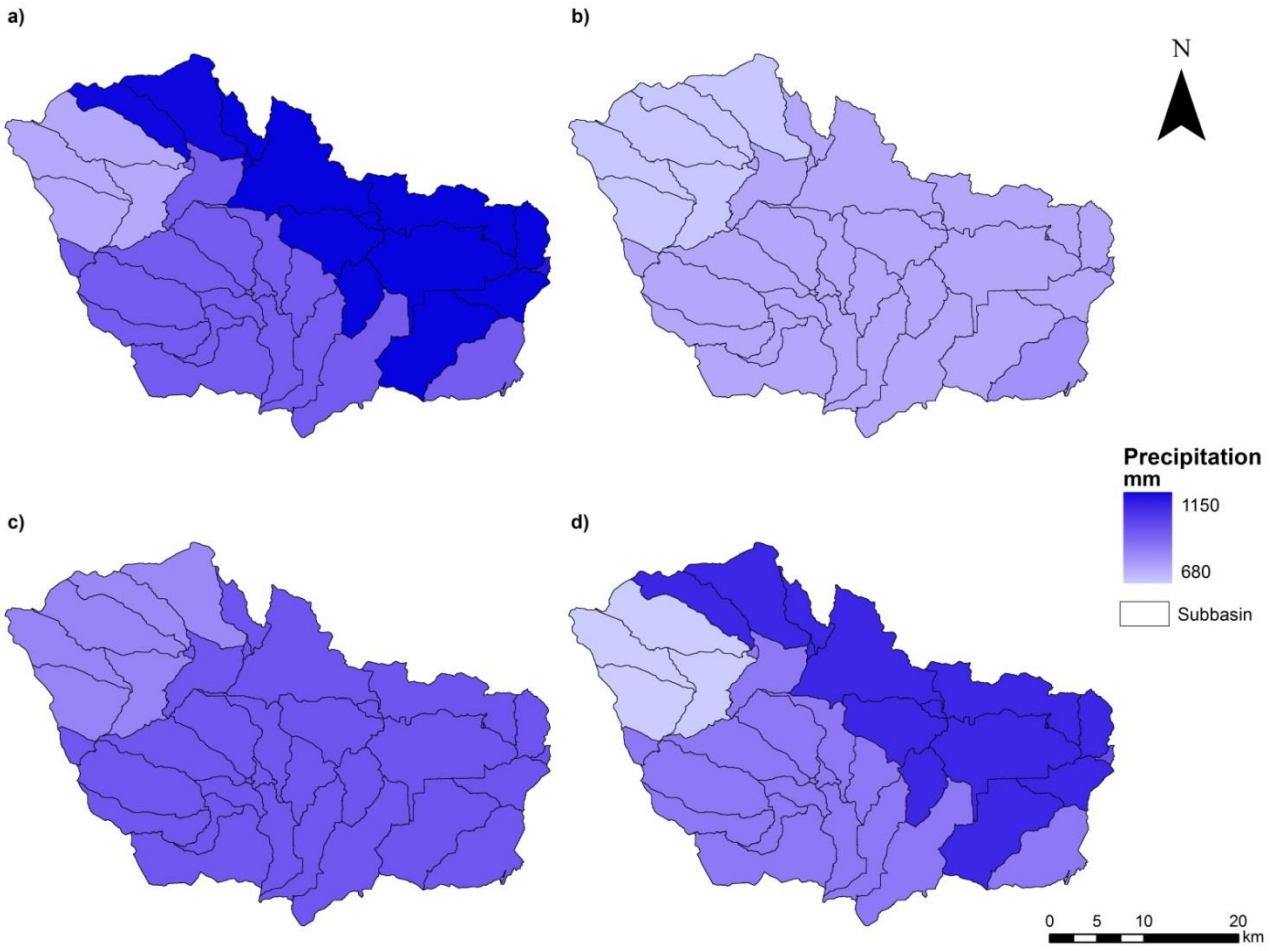

Figure V-6. a) Average annual precipitation by subbasin for the historical base line (1990-1999). b) Average annual precipitation by subbasin for the low precipitation scenario (2030-2039). c) Average annual precipitation by subbasin for the medium precipitation scenario (2030-2039). D) Average annual precipitation by subbasin for the high precipitation scenario (2030-2039).

5.3.4 SWAT Model Setup

In this study, ArcSWAT version 2009.93.7b that runs as an extension in ArcGIS 9.3 (ESRI 2009) was used for conducting the scenario analysis. Basin and subbasin boundaries were delineated using ArcSWAT; a maximum drainage area threshold of 1100 hectares was used to delineate 35 subwatersheds within the LARB (Figure V-7). Within each subwatershed, HRUs were generated on the basis of slope, soil, and land use. SWAT parameters were calibrated using streamflow records from a USGS gaging station on Chiltipin Creek (08189800); a major tributary of the Aransas River. Water diversions and return flows from waste water treatment plants were not incorporated in the SWAT model. While there is an unknown amount of water diversion within the LARB, there are seven point-source return flows (Schoenbaechler and Guthrie 2011). These anthropogenic modifications can impact the fluvial system, but return flows account for only a small percentage of freshwater inflow to the M-A estuarine system (Schoenbaechler and Guthrie 2011). Extensive calibration of SWAT for sediment and nutrient loads could not be conducted due to a lack of continuous records for these variables, but model parameters were adjusted until sediment and nutrient loads were within "ballpark" ranges from published estimates for these variables.

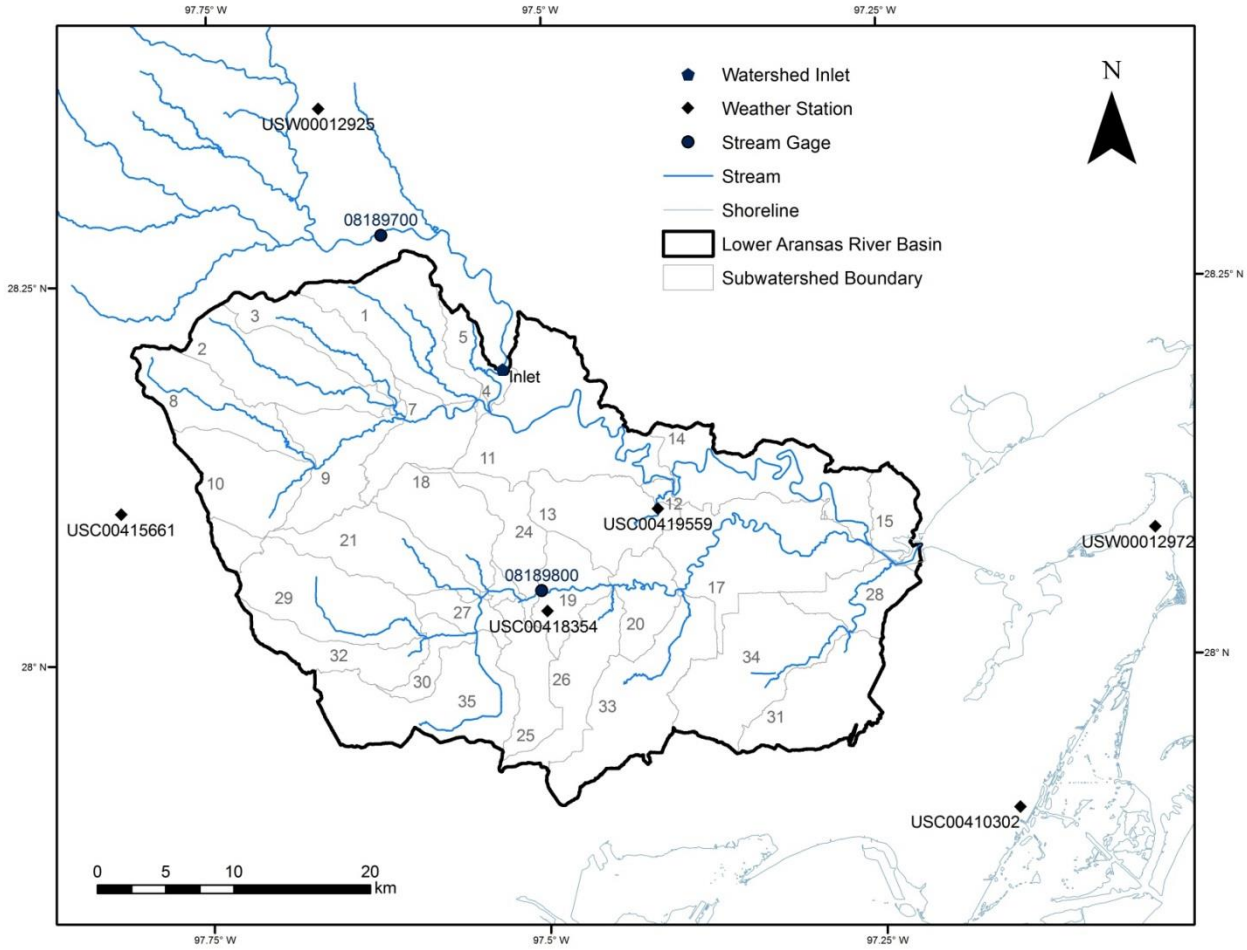

Figure V-7. Map of Lower Aransas River Basin (LARB) (delineated with ArcSWAT); stream network (stream network within the LARB delineated using ArSWAT); U.S, Geological Survey (USGS) stream gages used as watershed inlets (08189700) and for SWAT calibration (08189800); and National Climatic Data Center (NCDC) weather stations used as precipitation and temperature inputs. Note: Figure III-2 from Chapter III of this Thesis.

To incorporate LULC change, SWAT (version 2009) has a land use update feature where the land use component of affected HRUs are updated based on user specifications. The input files needed to properly depict LULC change for each HRU were developed using the SWAT2009-LUC tool developed by Pai and Saraswat (2011). Each LULC change scenario utilizes two land use updates; the first is for the 2010 LULC dataset used in developing the 2030 scenario of increased development; and the other is for the predicted expansion of developed land out to 2030 by the respective scenario.

The incorporation of the precipitation scenarios involved appending selected daily precipitation and temperature data to the historical time-series' for each scenario. Each scenario's respective time-series' of precipitation and temperature data was reloaded into the ArcSWAT interface.

5.3.5 Comparison between Scenarios and Associated Baselines

For the subbasin-scale, each output variable (stream/channel flow, sediment load, TN load, and TP load) was analyzed at an annual scale. Average annual quantities of material, volumes for water and mass for sediment/nutrients, transported out of each subbasin via the main channel were the basis for comparison between the scenario and historical baselines. The comparison was conducted by subtracting the predicted baseline (scenario or historical) quantity from the respective scenario value. For example, values from 8 of the 9 subbasins were compared to values from the scenario baseline (S5) by subtracting the S5 value from those for each respective scenario. The same approach was utilized when comparing scenario values to the HB. These differences in the output

variables were mapped to analyze the spatial configuration of hydrologic impacts under each scenario condition. The difference map of the LARB for each scenario was used to construct a 3x3 matrix of maps that displays how the variable of interest (e.g. stream/channel flow) varies across the 9 scenarios. Each row in the 3x3 map matrix represents a different scenario of increased development for the LARB (row 1: LD, row 2: MD, row 3: HD), while each column represents a different precipitation scenario (column 1: LP, column 2: MP, column 3: HP).

At the basin-scale, output variables were analyzed at annual, seasonal, and monthly time-scales. Average quantities of material transported out of the basin via the Aransas River (main channel) for each temporal scale were used to conduct the comparison between scenario predictions and those from each baseline (scenario and historical). Comparisons were conducted using graphical techniques (bar graphs) and by analyzing the difference between scenario and baseline predictions.

5.4 Results

5.4.1 Hydrologic Impacts at Subbasin Scale: Comparison between Scenarios

5.4.1.1 Stream/Channel Flow

Flows out (discharge) of each subbasin via the main channel for 8 of the 9 scenarios (S1, S2, S3, S4, S6, S7, S8, and S9) were compared to values from S5 (Figure V-8). Average annual stream/channel flows ranged from 2.39 thousand acre-feet for subbasins along the western and southern edge of the LARB, to 16.46 thousand acre-feet at the basin outlet for S5 (Figure V-8e). With regard to the comparisons, for LP scenarios (S1, S2, and S3), the effect of increased development is not obvious in the comparison (Figures V-8a, V-8b, and V-8c). MP scenarios (S5 and S6) portray the impacts of differing amounts of developed land more vividly with S6 exhibiting increases in stream/channel discharge for subbasins where some form of increased development occurs. To a lesser degree from S4 and S6, the effect of increased development is also noticeable for HP scenarios (S7, S8, and S9) for subbasins around the urban area of Sinton (Figures V-8g, V-8h, and V-8i).

Across all scenarios, the impacts to stream/channel discharge from various amounts of developed land are relatively small when compared to the effects caused by variable precipitation. In general, LP scenarios have lower stream/channel flows than MP scenarios within all subbasins, while HP scenarios have higher stream/channel flows than the LP and HP scenarios in subbasins that contain the Aransas River along the northern edge of the LARB (Figure V-8).

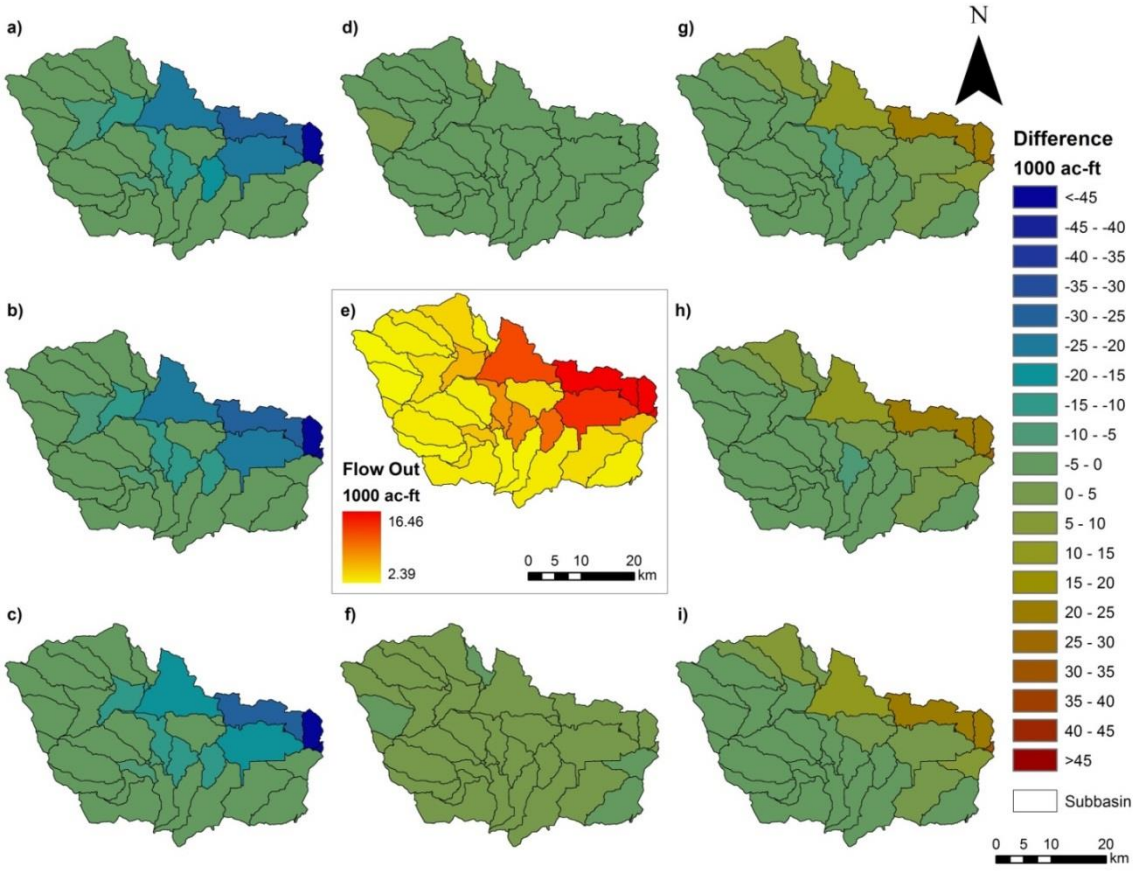

Figure V-8. Differences between scenario values and values for the scenario baseline (scenario 5) for average annual flow out of each subbasin via the main channel for the years 2030-2039. Each map represents a different scenario: a) difference between scenario 1 and the baseline; b) difference between scenario 2 and the baseline; c) difference between scenario 3 and the baseline; d) difference between scenario 4 and the baseline; e) average annual flow out (discharge) from each subbasin via the main channel under the scenario baseline (scenario 5) for the years 2030-2039; f) difference between scenario 6 and the baseline; g) difference between scenario 7 and the baseline; h) difference between scenario 8 and the baseline; i) difference between scenario 9 and the baseline.

5.4.1.2 Sediment Loads

Sediment loads transported out of each subbasin via the main channel for 8 of the 9 scenarios were compared to values from S5 (Figure V-9). Average annual sediment loads range from 2.1 thousand metric tons in subbasins along the western and southern edges of the LARB, to 97.1 thousand metric tons at the basin outlet for S5 (Figure V-9e). For LP scenarios (S1, S2, and S3), the effect of increased development is noticeable for subbasins in the central parts (near Sinton) of the LARB (Figures V-9a, V-9b, and V-9c). MP scenarios (S4 and S6) portray the impacts from development to a greater extent (Figures V-9d and V-9f); with S6 showing increases in sediment loads for subbasins near Sinton and major roads. The effect from greater amounts of developed land is also noticeable for HP scenarios (scenarios 7, 8, and 9), especially within subbasins around the Sinton area (Figures V-9g, V-9h, and V-9i).

The impacts to stream/channel sediment loads from increased amounts of developed land are comparable to the effects caused by variable precipitation. While the effects to sediment loads in streams/channels from variable precipitation occur more uniformly across the LARB, the impacts from increased development occur within subbasins in the vicinity of urban areas and major roads where developed land increases differently for each LULC scenario.

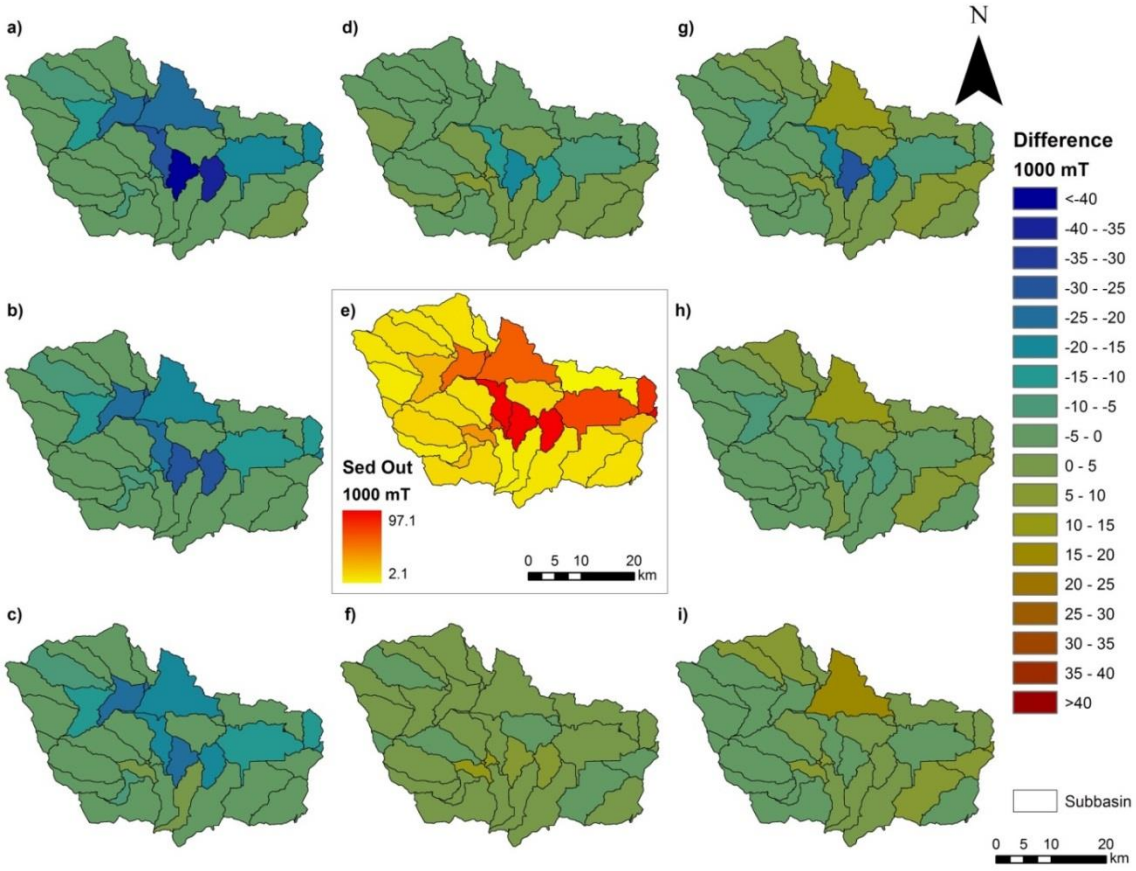

Figure V-9. Differences between scenario values and values for the scenario baseline (scenario 5) for average annual sediment load transported out of each subbasin via the main channel for the years 2030-2039. Each map represents a different scenario: a) difference between scenario 1 and the baseline; b) difference between scenario 2 and the baseline; c) difference between scenario 3 and the baseline; d) difference between scenario 4 and the baseline; e) average annual sediment load transported out of each subbasin via the main channel under the scenario baseline (scenario 5) for the years 2030-2039; f) difference between scenario 6 and the baseline; g) difference between scenario 7 and the baseline; h) difference between scenario 8 and the baseline; i) difference between scenario 9 and the baseline.

5.4.1.3 Total Nitrogen (TN) Loads

TN loads transported out of each subbasin via the main channel for 8 of the 9 scenarios were compared to values from S5 (Figure V-10). Average annual TN loads range from 6 metric tons in subbasins along the western and southern edges of the LARB, to 839 metric tons at the basin outlet for S5 (Figure V-10e). There is little or no difference as a result of increased development for the LP scenarios (S1, S2, and S3) (Figures V-10a, V-10b, and V-10c). MP scenarios (S4 and S6) also do not portray the impacts from increased amounts of developed land (Figures V-10d and V-10f). Similar to the other precipitation scenarios, there are no significant differences caused by the various amounts of developed land for HP scenarios (S7, S8, and S9) (Figures V-10g, V-10h, and V-10i).

For TN loads, the impacts from increasing development within the LARB are negligible compared to the differences between the precipitation scenarios. There are obvious similarities between the scenario maps in Figure V-9 and those from their respective precipitation scenario (Figures V-6b, V-6c, and V-6d).

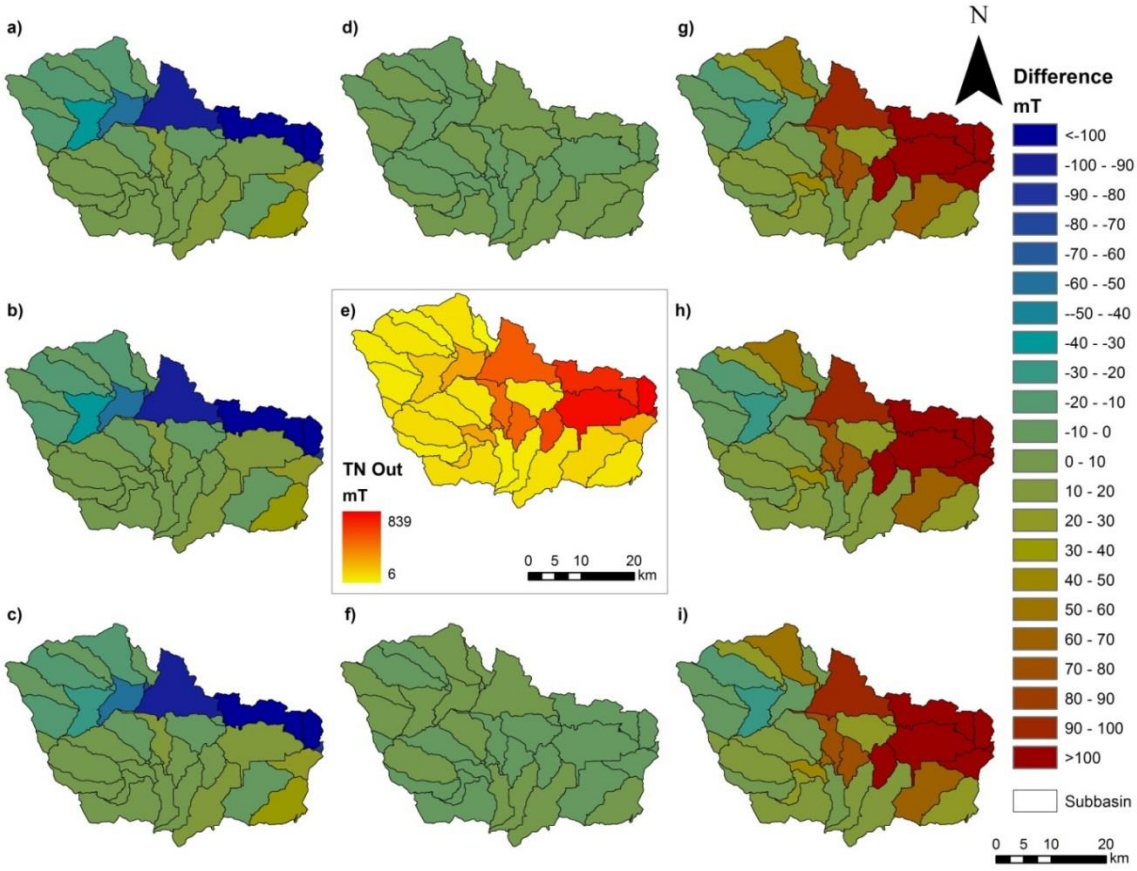

Figure V-10. Differences between scenario values and values for the scenario baseline (scenario 5) for average annual total nitrogen (TN) load transported out of each subbasin via the main channel for the years 2030-2039. Each map represents a different scenario: a) difference between scenario 1 and the baseline; b) difference between scenario 2 and the baseline; c) difference between scenario 3 and the baseline; d) difference between scenario 4 and the baseline; e) average annual TN load transported out of each subbasin via the main channel under the scenario baseline (scenario 5) for the years 2030-2039; f) difference between scenario 6 and the baseline; g) difference between scenario 7 and the baseline; h) difference between scenario 8 and the baseline; i) difference between scenario 9 and the baseline.

5.4.1.4 Total Phosphorus (TP) Loads

TP loads transported out of each subbasin via the main channel for 8 of the 9 scenarios were compared to values from S5 (Figure V-11). Average annual TP loads range from 0.53 metric tons in subbasins along the western and southern edges of the LARB, to 76.2 metric tons at the basin outlet for S5 (Figure V-11e). There is no obvious difference in TP loads due to the various amounts of increased development (S1, S2, and S3) for LP scenarios (Figures V-11a, V-11b, and V-11c). For MP scenarios (S4 and S6), there are modest increases in TP loads for most subbasins as the amount of developed land increases (Figures V-11d and V-11f). As for HP scenarios (S7, S8, and S9), subbasin 17 in the eastern portions of the LARB (Figure V-7) is the only area where TP loads are increasing as the amount of developed land increases (Figures V-11g, V-11h, and V-11i).

In a similar fashion to TN loads, differences in precipitation have a greater influence on TP loads than differences in the amount of developed land. It bears noting that the scenario maps for TP loads do not follow the trends exhibited by the precipitation maps for each scenario (Figures V-6b, V-6c, and V-6d) as closely as the TN load maps.

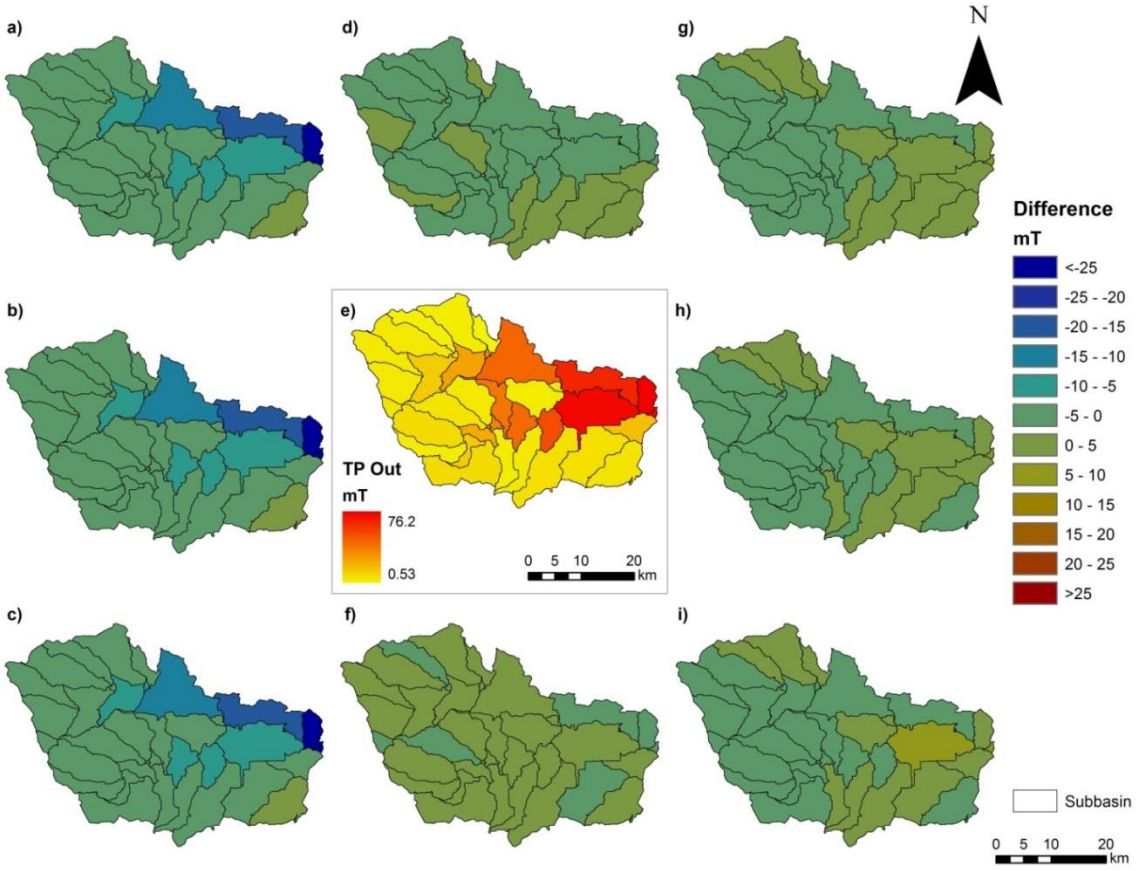

Figure V-11. Differences between scenario values and values for the scenario baseline (scenario 5) for average annual total phosphorus (TP) load transported out of each subbasin via the main channel for the years 2030-2039. Each map represents a different scenario: a) difference between scenario 1 and the baseline; b) difference between scenario 2 and the baseline; c) difference between scenario 3 and the baseline; d) difference between scenario 4 and the baseline; e) average annual TP load transported out of each subbasin via the main channel under the scenario baseline (scenario 5) for the years 2030-2039; f) difference between scenario 6 and the baseline; g) difference between scenario 7 and the baseline; h) difference between scenario 8 and the baseline; i) difference between scenario 9 and the baseline.

5.4.2 Hydrologic Impacts at Subbasin Scale: Comparison to Historical Baseline

5.4.2.1 Stream/Channel Flow

Flows out (discharge) of each subbasin via the main channel for the 9 scenarios were compared to values from the HB (Figure V-12). Average annual stream/channel flows ranged from 21.86 thousand acre-feet for subbasins along the western and southern edge of the LARB, to 198.98 thousand acre-feet at the basin outlet for the HB (Figure V-12j). For LP scenarios (S1, S2, and S3), all subbasin values for stream/channel flow fall below those form the HB; with little or no effect to stream/channel flow as a result of increased development (Figures V-12a, V-12b, and V-12c). With regard to the MP scenarios (S4, S5, and S6), 17 subbasins in the western and southwestern portions of the LARB exhibit values that are greater than those from the HB (Figures V-12d, V-12e, and V-12f). In terms of the effect of increased development, only S6 (Figure V-12f) portrays the impact of an increased amount of developed land. This is because only one subbasin (subbasin 19) in the Sinton area exhibits an increase in stream/channel discharge when compared to scenarios 4 and 5 (Figures V-12d and V-12e, respectively). For HP scenarios (scenarios 7, 8, and 9), most subbasins have stream/channel flow values slightly below those from the HB, with the exception of a few subbasins in the central (longitudinal) parts of the LARB (Figures V-12g, V-12h, and V-12i). Furthermore, the effect of increasing amounts of developed land is exhibited because there is a higher count of subbasins with stream/channel flows greater than those from the HB for every scenario that has a larger quantity of developed land (Figures V-12g, V-12h, and V-12i).

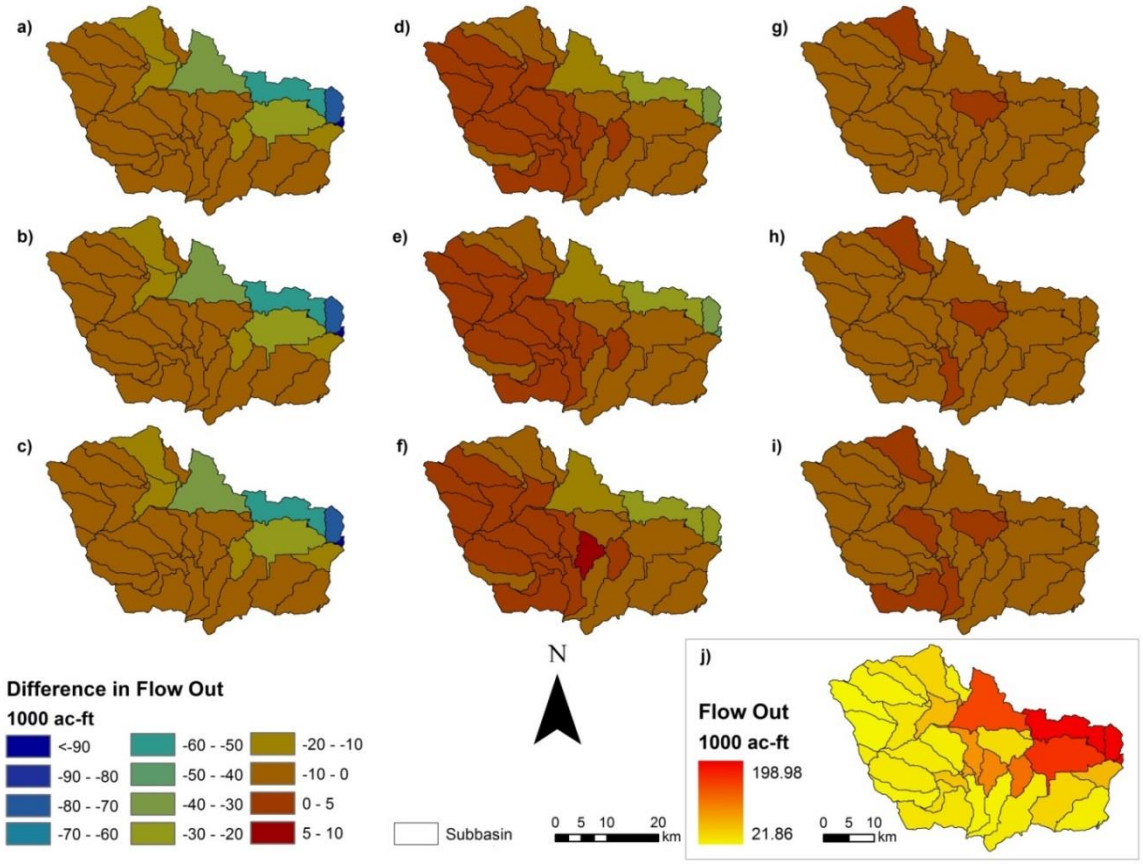

Figure V-12. Differences between scenario values (2030-2039) and values for the historical baseline (1990-1999) for average annual flow out of each subbasin via the main channel. Each map represents a different scenario: a) difference between scenario 1 and the historical baseline; b) difference between scenario 2 and the historical baseline; c) difference between scenario 3 and the historical baseline; d) difference between scenario 4 and the historical baseline; e) difference between scenario 5 and the historical baseline; f) difference between scenario 6 and the historical baseline; g) difference between scenario 7 and the historical baseline; h) difference between scenario 8 and the historical baseline; i) difference between scenario 9 and the historical baseline; j) average annual flow out (discharge) from each subbasin via the main channel for the historical baseline (1990-1999).

5.4.2.2 Sediment Loads

Sediment loads transported out of each subbasin via the main channel for the 9 scenarios were compared to values from the HB (Figure V-13). Average annual sediment loads ranged from 2.7 thousand metric tons for subbasins along the western and southwestern edge of the LARB, to 60.7 thousand metric tons at the basin outlet for the HB (Figure V-13j). For LP scenarios (S1, S2, and S3), most subbasin values for sediment loads fall below those form the HB, but subbasins in the Sinton area have values greater than those for the baseline (Figures V-13a, V-13b, and V-13c). The impacts to sediment loads from increased development is apparent for subbasins in the Sinton area with S2 and S3 each having a higher number of subbasins with values greater than those from the HB (Figures V-13a, V-13b, and V-13c). For MP scenarios (S4, S5, and S6), 20 or more subbasins in the central and southwestern portions of the LARB exhibit values that are greater than those from the HB (Figures V-13d, V-13e, and V-13f). In terms of the effect of increased development, sediment loads increase as the amount of developed land increases; with the greatest differences between MP and HB values occurring in areas around Sinton (Figures V-13d, V-13e, and V-13f). For HP scenarios (scenarios 7, 8, and 9), most subbasins have sediment loads greater than those from the HB (Figures V-13g, V-13h, and V-13i). Once again, the effect of increasing amounts of developed land is exhibited because subbasins in the Sinton have higher sediment loads for every scenario that has a larger quantity of developed land (Figures V-13g, V-13h, and V-13i).

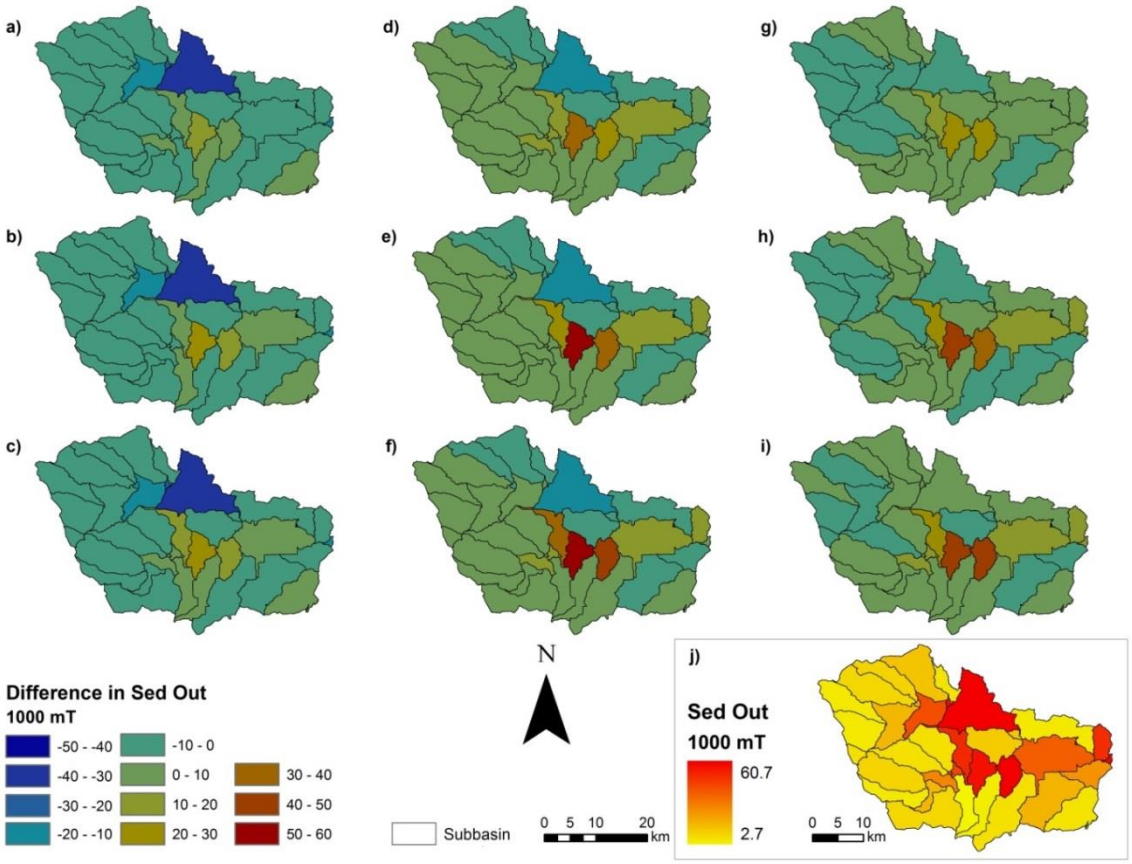

Figure V-13. Differences between scenario values (2030-2039) and values for the historical baseline (1990-1999) for average annual sediment load transported out of each subbasin via the main channel. Each map represents a different scenario: a) difference between scenario 1 and the historical baseline; b) difference between scenario 2 and the historical baseline; c) difference between scenario 3 and the historical baseline; d) difference between scenario 4 and the historical baseline; e) difference between scenario 5 and the historical baseline; f) difference between scenario 6 and the historical baseline; g) difference between scenario 7 and the historical baseline; h) difference between scenario 8 and the historical baseline; i) difference between scenario 9 and the historical baseline; j) average annual sediment load transported out of each subbasin via the main channel for the historical baseline (1990-1999).

5.4.2.3 Total Nitrogen (TN) Loads

TN loads transported out of each subbasin via the main channel for the 9 scenarios were compared to values from the HB (Figure V-14). Average annual TN loads ranged from 15 metric tons for subbasins along the western and southern edge of the LARB, to 1391 metric tons at the basin outlet for the HB (Figure V-14j). For LP scenarios (S1, S2, and S3), TN loads for most subbasins fall below those from the HB, with three subbasins in the southern portions of the LARB have values slightly greater than those for the HB (Figures V-14a, V-14b, and V-14c). There are little or no impacts to TN loads as a result of increased development. For MP scenarios (S4, S5, and S6), none of the subbasins have TN loads that are greater than those from the HB (Figures V-14d, V-14e, and V-14f); with no effect from increased development. As for HP scenarios (S7, S8, and S9), 13 subbasins have TN loads greater than those from the HB (Figures V-14g, V-14h, and V-14i), but once again there is no noticeable impact from increased amounts of developed land.

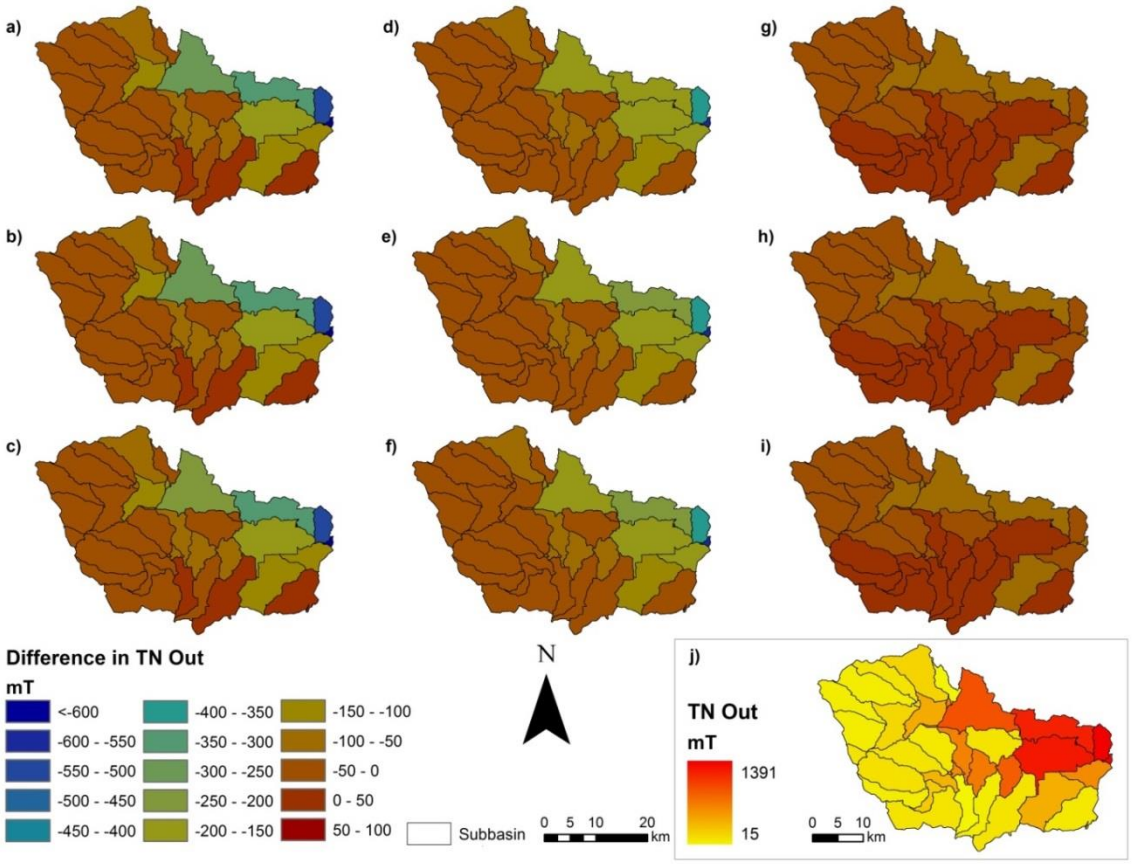

Figure V-14. Differences between scenario values (2030-2039) and values for the historical baseline (1990-1999) for average annual total nitrogen (TN) load transported out of each subbasin via the main channel. Each map represents a different scenario: a) difference between scenario 1 and the historical baseline; b) difference between scenario 2 and the historical baseline; c) difference between scenario 3 and the historical baseline; d) difference between scenario 4 and the historical baseline; e) difference between scenario 5 and the historical baseline; f) difference between scenario 6 and the historical baseline; g) difference between scenario 7 and the historical baseline; h) difference between scenario 8 and the historical baseline; i) difference between scenario 9 and the historical baseline; j) average annual TN load transported out of each subbasin via the main channel for the historical baseline (1990-1999).

5.4.2.4 Total Phosphorus (TP) Loads

TP loads transported out of each subbasin via the main channel for the 9 scenarios were compared to values from the HB (Figure V-15). Average annual TP loads ranged from 0.7 metric tons for subbasins along the western edge of the LARB, to 113.9 metric tons at the basin outlet for the HB (Figure V-15j). For LP scenarios (S1, S2, and S3), all subbasin values for TP loads fall below those from the HB (Figures V-15a, V-15b, and V-15c); with no noticeable impacts to TP loads as a result of increased development. For MP scenarios (S4, S5, and S6), none of the subbasins have values that are greater than those from the HB (Figures V-15d, V-15e, and V-15f); and there is no effect from increased development. As for HP scenarios (scenarios 7, 8, and 9), the same trend continues with no subbasin having TP load values greater than those from the HB (Figures V-15g, V-15h, and V-15i). Furthermore, there is no noticeable impact from increased amounts of developed land to TP loads for HP scenarios.

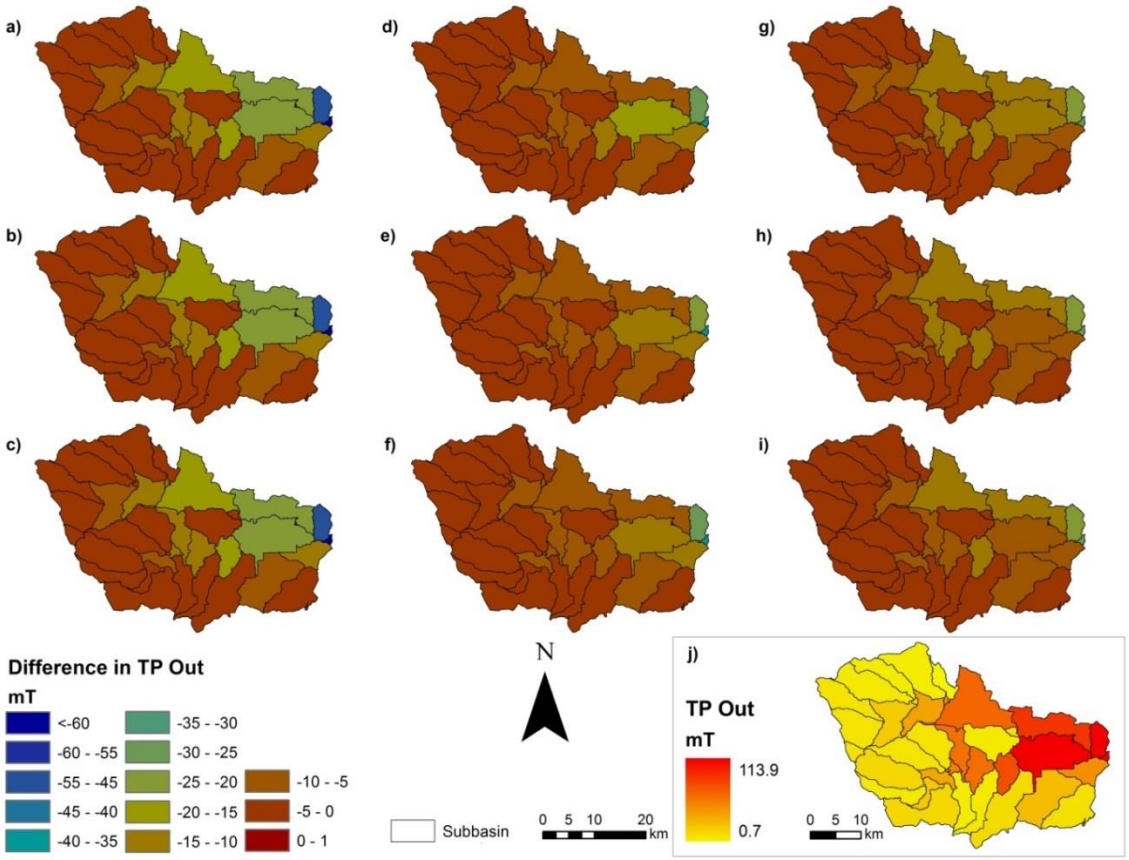

Figure V-15. Differences between scenario values (2030-2039) and values for the historical baseline (1990-1999) for average annual total phosphorus (TP) load transported out of each subbasin via the main channel. Each map represents a different scenario: a) difference between scenario 1 and the historical baseline; b) difference between scenario 2 and the historical baseline; c) difference between scenario 3 and the historical baseline; d) difference between scenario 4 and the historical baseline; e) difference between scenario 5 and the historical baseline; f) difference between scenario 6 and the historical baseline; g) difference between scenario 7 and the historical baseline; h) difference between scenario 8 and the historical baseline; i) difference between scenario 9 and the historical baseline; j) average annual TP load transported out of each subbasin via the main channel for the historical baseline (1990-1999).

5.4.3 Hydrologic Impacts at Basin Scale

5.4.3.1 Annual Scale

Average annual freshwater inflows and delivered loads of sediment, TN, and TP to Copano Bay from the Aransas River (LARB outlet) were analyzed for the HB (1990-1999) and each scenario (2030-2039) that incorporated various amounts of developed land and precipitation for the LARB (Table V-3). Freshwater inflows for the HB had an annual average of 199.0 thousand acre-feet, which was higher than the average annual freshwater inflows for any of the scenarios which ranged from 107.2 thousand acre-feet for S1 to 188.0 thousand acre-feet for S9. As expected, there is a general increase in flow quantities amongst the scenarios as the amount of developed land and precipitation increases.

Average annual sediment loads at the LARB outlet are 60.7 thousand metric tons for the HB that is most similar to values from S4. Sediment loads for the scenarios ranged from 45.3 thousand metric tons for S1 to 76.4 thousand metric tons for S9. Similar to freshwater inflows, sediment loads gradually increase as the quantity of developed land and precipitation increases.

Average annual delivered TN loads to Copano Bay were 1391.0 metric tons for the HB that is greater than all scenario values for TN loads. For the scenarios, TN loads ranged from 754.1 metric tons for S1 to 1324.4 metric tons for S9. With the exception of S6, there is a gradual increase in TN loads with more development and precipitation within the LARB.

As for TP, average annual loads were 113.9 metric tons for the HB, which again is greater than any TP load from the scenarios. TP loads for the scenarios range from 50.0 metric tons for S1 to 85.7 metric tons for S9 with the same type of increasing trend exhibited by scenarios for TN.

Table V-3. Average annual freshwater inflows and delivered loads of sediment, total nitrogen (TN), and total phosphorus (TP) delivered to Copano Bay under historical baseline or scenario conditions. Note: LD = lower amounts of developed land; MD = medium ammounts of developed land; HD = higher amounts of developed land; LP = lower amounts of precipitation; MP = medium amounts of precipitation; HP = higher amounts of precipitation

Scenario/Baseline	Time-Period	Freshwater Inflows 1000 acre-feet	Delivered Sediment Load 1000 mT	Delivered TN Load mT	Delivered TP Load mT
Historical	1990 - 1999	199.0	60.7	1391.0	113.9
S1 (LD + LP)	2030 - 2039	107.2	45.3	754.1	50.0
S2 (MD + LP)	2030 - 2039	107.6	48.9	755.3	50.4
S3 (HP + LP)	2030 - 2039	108.7	50.5	755.4	50.7
S4 (LD + MP)	2030 - 2039	157.4	60.4	837.2	75.5
S5 (MD + MP)	2030 - 2039	157.8	64.8	839.3	76.2
S6 (HD + MP)	2030 - 2039	159.1	67.7	836.0	75.8
S7 (LD + HP)	2030 - 2039	186.5	70.1	1321.7	84.5
S8 (MD + HP)	2030 - 2039	186.9	74.4	1320.3	84.7
S9 (HD + HP)	2030 - 2039	188.0	76.4	1324.4	85.7

5.4.3.2 Sub-Annual Scales

Freshwater inflows and delivered loads of sediment, TN, and TP to Copano Bay from the Aransas River were analyzed for the HB (1990-1999) and 9 scenarios (2030-2039) at seasonal and monthly scales. Fall is the season with the highest freshwater inflows for the HB and all scenarios. With the exception of the MP scenarios (S4, S5,

and S6) that experience their lowest freshwater inflows in the winter; spring is the season with the lowest freshwater inflows for all other scenarios and the HB (Figure V-16a). The impacts from variable precipitation are far more significant than those from various amounts of developed land. For the HB and scenarios with LP and HP, October is the month with the greatest freshwater inflows and July is when freshwater inflows are at their lowest. July and October are the months with the greatest freshwater inflows for the MP scenarios; and December is the month with the lowest.

Similar to freshwater inflows, fall is the season with the greatest delivered sediment load to Copano Bay for the HB and all scenarios (Figure V-17a). Summer is the season with the lowest sediment loads for the HB and scenarios with MP and HP. For LP scenarios, spring is the season with the lowest sediment loads. With the exception of LP scenarios where August is the month with the greatest average sediment loads, October is the month with the greatest delivered sediment loads to Copano Bay for the HB and other scenarios (Figure V-17b). July is the month with the lowest sediment loads for the HB and scenarios with LP and HP. For MP scenarios, December is the month with the lowest freshwater inflows. While the influence of varying amounts of developed land is more distinct between the scenarios, this distinction is not as profound as those exhibited by varying amounts of precipitation.

a)

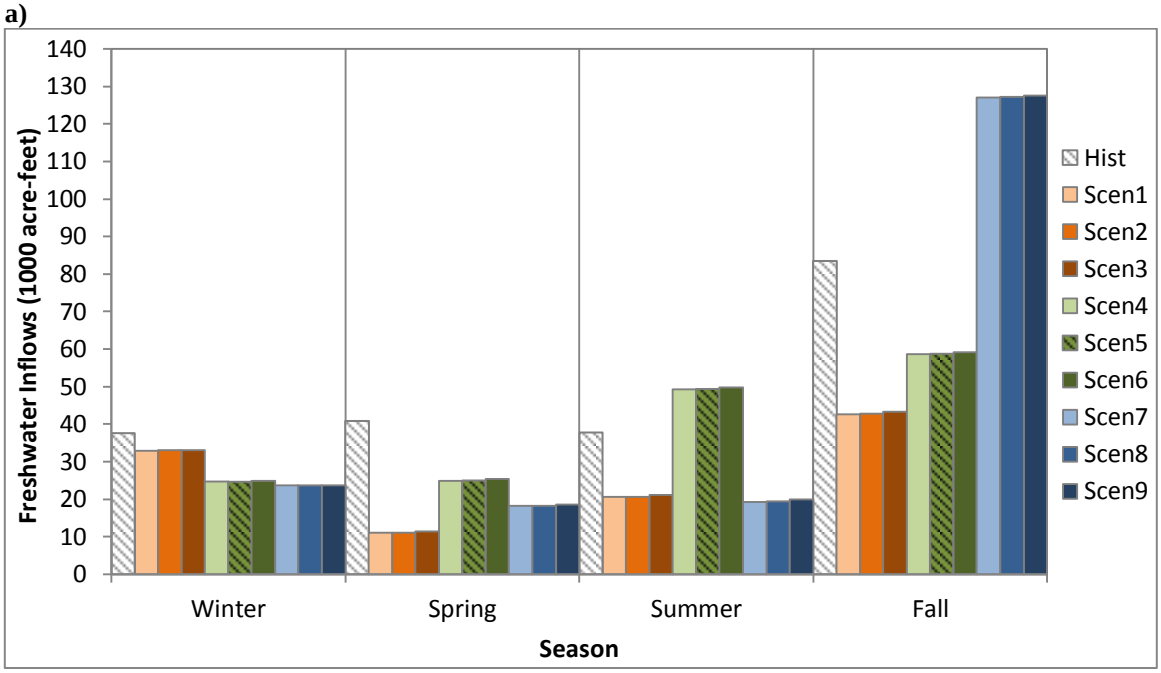

b)

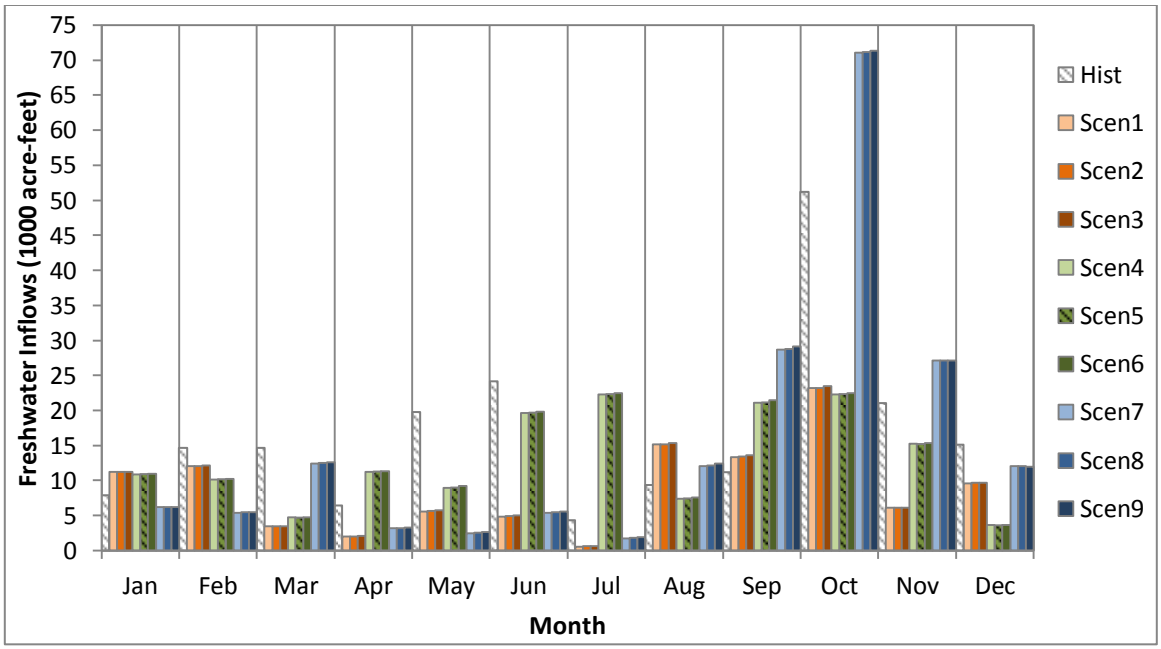

Figure V-16. a) Average seasonal freshwater inflows to Copano Bay from the Aransas River for the historical (Hist) baseline (1990-1999) and each scenario (2030-2039). b) Average monthly freshwater inflows to Copano Bay from the Aransas River for the historical (Hist) baseline (1990-1999) and each scenario (2030-2039). Note: baselines (historical and scenario 5) each have diagonal hatches.

a)

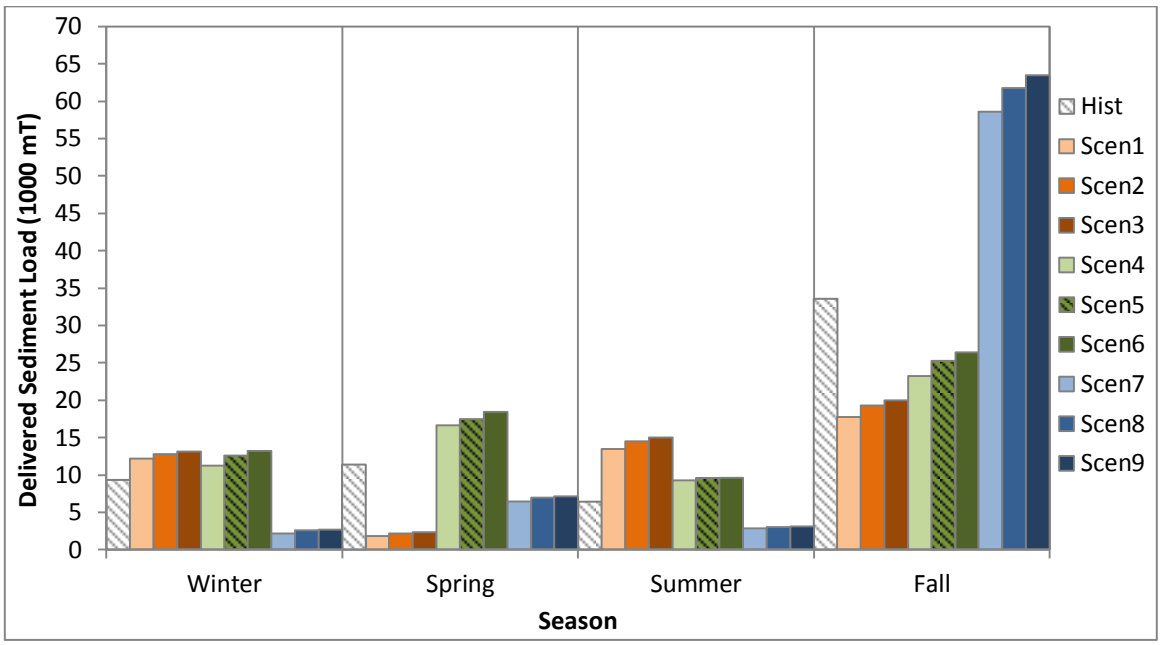

b)

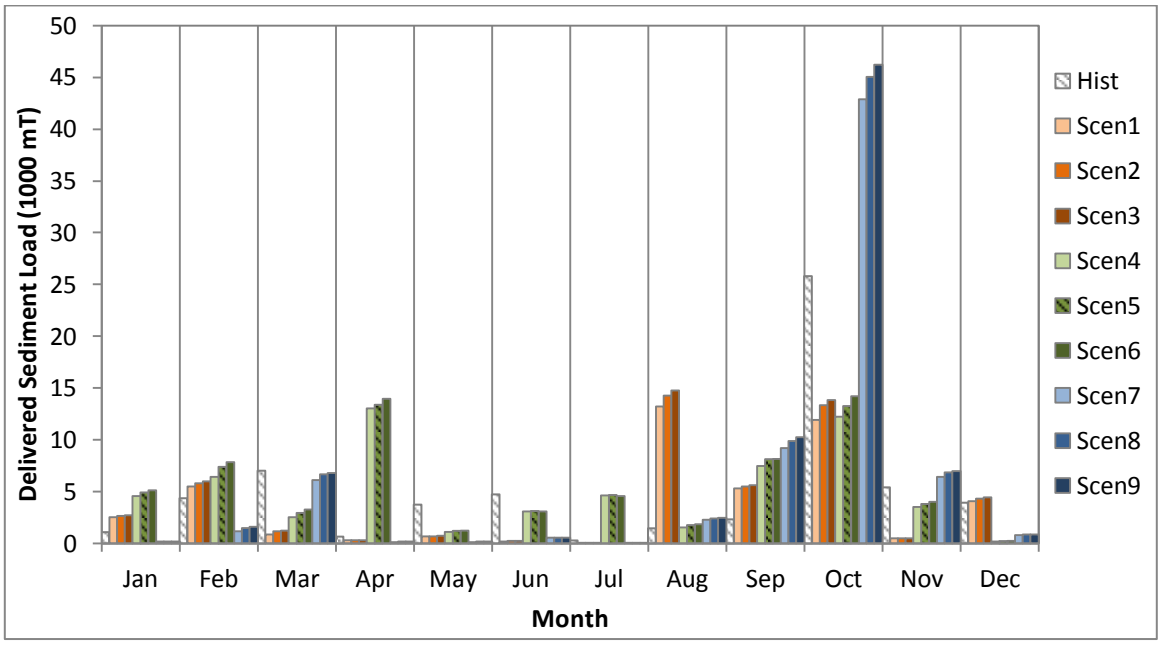

Figure V-17. a) Average seasonal delivered sediment load to Copano Bay from the Aransas River for the historical (Hist) baseline (1990-1999) and each scenario (2030-2039). b) Average monthly delivered sediment load to Copano Bay from the Aransas River for the historical (Hist) baseline (1990-1999) and each scenario (2030-2039). Note: baselines (historical and scenario 5) each have diagonal hatches.

The greatest seasonal average delivered TN loads to Copano Bay occur in the fall season for the HB and scenarios with MP and HP. For LP scenarios, winter is the season with the greatest TN loads. The spring and summer are the seasons with the lowest TN loads for the HB and all scenarios. October is the month with the greatest TN loads for the HB and all scenarios. July is the month with the lowest average TN loads for the HB and scenarios with LP and HP. December is when the lowest average TN loads occur for the MP scenarios. The effect to TN loads from the various levels of increased development is negligible when compared to the impacts cause by variable precipitation.

Similar to sediment loads, the greatest seasonal average delivered TP loads to Copano Bay occurs in the fall season for the HB and all scenarios. For LP scenarios, fall is the season with the greatest TP loads. Summer is the season with the lowest TP loads for the HB and all scenarios. October is the month with the greatest TP loads for the HB and all scenarios. July is the month with lowest average TP loads for the HB and scenarios with LP and HP. July is when the lowest average TP loads occur for the MP scenarios. The impacts to TP loads from the various amounts of increased development are slight when compared to the impacts cause by variable precipitation.

a)

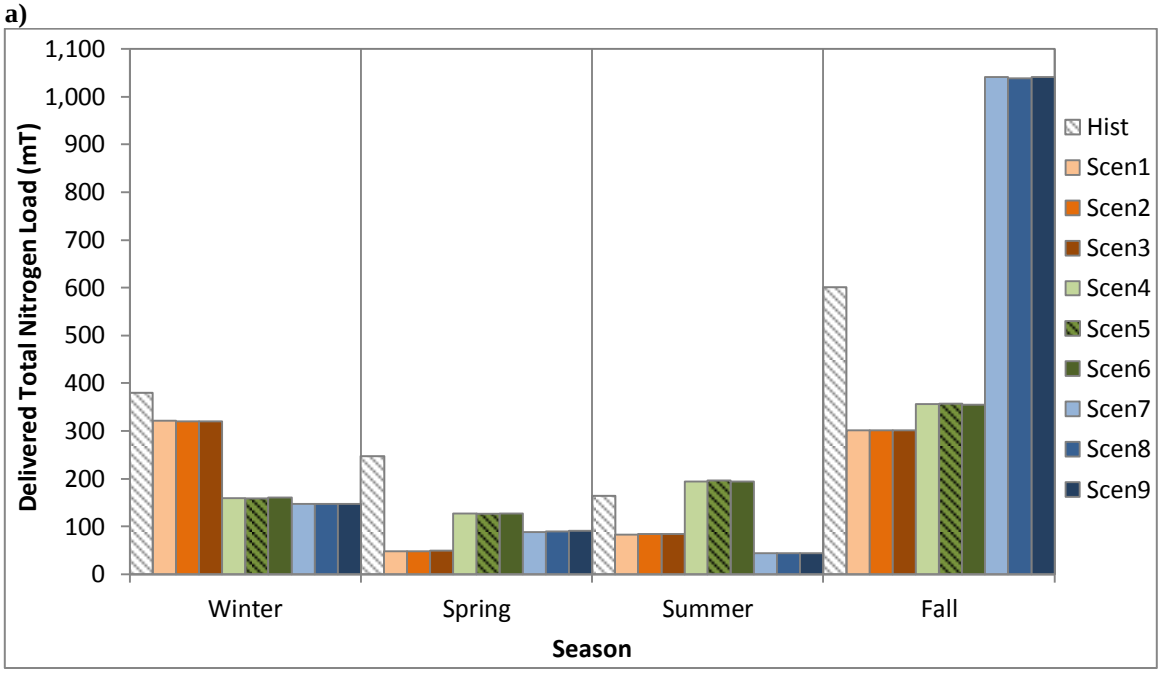

b)

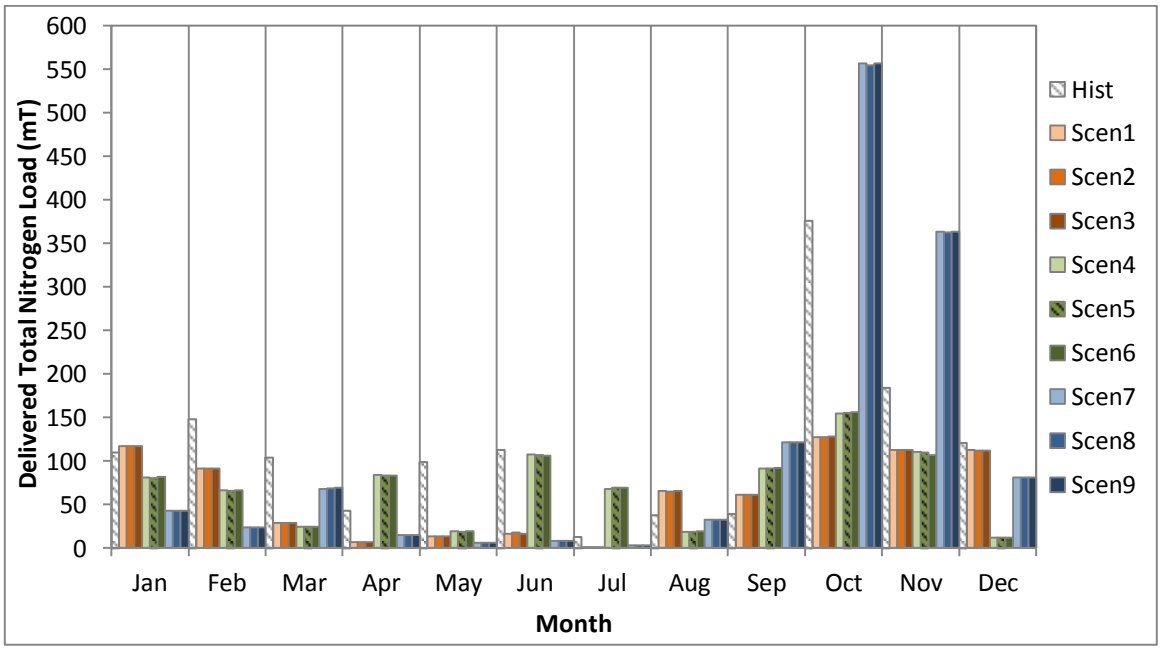

Figure V-18. Average seasonal delivered total nitrogen load to Copano Bay from the Aransas River for the historical (Hist) baseline (1990-1999) and each scenario (2030-2039). b) Average monthly delivered total nitrogen load to Copano Bay from the Aransas River for the historical (Hist) baseline (1990-1999) and each scenario (2030-2039). Note: baselines (historical and scenario 5) each have diagonal hatches.

a)

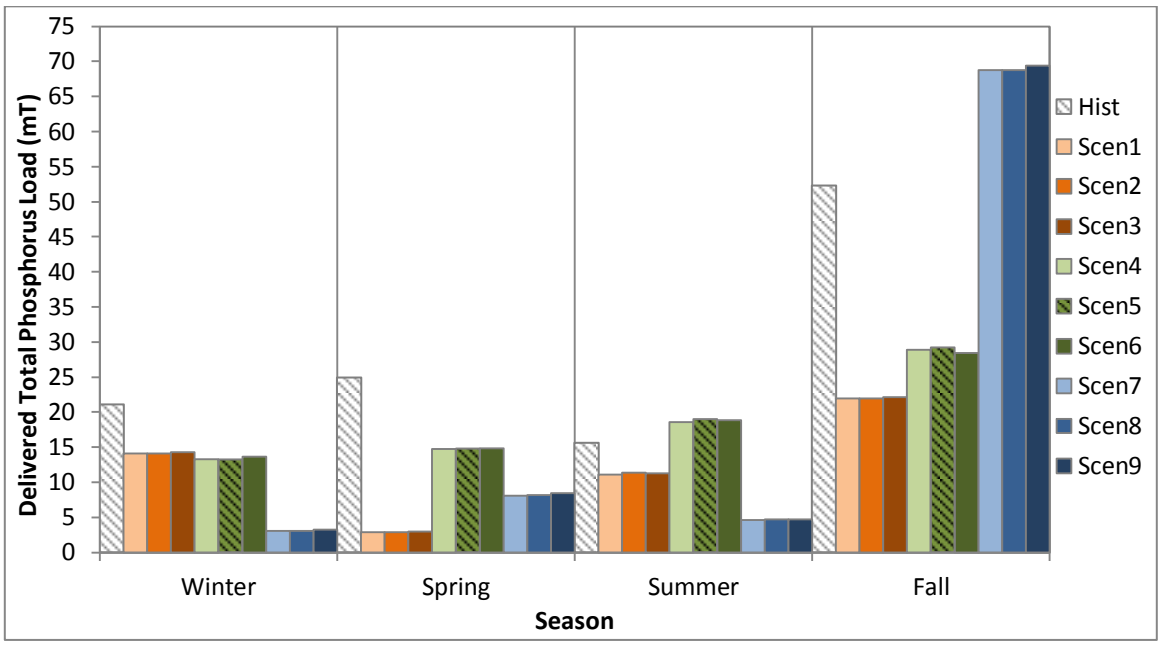

b)

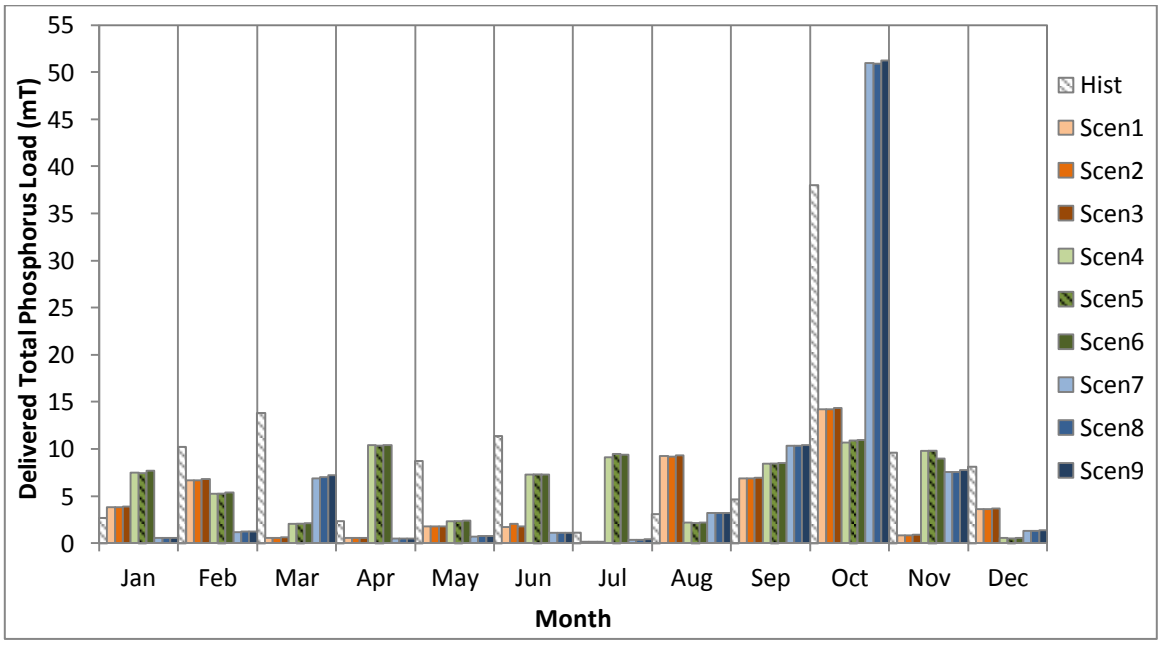

Figure V-19. Average seasonal delivered total phosphorus load to Copano Bay from the Aransas River for the historical (Hist) baseline (1990-1999) and each scenario (2030-2039). b) Average monthly delivered total phosphorus load to Copano Bay from the Aransas River for the historical (Hist) baseline (1990-1999) and each scenario (2030-2039). Note: baselines (historical and scenario 5) each have diagonal hatches.

5.5 Discussion

5.5.1 Hydrologic Impacts at Subbasin Scale: Comparison between Scenarios

5.5.1.1 Stream/Channel Flow

Average annual stream/channel flows out of each subbasin for 8 scenarios for the time-period 2030-2039 were compared to flows from S5 for the same time-period (Figure V-8). Noticeable differences exist across most scenarios, with the impacts from variable amounts of precipitation generally outweighing those from variable amounts of developed land. For subbasins in the western parts of the LARB, differences in the stream/channel flow quantities do not vary significantly across the scenarios and this is mostly due to fairly similar amounts of precipitation (Figure V-6) and developed land (Figure V-3) for all scenarios. Subbasins along the northeastern edge and in the central parts of the LARB, where the Aransas River and Chiltipin Creek are found (Figure V-7), are the subbasins most impacted by the variations in precipitation and the degree of development. Stream/channel flows out of subbasins along the northeastern boundary of the LARB are mostly impacted by the variations in precipitation because these are the areas with the greatest variation in precipitation (Figure V-6). While stream/channel flows out of the central subbasins are most certainly impacted by precipitation variability, these areas are where most of the expansion of developed land occurs between scenarios and thus is where the associated impacts from increased development occur. It can be inferred that for the conditions used in this analysis, the variations in precipitation impact stream/channel flows throughout most of the LARB, while the

variations in the amounts of developed land cause impacts at more local scales in the vicinity of where the expansion of developed land is occurring.

5.5.1.2 Sediment Loads

Average annual sediment loads transported out of each subbasin via the main channel for 8 scenarios for the time-period 2030-2039 were compared to sediment loads from S5 for the same time-period (Figure V-9). The spatial trends in the differences for sediment loads across the scenarios (Figure V-9) are somewhat similar to the spatial trends from stream/channel flows (Figure V-10). This is to be expected as only mechanisms associated with the action of water (rain-drop impact, sheet erosion, and channel erosion) are utilized to model soil erosion and sediment transport. Nonetheless, the difference in the amount of influence to sediment loads that the various amounts of precipitation and developed land each have is not equal between sediment loads and stream/channel flows. Furthermore, the impact to sediment loads from the amount of development is distributed across the LARB near urban areas and major roads. This is most apparent for scenarios that had medium amounts of precipitation (S4 and S6) because the spatial distribution of precipitation across the LARB is more uniform (Figure V-6c) and the increases in sediment loads from S4 to S6 are fairly significant. Conceptually, this is expected because an increase in the amount of developed land reduces infiltration leaving higher quantities of water on the surface to erode the soil and transport sediment.

5.5.1.3 Total Nitrogen (TN) Loads

Average annual TN loads transported out of each subbasin via the main channel for 8 scenarios for the time-period 2030-2039 were compared to TN loads from S5 for the same time-period (Figure V-10). The spatial trend of differences in TN loads amongst the scenarios is similar to the trend of differences for stream/channel flow (Figure V-8), and it more closely matches the stream/channel flow spatial distribution than the differences for sediment loads (Figure V-9). This is because there are little or no impacts to TN loads from increased amounts of developed land. Again, this makes intuitive sense as flows of water are the only transport mechanism being modeled. Furthermore, the LARB is a highly agricultural region, but the application of fertilizer was not incorporated into SWAT simulations. The amount of precipitation received by subbasins ultimately governs SWAT simulations of the transport of TN loads via the main channel in the subbasin.

5.5.1.4 Total Phosphorus (TP) Loads

Average annual TP loads transported out of each subbasin via the main channel for 8 scenarios for the time-period 2030-2039 were compared to TP loads from S5 for the same time-period (Figure V-10). The spatial trend of differences in TP loads amongst the scenarios is similar to the trend of differences for sediment loads (Figure V-9). This is because phosphorus tends to bind to soil/sediment and phosphorus will be transported along with sediment. Given the impact that increasing amounts of developed land have on sediment loads, it will consequently have an impact on TP loads.

5.5.2 Hydrologic Impacts at Subbasin Scale: Comparison to Historical Baseline

5.5.2.1 Stream/Channel Flow

To analyze how scenario values compare to those modeled using non-synthetic data, average annual stream/channel flows out of each subbasin for all scenarios for the time-period 2030-2039 were compared to flows from the HB for the time-period 1990-1999 (Figure V-12). The HB represents a condition with lower amounts of developed land than all scenarios (Figure V-3a), but with greater amounts of annual precipitation (Figure V-6a). There are rather large differences between the HB and scenarios with LP and MP that is mostly due to differences in the amounts and spatial distribution of precipitation. HP scenarios are the most similar to the HB because the quantity and spatial distribution of precipitation is very similar. Differences between the HP scenarios and the HB are mostly due to greater amounts of developed land for the scenarios in central parts of the LARB. It is interesting to note that the impacts from developed land are more local and they do not tend to propagate downstream when analyzing average annual stream/channel flows. While increases in stream/channel flows due to increasing amounts of developed land are seemingly modest, it increases the potential for damages associated with flooding when large precipitation events occur.

5.5.2.2 Sediment Loads

Average annual sediment loads transported out of each subbasin via the main channel for all scenarios for the time-period 2030-2039 were compared to sediment loads from the HB for the time-period 1990-1999 (Figure V-12). Given that sediment transport is governed by the action of water within SWAT, sediment loads for HP

scenarios most closely resemble those from the HB, as expected. The impacts to sediment loads from increased amounts of developed land are quite significant because sediment loads are greater for subbasins in the Sinton area than those from the HB regardless of the amount of precipitation. To model soil erosion outside of channels, SWAT utilizes the Modified Universal Soil Loss Equation (MUSLE) that does not account for sediment supplies and variable storage of sediment within subbasins. The utilization of MUSLE increases the chances that SWAT will over-predict soil erosion and sediment transport; nonetheless increased amounts of erosion due to greater amounts of developed land can have serious implications to surrounding agricultural areas and sedimentation rates within the estuary downstream.

5.5.2.3 Total Nitrogen (TN) Loads

Average annual TN loads transported out of each subbasin via the main channel for all scenarios for the time-period 2030-2039 were compared to TN loads from the HB for the time-period 1990-1999 (Figure V-13). Given that the amount of precipitation an area receives largely governs TN loads, HP scenarios most closely resemble the HB. Nonetheless, it is interesting to note that for HP scenarios, subbasins in southern portions of the LARB have greater TN loads than those from the HB. While these subbasins receive greater amounts of annual precipitation with the HB (Figures V-5a and V-5d), there is a greater amount of developed land within these subbasins under scenario conditions. It seems that greater amounts of precipitation coupled with large increases in developed land can cause increases in average annual TN loads. While fertilizer applications for agricultural areas was not incorporated in SWAT simulations, results

presented here indicate that wet time periods and increased development can lead to larger TN loads being transported downstream to Copano Bay and pose negative impactions to estuarine ecology.

5.5.2.4 Total Phosphorus (TP) Loads

Average annual TP loads transported out of each subbasin via the main channel for all scenarios for the time-period 2030-2039 were compared to TP loads from the HB for the time-period 1990-1999 (Figure V-14). TP loads for all scenarios are below those from the HB. Furthermore, there are no discernible impacts as a result of increased development. The lack of an impact from increased amounts of developed land is somewhat unexpected given the association that TP loads have with sediment loads. Differences between sediment loads for scenarios with the amount of precipitation were attributed to differing amounts of developed land (e.g. Figures V-13d, V-13e, and V-13f). The classification scheme used in Figure V-15 maps differences between TP loads with a 5,000 metric ton interval; and the differences in TP loads due to the amounts of development are small enough that they are not captured using the class interval utilized in constructing the maps.

5.5.3 Hydrologic Impacts at Basin Scale

5.5.3.1 Annual Scale

Average annual freshwater inflows and delivered loads of sediment, TN, and TP to Copano Bay from the Aransas River (LARB outlet) were analyzed for the HB and each scenario (Table V-3). Freshwater inflows for the HB were higher than those for any of the scenarios and this is because there was a higher average annual precipitation for

this time-period. With regard to the scenarios, the impacts from variable precipitation cause the greatest differences in freshwater inflows amongst the scenarios. Nonetheless, increasing amounts of developed land cause increases in freshwater inflows across scenarios with the same amount of precipitation. It bears noting that the level of impact to average annual freshwater inflows becomes more significant as the amount of precipitation decreases. For HP scenarios, there is a percent difference of 0.8% between the low and high development scenarios, while there is a percent difference of 1.4% for LP scenarios. This is likely due to differences in the spatial distribution of precipitation for each scenario (Figure V-6). For the LP scenarios, quantities of precipitation are distributed more uniformly across the lower portions of the LARB where increased development occurs, while the HP scenarios have the greatest amount of precipitation occurring along northern portions where there is less development. Regardless of the location where increased development occurs, it can cause changes to freshwater inflow quantities and potentially affect the salinity balance within the M-A estuarine system.

For sediment loads, unlike the trend exhibited by freshwater inflows, sediment loads for the HB are greater than 4 of the 9 scenarios (S1, S2, S4, and S4). This is because the amount of developed land has a significant influence on sediment loads. While the HB received a higher amount of precipitation, the amount of development for the HB is lower. Given that freshwater inflows govern the transport of sediment to the coast within SWAT, the scenarios exhibit a similar trend of increasing sediment loads with increasing amounts of precipitation and developed land. On the other hand, the degree of influence from variations in the amount of developed land is greatest for MP

scenarios, as opposed to freshwater inflows where the influence from development was greatest for the LP scenarios. For sediment loads from MP scenarios, there is a percent difference of 12.1% between the LD and HD scenarios, while there is a percent difference of 11.5% between sediment loads for LP scenarios with LD and HD. Given that the spatial distribution of precipitation is similar between the LP and MP scenarios (Figures V-6b and V-6c), the greater amounts of precipitation allow for more soil erosion and sediment transport to occur. Modeled sediment loads for the LARB are fairly sensitive to the amount of developed land, which indicates that rapid increases in urbanization can ultimately alter sedimentation rates within Copano Bay.

Average annual TN loads exhibited much of the same trend exhibited by freshwater inflows. TN loads for the HB were greater than those from every scenario due to greater amounts of precipitation. With the exception of S6, there is a trend of increasing TN loads as the amount of precipitation and developed land increases. Excluding S6, the variation between TN loads as a result of the amount of development for scenarios with same amount of precipitation is very small. LP scenarios exhibited the greatest impact from variable development with a percent difference of 0.2% between the LD and HD scenarios. S6 had a decline in TN loads and part of this decline might be due to model error and/or decreases in plant matter modeled within SWAT as a result of losses in vegetated and agricultural surfaces that transitioned to developed land. While increased TN loads reaching Copano Bay as a result of increased precipitation and developed land could cause imbalances in nutrient cycles for the estuary due to overloading, the removal of vegetation for the conversion to developed land can

decrease TN loads reaching the estuary and cause imbalances in these nutrient cycles due to a reduced supply of nitrogen.

For average annual TP loads, the trend is fairly similar to that of TN, but with a more distinctive impact from increased amounts of developed land. The impacts from variable amounts of developed land are fairly similar with a percent difference of 1.4% between the LD and HD scenarios with low and high amounts of precipitation. Similar to TN, there is a decline in TP loads for S6, and this decline could be due to model error and/or losses of vegetated surfaces. Once again, nutrient cycles of the M-A estuarine system can potentially be disrupted by changes in the inputs of TP.

5.5.3.2 Sub-Annual Scales

Freshwater inflows and delivered loads of sediment, TN, and TP to Copano Bay from the Aransas River were analyzed for the HB (1990-1999) and 9 scenarios (2030-2039) at seasonal and monthly scales. In terms of freshwater inflows, the impacts from variable precipitation significantly outweigh the impacts from variable amounts of developed land. Fall is the season with the greatest freshwater inflows with the HP scenarios having the greatest peaks that are significantly higher than the peak for any other scenario and the HB (Figure V-16a). The large peak flows that occur in fall for the HB are mostly from October where freshwater inflows are greater than HP and LP scenario inflows by 20.0 and 47.9 thousand acre-feet, respectively. It is interesting to note that the HP scenarios only have the highest freshwater inflows in the fall with the MD scenarios having higher freshwater inflows for all other seasons. This indicates that large storms in the fall, such as tropical storms, can dramatically skew statistics made at

annual scales and highlights the importance of conducting scenario analyses at various time-scales with multiple precipitation scenarios. While the impacts from increased development are seemingly negligible when compared to how variable precipitation affects the watershed hydrology for the LARB, the water balance is being altered with decreased amounts of infiltration as development increases that could potentially affect future groundwater supplies for irrigators and communities in the LARB region.

Similar to freshwater inflows, the fall months are the time of the year with the greatest delivered sediment loads to Copano Bay for all scenarios (Figure V-17a). Interestingly, MP scenarios had the greatest freshwater inflows for the summer months, but the LP scenarios have the greatest delivered sediment loads in the summer. It seems that while the MP scenarios had higher amounts of precipitation during the summer, precipitation events in August for the LP scenarios were of sufficient intensity to cause greater amounts of erosion and sediment transport. The impacts to sediment loads from increased amounts of developed land are more apparent with an average percent difference of 11.6% between the HD and LD scenarios for all seasons. This is to be expected as the expansion of developed land often involves the removal of vegetated surfaces that anchor soils and reduce erosion. Furthermore, a reduction in infiltration leaves greater quantities of water on the surface that can travel at greater velocities and thus transport larger quantities of sediment. Given the sensitivity of sediment transport to increased amounts of developed land, an increasing trend for delivered sediment loads to Copano Bay can be expected as the region becomes more developed. This can lead to

alterations in sedimentation rates for the M-A estuary and cause implications with the regard to the ecology and infrastructure of areas along the coast in the region.

The trends in seasonal and monthly average delivered TN loads to Copano Bay are fairly similar to those from freshwater inflows (Figures V-16 and V-18), with fall and winter being the seasons with the greatest delivered TN loads. However, the degree of influence from increased amounts of developed land is different between TN loads and freshwater inflows. Increased development does not necessarily lead to higher TN loads with some months exhibiting lower TN loads for HD scenarios than any of the other development scenarios with the same precipitation. While this difference in TN loads is relatively small and it might be attributed to model error, losses of vegetated surface (conversion to developed) and lower than average temperatures can also cause TN loads to decrease. However, SWAT assumes that TN loads cannot be exhausted and the non-incorporation of fertilizer applications for agricultural purposes indicates that SWAT estimates are somewhat unreliable. Regardless of whether TN loads are completely accurate, the scenario analysis indicates that TN loads are closely related to the amounts of precipitation the area receives. Given the potential that nitrogen has in causing negative ecological implications for coastal areas, understanding the factors influencing TN loads for the region will be important in managing the M-A estuarine system.

Delivered TP loads to Copano Bay, on the other hand, display a seasonal and monthly trend that is more similar to sediment loads. With the exception of the MP scenarios, there is a general increase in TP loads with increasing amounts of developed

land. As for the MP scenarios, some months exhibit a lower TN load for HD scenarios than for scenarios with LD and MD. Again, this might be due to model error, losses of vegetation, or temperature variations. Nonetheless, this analysis highlights the importance of sediment transport in the delivery of phosphorus to the coast. Proper management of sediment transport within the Aransas region will aid the management of phosphorus delivery to the M-A estuarine system.

5.6 Conclusion

Watershed hydrology and water quality of coastal watersheds can be impacted by changes in the amount of developed land within the watershed and variability in the amount of precipitation the area receives. The LARB on the Coastal Bend of Texas is an area that has been experiencing a steady increase in the amount of developed land within the basin from 1990 to 2010. Furthermore, the semi-arid region is subject to variations in precipitation from extended drought to seasonal tropical storms that occasionally bring large amounts of precipitation to the region. Given the importance of freshwater inflows and the delivery of sediments and nutrients from the Aransas River Basin to the estuary downstream; a scenario analysis for LARB was conducted that analyzed how stream/channel flows and loads of sediment, TN, and TP were impacted using hypothetical future conditions for the time-period 2030-2039 that each had varying amounts of developed land and precipitation for the watershed.

Three LULC change scenarios that predicted differing amounts of developed land (low development (LD), medium development (MD), and high development (HD)) were combined with three precipitation scenarios that predict differing amounts annual

precipitation (low precipitation (LP), medium precipitation (MP), and high precipitation (HP)). Each individual LULC change scenario was combined with a precipitation scenario to have a total of 9 scenarios used in this analysis. The scenarios were incorporated into a SWAT model calibrated to the hydrological conditions of the LARB. To analyze how stream/channel flows and loads of sediment, TN, and TP were impacted under each scenario condition, comparisons were made between scenarios themselves and comparisons with a historical baseline (HB). Comparisons between the scenarios and the HB were conducted at the subbasin and basin scale by analyzing the variables of interest at the subbasin and basin outlet.

At the subbasin scale, the impacts to stream/channel flows and loads of sediment, TN, and TP from variable amounts of precipitation generally outweighed the impacts from various amounts of developed land within the LARB. Scenarios exhibited a general increase in all output variables of interest as the amount of precipitation and developed land increased. Subbasins being impacted by the differing amounts of precipitation were more evenly distributed across the LARB, while impacts from differing amounts of developed land were situated in subbasins where most of the increases in developed land occurred. Given that the action/flow of water was the only mechanism used to model the transport of associated constituents, large variations in material loads (sediment, TN, and TP) were generally governed by variations in stream/channel flows. However, sediment loads were the output variable most affected by the differing amounts of developed land causing the spatial pattern in changes to sediment loads to sometimes differ from the spatial pattern for stream/channel flows.

Furthermore, phosphorus has a tendency to bind to soil/sediment particles and thus the spatial pattern in changes to TP loads was often similar to the spatial pattern for sediment loads. It can be inferred that the spatial pattern of changes to TN loads is more similar to the pattern for stream/channel flows, while the spatial pattern for TP loads is more similar to the spatial pattern for sediment loads.

With regard to the comparison to the HB at the subbasin scale, the HB predicted higher values for most of the output variables of interest. The conditions for the HB in 1990-1999 are characterized with having a lower amount of developed land and a greater amount of precipitation when compared to the conditions for the 9 scenarios. Differences between the HB and scenarios are generally depicted by differences in the quantity and spatial distribution of precipitation. However, as a result of greater amounts of developed land, stream/channel flows and sediment loads are often greater for some scenarios than those from the HB for subbasins in the vicinity of where increases in developed land occur. Although the same types of differences between the HB and scenarios are not depicted for TN and TP loads. This indicates that certain aspects of the local hydrology for particular subbasins can change significantly as a result of increases in the amount of developed land regardless of how precipitation varies.

At the basin scale, with the exception of the HB, there is a general trend of increasing values for the output variables of interest as the amount of precipitation and developed land increases when analyzing the variables at an annual scale. The HB had the highest average annual freshwater inflows and delivered loads of TN and TP largely due to higher amounts of precipitation. Average annual delivered sediment loads for 5 of

the 9 scenarios were greater than the sediment load for the HB due to greater amounts of developed land for these 5 scenarios. At sub-annual scales, the character of the precipitation scenarios becomes more apparent with the HP scenario only having the highest values for the variables of interest in the fall months. At least one of the other precipitation scenarios predicts higher values for output variables for all other non-fall seasons. This highlights the importance of analyzing the seasonal and monthly variability in watershed hydrology when conducting scenario analyses. Nonetheless, much of the same trends associated with varying amounts of developed land (increases in model outputs) are exhibited when analyzing scenarios with similar precipitation at sub-annual scales. This indicates that precipitation variability largely controls the quantity and seasonal variation of freshwater inflows, while LULC can be a major control of water quality and potentially compound the effects from variations in precipitation.

The delivery of freshwater, sediment, and nutrients to the coast by drainage basins is intimately connected with the climatic and landscape characteristics of the region. The LARB is no exception with the precipitation regime and character of LULC within the watershed having a profound effect on the quantity and quality of freshwater inflows. Results from this analysis suggest that precipitation variability has the greatest impact on freshwater inflows and delivered loads of sediment and nutrients to the M-A estuarine system. It is important to note that precipitation variability is something that cannot be managed, but it a different story for the ways in which land is used. Analyses such as the one presented here provide insight into how LULC and precipitation interact

to cause changes in watershed hydrology and water quality that can be used to better manage coastal watersheds and maintain the ecological integrity of bays and estuaries when there are large uncertainties in regional characteristics for the future.

CHAPTER VI

SUMMARY AND CONCLUSIONS

6.1 Summary

6.1.1 Land Change Analysis

The quantity and spatial distribution of land-use/land-cover (LULC) change within the Mission-Aransas Coastal Region (MACR) from 1990 to 2010 was analyzed. Portions of two Landsat Thematic Mapper images (1990 and 2010) were classified to a modified Anderson Level I classification with an overall accuracy of 88% and 84%, respectively, for each image. Cultivated land and rangeland are the dominant LULC; with the developed land comprising an average of 4.3% of the land area for the two images.

A relatively large degree of LULC change occurred within the MACR from 1990 to 2010 with 27.1% of the MACR experiencing some form of change. Rangeland was the LULC that experienced the most change. The proportion of total coverage for developed land didn't differ very dramatically from 1990 to 2010, but developed land experienced an increase of 44.9%.

6.1.2 SWAT Calibration

An assessment of the capabilities of SWAT to model freshwater inflows and loadings of sediment and nutrients (TN and TP) from the Lower Aransas River Basin (LARB) was conducted. SWAT was calibrated for monthly mean daily streamflow using data from a USGS stream gage on Chiltipin Creek. Evaluation of the calibrated model

indicated that the model had a good performance with an Nashe-Sutcliffe model efficiency coefficient (NS) of 0.66, coefficient of determination (R^2) of 0.66, and percent difference between average observed and predicted values (PD) of 5.57 for the calibration period (Jan-1972 to Dec-1981); and an NS of 0.76, R^2 of 0.78, and PD of 40.68 for the validation period (Jan-1982 to Sep-1991). Parameters that influence the transport of sediment and nutrients were adjusted so that model outputs resembled published estimates as closely as possible.

A family of correction factors that incorporate measured and modeled uncertainty in common GOF indicators were computed for monthly mean daily streamflow. Three uncertainty distributions (normal, lognormal, and uniform) and four Cv values (0.026, 0.085, 0.192, and 0.256) were utilized in the computation of correction factors. The level of agreement generally increased as the Cv (uncertainty) increased with correction factors that utilized the normal distributions yielding the most promising results.

Using the calibrated model, freshwater inflows and loads of sediment and nutrients (TN and TP) to the M-A estuary from the Aransas River were estimated for the years 1972-2010. Mean annual freshwater inflows was 188.93 million cubic meters, with mean annual delivered loads of 33.27 thousand metric tons for TSS, 1111.05 metric tons for TN, and 94.47 metric tons for TP.

6.1.3 Scenario Development

Three LULC change scenarios and three precipitation scenarios were developed to be used in a SWAT hydrological model calibrated to conditions for the LARB. Each

LULC change scenario represents a different amount of developed land within the LARB. A Multi-Layer perceptron (MLP) neural network was used to conduct a training procedure that modeled LULC change using historical LULC images (for1990 and 2010) and predictor variables. The training procedure yielded an accuracy rate of 63.7%. A Markov chain process was used to generate three scenarios of increased development (low: 23.5%, medium: 35.3%, and high: 70.6%) within the LARB.

Precipitation data from 1950 to 2012 was analyzed at an annual scale to select 28 years of weather data that comprised each precipitation scenario (low, medium, and high). A 14-year moving average was used to select two 14-year periods for each precipitation scenario. Average annual precipitation for the low, medium, and high scenarios is 763, 907, and 996 mm, respectively.

6.1.4 Scenario Analysis

A scenario analysis for the LARB was conducted that analyzed how stream/channel flows and loads of sediment, TN, and TP were impacted using hypothetical future conditions for the time-period 2030-2039 that each had varying amounts of developed land and precipitation for the watershed.

Three LULC change scenarios that predicted differing amounts of developed land (low development, medium development, and high development) were combined with three precipitation scenarios that predict differing amounts annual precipitation (low precipitation, medium precipitation, and high precipitation). Each LULC change scenario was combined with a precipitation scenario to have a total of 9 scenarios that were each incorporated into the calibrated SWAT model. Comparisons were made

between scenarios and a historical baseline. Comparisons were conducted at the subbasin and basin scale by analyzing differences in stream/channel flows and loads of sediment, TN, and TP.

At the subbasin scale, the impacts to stream/channel flows and loads of sediment, TN, and TP from variable amounts of precipitation generally outweighed the impacts from various amounts of developed land within the LARB. Scenarios exhibited a general increase in all output variables of interest as the amount of precipitation and developed land increased. Subbasins being impacted by the differing amounts of precipitation were more evenly distributed across the LARB, while impacts from differing amounts of developed land were situated in subbasins where most of the increases in developed land occurred. Sediment loads were the output variable most affected by the differing amounts of developed land. Furthermore, phosphorus has a tendency to bind to soil/sediment particles and thus the spatial pattern in changes to TP loads was often similar to the spatial pattern for sediment loads. The spatial pattern of changes to TN loads is more similar to the pattern for stream/channel flows, while the spatial pattern for TP loads is more similar to the spatial pattern for sediment loads.

At the basin scale, there is a general trend of increasing values for the output variables of interest as the amount of precipitation and developed land increases when analyzing the variables at an annual scale. The historical baseline had the highest average annual freshwater inflows and delivered loads of TN and TP largely due to higher amounts of precipitation. At sub-annual scales, fall was found to be wettest time of the year with spring being the driest. Similar trends associated with increasing

amounts of developed land (increases in model outputs) are exhibited when analyzing scenarios with similar precipitation at sub-annual scales. Precipitation variability largely controlled the quantity and seasonal variation of freshwater inflows, while LULC largely affected sediment loads.

6.2 Main Conclusions

The research presented in this thesis addressed the following question: How are streamflow, sediment flow, and nutrient transport into the Mission-Aransas estuarine system impacted by interactive variations in precipitation and land-use/land-cover change? Results from the research presented here allow one to make the following three conclusions regarding the research question:

1. Impacts to the quantity and quality of freshwater inflows from precipitation variability outweighed the impacts from increased amounts of developed land in SWAT simulations. While the amount of developed land increased substantially amongst the scenarios in relative terms, developed land still only constituted a small proportion of the watershed area. Precipitation is the main input of freshwater to the Aransas River Basin and variations in precipitation cause large fluctuations in freshwater inflows and associated sediment and nutrient loads.
2. Impacts to watershed hydrology and water quality from increased amounts of developed land tended to be more local in the vicinity of where the expansion of developed land is occurring, while impacts from precipitation variability were more evenly distributed across the Lower Aransas River Basin. This is because

the influence from increased development was more apparent at the subbasin scale, while the influence from variable precipitation was significant across the basin and subbasins scales.

3. Sediment transport is the process most impacted by increases in developed land for SWAT simulations. More calibration of SWAT is needed for sediment load estimates to be considered reliable, however there were distinct differences between scenarios with the same precipitation and differing amounts of developed land. A reduction in groundwater infiltration and the removal of vegetated surface is a characteristic of increasing development that greatly increases the potential for soil erosion and sediment transport.

The research presented in this thesis provides useful knowledge regarding the hydrological characteristics of the Mission-Aransas region through a case study application of the SWAT hydrological model. This knowledge will inform the management of watersheds upstream of the M-A estuary and elsewhere. Furthermore, this research contributes to the body of knowledge aimed at understanding the changes occurring in coastal regions of Texas.

REFERENCES

Allan, J. D. 2004. Landscapes and riverscapes: The influence of land use on stream ecosystems.

Anderson, James R., Ernest E. Hardy, John T. Roach, and Richard E. Witmer. 1976. "Land use and land cover classification system for use with remote sensor data." *U S Geol Surv, Prof Pap* (964).

ArcGIS Desktop Version 9.3.1. Environmental Systems Research Institute, Inc., Redlands, California, USA.

Arismendez, S. S., H. C. Kim, J. Brenner, and P. A. Montagna. 2009. "Application of watershed analyses and ecosystem modeling to investigate land-water nutrient coupling processes in the Guadalupe Estuary, Texas." *Ecological Informatics* no. 4 (4):243-253.

Arnold, J. G., R. Kiniry, R. Srinivasan, J. R. Williams, E. B. Haney, and S. L. Neitsch. 2011. Soil and Water Assessment Tool: Input/Output File Documentation Version 2009. College Station, TX: Grassland, Soil and Water Research Laboratory - Agricultural Research Service, Blackland Research Center - Texas AgriLife Research, Texas Water Resources Institute.

Arnold, J. G., D. N. Moriasi, P. W. Gassman, K. C. Abbaspour, M. J. White, R. Srinivasan, C. Santhi, R. D. Harmel, A. Van Griensven, M. W. Van Liew, N. Kannan, and M. K. Jha. 2012. "SWAT: Model use, calibration, and validation." *Transactions of the ASABE* no. 55 (4):1491-1508.

Borah, D. K., and M. Bera. 2004. "Watershed-scale hydrologic and nonpoint-source pollution models: Review of applications." *Transactions of the American Society of Agricultural Engineers* no. 47 (3):789-803.

Breuer, L., J. A. Huisman, and H. G. Frede. 2006. "Monte Carlo assessment of uncertainty in the simulated hydrological response to land use change." *Environmental Modeling & Assessment* no. 11 (3):209-218. doi: 10.1007/s10666-006-9051-9.

Brock, D., M. Wentzel, J. Matsumoto, and R. Solis. 2008. Values and Constraints for the TXEMP Model Used in the Freshwater Inflow Analysis of the Mission-Aransas Estuary. Austin, TX: Texas Water Development Board: Surface Water Resources

Division: Bays & Estuaries Programs, Texas Parks and Wildlife Department: Coastal Fishery Division.

Chang, H. 2004. "Water quality impacts of climate and land use changes in southeastern Pennsylvania." *Professional Geographer* no. 56 (2):240-257.

Chen, Grace F. 2010. Freshwater Inflow Reccomendations for the Mission-Aransas Estuarine System. Austin, TX: Texas Parks and Wildlife Department: Ecosystem Resources Program: Coastal Fisheries Division.

Congalton, R G, and K Green. 2009. *Assessing the Accuracy of Remotely Sensed Data: Principles and Practices*. Boca Raton, FL: CRC Press.

Correll, D. L., T. E. Jordan, and D. E. Weller. 1992. "Nutrient flux in a landscape: Effects of coastal land use and terrestrial community mosaic on nutrient transport to coastal waters." *Estuaries* no. 15 (4):431-442.

Duda, P. B., P. R. Hummel, A. S. Donigian Jr, and J. C. Imhoff. 2012. "BASINS/HSPF: Model use, calibration, and validation." *Transactions of the ASABE* no. 55 (4):1523-1547.

Eastman, J. R. 2012. IDRISI Selva Manual. Worcester, MA: Clark Labs, Clark University.

Engel, B., D. Storm, M. White, J. Arnold, and M. Arabi. 2007. "A hydrologic/water quality model application protocol." *Journal of the American Water Resources Association* no. 43 (5):1223-1226.

Environment for Visualizing Images (ENVI) 4.7. ITT Visual Information Solutions, Boulder, CO.

Estevez, E. D. 2002. "Review and assessment of biotic variables and analytical methods used in estuarine inflow studies." *Estuaries* no. 25 (6 B):1291-1303.

Foley, J. A., R. DeFries, G. P. Asner, C. Barford, G. Bonan, S. R. Carpenter, F. S. Chapin, M. T. Coe, G. C. Daily, H. K. Gibbs, J. H. Helkowski, T. Holloway, E. A. Howard, C. J. Kucharik, C. Monfreda, J. A. Patz, I. C. Prentice, N. Ramankutty, and P. K. Snyder. 2005. "Global consequences of land use." *Science* no. 309 (5734):570-574.

Franczyk, J., and H. Chang. 2009. "The effects of climate change and urbanization on the runoff of the Rock Creek basin in the Portland metropolitan area, Oregon, USA." *Hydrological Processes* no. 23 (6):805-815.

Gassman, P. W., M. R. Reyes, C. H. Green, and J. G. Arnold. 2007. "The soil and water assessment tool: Historical development, applications, and future research directions." *Transactions of the ASABE* no. 50 (4):1211-1250.

Google Earth 6.1.0.5001. Google Inc., Mountain Vew, CA.

Harmel, R. D., R. J. Cooper, R. M. Slade, R. L. Haney, and J. G. Arnold. 2006. "Cumulative uncertainty in measured streamflow and water quality data for small watersheds." *Transactions of the ASABE* no. 49 (3):689-701.

Harmel, R. D., P. K. Smith, and K. W. Migliaccio. 2010. "Modifying goodness-of-fit indicators to incorporate both measurement and model uncertainty in model calibration and validation." *Transactions of the ASABE* no. 53 (1):55-63.

Harris, G. P. 2001. "Biogeochemistry of nitrogen and phosphorus in Australian catchments, rivers and estuaries: Effects of land use and flow regulation and comparisons with global patterns." *Marine and Freshwater Research* no. 52 (1):139-149.

Howarth, R., D. Swaney, G. Billen, J. Garnier, B. Hong, C. Humborg, P. Johnes, C. M. Mörth, and R. Marino. 2011. "Nitrogen fluxes from the landscape are controlled by net anthropogenic nitrogen inputs and by climate." *Frontiers in Ecology and the Environment* no. 10 (1):37-43. doi: 10.1890/100178.

IDRISI Selva. Clark Labs, Clark University, Worcester, MA.

ITT Visual Information Solutions, ENVI. 2009a. Atmospheric Correction Module: QUAC and FLAASH User's Guide.

Kirsch, K., A. Kirsch, and J. G. Arnold. 2002. "Predicting Sediment and Phosphorus Loads in the Rock River Basin Using Swat." *Transactions of the American Society of Agricultural Engineers* no. 45 (6):1757-1769.

Lee, T., R. Srinivasan, J. Moon, and N. Omani. 2011. "Estimation of fresh water inflow to bays from gaged and ungaged watersheds." *Applied Engineering in Agriculture* no. 27 (6):917-923.

Legates, D. R., and G. J. McCabe Jr. 1999. "Evaluating the use of 'goodness-of-fit' measures in hydrologic and hydroclimatic model validation." *Water Resources Research* no. 35 (1):233-241.

McElroy, A. D., S. Y. Chiu, J. W. Nebgen, A. Aleti, and F. W. Bennet. 1976. Loading functions for assessment of water pollution from nonpoint sources. Environmental Protection Agency.

Morehead, S., T. G. Beyer, and K. Dunton. 2007. Community Characterization of the Mission-Aransas National Estuarine Research Reserve and Surrounding Areas. Port Aransas, Texas: University of Texas at Austin - Marine Science Institute.

Moriasi, D. N., J. G. Arnold, M. W. Van Liew, R. L. Bingner, R. D. Harmel, and T. L. Veith. 2007. "Model evaluation guidelines for systematic quantification of accuracy in watershed simulations." *Transactions of the ASABE* no. 50 (3):885-900.

Moriasi, D. N., B. N. Wilson, K. R. Douglas-Mankin, J. G. Arnold, and P. H. Gowda. 2012. "Hydrologic and water quality models: Use, calibration, and validation." *Transactions of the ASABE* no. 55 (4):1241-1247.

Nash, J. E., and J. V. Sutcliffe. 1970. "River flow forecasting through conceptual models part I — A discussion of principles." *Journal of Hydrology* no. 10 (3):282-290. doi: http://dx.doi.org/10.1016/0022-1694(70)90255-6.

NCDC. 2012. National Climatic Data Center. National Oceanic and Atmospheric Administration.

Neitsch, S. L., J. G. Arnold, J. R. Kiniry, and J. R. Williams. 2011. Soil and Water Assessment Tool, Theoretical Documentation, Version 2009. Grassland, Soil and Water Research Laboratory - Agricultural Research Service, Blackland Research Center - Texas AgriLife Research.

NERRS. 2006. National Estuarine Research Reserve System: Strategic Plan 2005-2010. Silver Spring, MD: NOAA, National Oceanographic and Atmospheric Administration.

NOAA. 2012. Digital Coast: NOAA Coastal Services Center.

NWIS. 2012. National Water Information System: Web Interface. United States Geological Survey.

Pai, N., and D. Saraswat. 2011. "SWAT2009-LUC: A tool to activate the land use change module in SWAT 2009." *Transactions of the ASABE* no. 54 (5):1649-1658.

Pontius, R. G., and M. Millones. 2011. "Death to Kappa: Birth of quantity disagreement and allocation disagreement for accuracy assessment." *International Journal of Remote Sensing* no. 32 (15):4407-4429.

Powell, G. L., J. Matsumoto, and D. A. Brock. 2002. "Methods for determining minimum freshwater inflow needs of Texas bays and estuaries." *Estuaries* no. 25 (6 B):1262-1274.

Praskievicz, S., and H. Chang. 2009. "A review of hydrological modelling of basin-scale climate change and urban development impacts." *Progress in Physical Geography* no. 33 (5):650-671.

Praskievicz, S., and H. Chang. 2011. "Impacts of climate change and urban development on water resources in the Tualatin River Basin, Oregon." *Annals of the Association of American Geographers* no. 101 (2):249-271.

Price, K. 2011. "Effects of watershed topography, soils, land use, and climate on baseflow hydrology in humid regions: A review." *Progress in Physical Geography* no. 35 (4):465-492.

Rebich, R. A., N. A. Houston, S. V. Mize, D. K. Pearson, P. B. Ging, and C. Evan Hornig. 2011. "Sources and Delivery of Nutrients to the Northwestern Gulf of Mexico from Streams in the South-Central United States." *Journal of the American Water Resources Association* no. 47 (5):1061-1086.

Sahoo, D., and P. K. Smith. 2009. "Hydroclimatic trend detection in a rapidly urbanizing semi-arid and coastal river basin." *Journal of Hydrology* no. 367 (3-4):217-227.

Saleh, A., J. G. Arnold, P. W. Gassman, L. M. Hauck, W. D. Rosenthal, J. R. Williams, and A. M. S. McFarland. 2000. "Application of SWAT for the Upper North Bosque River Watershed." *Transactions of the American Society of Agricultural Engineers* no. 43 (5):1077-1087.

Santhi, C., J. G. Arnold, J. R. Williams, W. A. Dugas, R. Srinivasan, and L. M. Hauck. 2001. "Validation of the SWAT model on a large river basin with point and nonpoint sources." *JAWRA Journal of the American Water Resources Association* no. 37 (5):1169-1188. doi: 10.1111/j.1752-1688.2001.tb03630.x.

Scavia, D., J. C. Field, D. F. Boesch, R. W. Buddemeier, V. Burkett, D. R. Cayan, M. Fogarty, M. A. Harwell, R. W. Howarth, C. Mason, D. J. Reed, T. C. Royer, A. H. Sallenger, and J. G. Titus. 2002. "Climate change impacts on U.S. coastal and marine ecosystems." *Estuaries* no. 25 (2):149-164.

Schoenbaechler, Caimee, and Carla G. Guthrie. 2011. Coastal Hydrology for the Mission-Aransas Estuary. Austin, TX, USA: Texas Water Development Board: Surface Water Resources Division - Bays and Estuaries Program.

Tang, Z., B. A. Engel, B. C. Pijanowski, and K. J. Lim. 2005. "Forecasting land use change and its environmental impact at a watershed scale." *Journal of Environmental Management* no. 76 (1):35-45.

Thomson, A. M., R. A. Brown, N. J. Rosenberg, R. Srinivasan, and R. C. Izaurralde. 2005. "Climate change impacts for the conterminous USA: An integrated assessment: Part 4: Water resources." *Climatic Change* no. 69 (1):67-88.

Tong, S. T. Y., and W. Chen. 2002. "Modeling the relationship between land use and surface water quality." *Journal of Environmental Management* no. 66 (4):377-393.

Welborn, C. T., and R. B. Bezant. 1978. Sediment Yields for Selected Streams in Texas. United States Geological Survey.

Williams, J. R., and R. W. Hann. 1978. Optimal operation of large agricultural watersheds with water quality constraints. Texas Water Resources Institute - Texas A&M University.

Winchell, M., R. Srinivasan, M. Di Luzio, and J. Arnold. 2010. ArcSWAT Interface For SWAT2009: User's Guide. Temple, Texas, USA: Blackland Research and Extension Center - Texas AgriLife Research, Grassland Soil and Water Research Laboratory - USDA Agricultural Research Service.

Wu, K., and Y. J. Xu. 2006. "Evaluation of the applicability of the SWAT model for coastal watersheds in southeastern Louisiana." *Journal of the American Water Resources Association* no. 42 (5):1247-1260.